NASA CR-145072
BBN Report #3245

EXPLORATORY INVESTIGATION OF AEROACOUSTIC OPTIMIZATION OF THE VARIABLE IMPEDANCE EDGE CONCEPT APPLIED TO UPPER SURFACE BLOWN CONFIGURATIONS

by

R.E. Hayden

Prepared Under Contract No. NAS1-13896

By
Bolt Beranek and Newman Inc.
Cambridge, Mass. 02138

for

NASA

National Aeronautics and
Space Administration
Langley Research Center
Hampton, Virginia 23665

1. Report No.	2. Government Accession No.	3. Recipient's Catalog No.
NASA CR-2714		

4. Title and Subtitle	5. Report Date
EXPLORATORY INVESTIGATION OF AEROACOUSTIC OPTIMIZATION OF THE VARIABLE IMPEDANCE EDGE CONCEPT APPLIED TO UPPER SURFACE BLOWN CONFIGURATIONS	November 1976
	6. Performing Organization Code: ---

7. Author(s)	8. Performing Organization Report No.
Richard E. Hayden	3245
	10. Work Unit No.: ---

9. Performing Organization Name and Address	11. Contract or Grant No.
Bolt Beranek and Newman Inc. 50 Moulton Street Cambridge, Massachusetts 02138	NAS1-13896
	13. Type of Report and Period Covered: Contractor Report

12. Sponsoring Agency Name and Address	14. Sponsoring Agency Code
NASA Langley Research Center Hampton, Virginia 23665	---

15. Supplementary Notes

NASA Langley Research Technical Monitor: Donald L. Lansing

16. Abstract

The noise generated by aircraft propulsive lift systems is a potential problem in both the community and inside the aircraft itself. This study investigates the feasibility of using porous surfaces on lift augmenting flaps to reduce the noise at the source, without adversely affecting aerodynamic performance. Numerous flap configurations were tested on a USB (upper surface blowing) type powered lift model (approximately 1/5 full scale). Significant reductions of far field noise and aeroacoustic pressures were found, and many configurations exhibited aerodynamic characteristics comparable to unmodified configurations of the nozzle/flap system.

17. Key Words (Suggested by Author(s))	18. Distribution Statement
Airfoil Noise; Powered Lift Noise Reduction Porous Surfaces; Interior Noise USB Noise and Aerodynamics V/STOL Noise and Aerodynamics	Unclassified

19. Security Classif. (of this report)	20. Security Classif. (of this page)	21. No. of Pages	22. Price*
Unclassified	Unclassified		

* For sale by the National Technical Information Service, Springfield, Virginia 22161

TABLE OF CONTENTS

TABLE OF CONTENTS (Continued)

LIST OF FIGURES AND TABLES

LIST OF FIGURES AND TABLES (Continued)

LIST OF FIGURES AND TABLES (Continued)

SECTION 1

INTRODUCTION AND SUMMARY

1.1 Motivation for this Study

Lift augmentation of jet aircraft using deflected jet streams results in noise sources being generated by the process of flow interaction with the lifting surfaces. The upper surface blown flap, a propulsive lift concept derived from the long-known Coanda effect, is currently of interest due to its relative simplicity and potential for achieving high turning angles and high propulsive lift efficiencies. The upper surface blowing (USB) concept has been studied extensively in the last few years to achieve an improved understanding of both aerodynamic and acoustic characteristics. The acoustic studies have revealed a potentially serious noise problem of both community impact and cabin interior noise levels. This problem is a high level of low frequency noise during powered lift modes of flight. Additionally, the levels in the high frequency part of USB-radiated sound spectra, that part which dominates the currently accepted measure of aircraft community noise impact - perceived noise level, are several dB above the levels needed to achieve noise goals for future aircraft.

Thus, the noise from the USB propulsive lift system must be reduced over a wide range of frequencies. Noise due to propulsive lift devices must be reduced at the source, since the sources occur over a large portion of the lifting surface and are not amenable to conventional muffling. The sources may be reduced by gross configuration variations such as exit velocity reductions, nozzle aspect ratio changes and nozzle location, flap chord length, and turning radii. However, aerodynamic and airframe integration studies carried out on model and full scale flight aircraft (e.g., Boeing-USAF YC-14 AMST) have shown that the available range of variations of these gross parameters is quite limited when one is faced with achieving a particular powered lift thrust/weight ratio, cruise performance, etc. Thus, consideration of flap modifications as a means of achieving necessary noise reduction has become necessary.

The variable impedance (porous) edge concept is a promising means for reducing flow/surface interaction noise arising at the trailing edge of airfoils or lift-augmenting flaps. The porous or variable impedance edge reduces noise generation by making the trailing edge surface "impedance discontinuity" gradual instead of abrupt, as would be the case for rigid surfaces,

thus allowing a gradual acceleration of the flow by the otherwise non-radiating turbulent eddies. Reduced unsteady flow acceleration (fluctuating forces) results in reduced sound radiation. There are also some effects of porous surfaces on unsteady parts of the flow field, which could reduce the basic "forcing function" of the sound source. At present, the relative effects of porous edges as "impedance matchers" and "turbulence reducers" are not established. However, several edge configurations have been tested which show that substantial broadband noise reduction can be achieved, and that aerodynamic performance can be retained. There is a need to optimize the noise reduction and aerodynamic effectiveness of a turning flap for a USB configuration before large-scale applications are undertaken.

Several studies of the variable impedance edge concept have been conducted to date which indicate the promise of the concept. Bolt Beranek and Newman Inc. (BBN) has conducted "in-house" research which led to a patent on the concept (Hayden and Chanaud, 1973, 1974), BBN performed a NASA Langley-funded study on the application of the concept to under-the-wing externally blown flap (EBF) systems (Hayden *et al*, 1972a), and a preliminary study of an upper surface blown configuration was also conducted by BBN for NASA Langley Research Center (Hayden *et al*, 1972b). NASA has conducted some in-house studies on a USB configuration, using porous trailing edge configurations. All studies showed some noise reduction, but the amount of noise reduction varied significantly between studies. The reasons for the variations are believed to be (1) incomplete identification and treatment of all noise-producing regions, (2) too large or too small an impedance discontinuity (i.e., materials and design factors), and (3) non-representative test environment (i.e., reverberant space instead of free field).

In a NASA Langley Research Center-sponsored study of techniques to reduce community noise from USB configurations (Hayden *et al*, 1972b), BBN achieved a substantial noise reduction in the hemisphere *below the wing* over a wide frequency range. Correlation techniques were used to locate all important source regions of the flap and two types of treatment applied (Fig. 1) - a simple porous insert, and one with a backing which formed a cavity below the porous surface. Noise reductions were substantial, as shown in Fig. 2. Since no evaluation of aerodynamic performance was made, the potential of this concept for reducing noise on flightworthy aircraft remained uncertain.

More recently, Bohn (1975) carried out a series of tests on undeflected wall jets which showed noise reductions of the same magnitude as the early studies, but with a strong dependence on the details of the backing cavity.

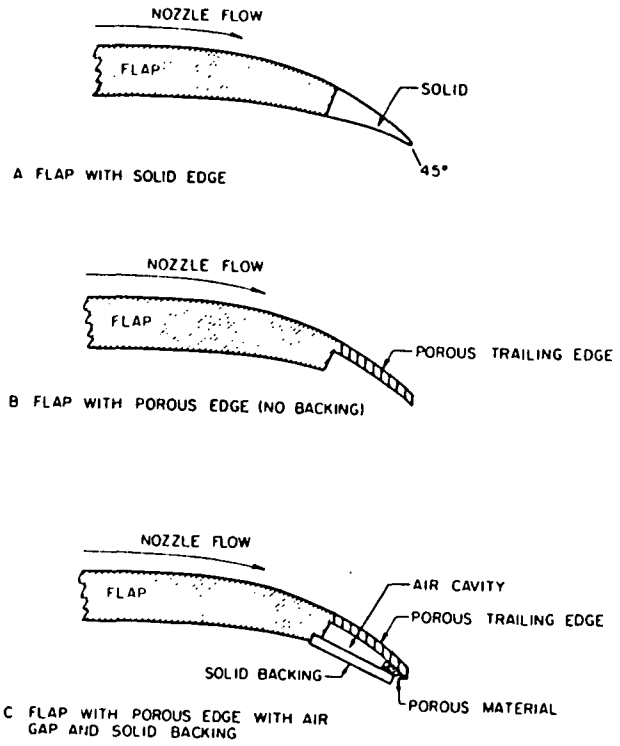

FIG. 1. VARIABLE IMPEDANCE EDGE CONFIGURATIONS (From Hayden, 1972b; also 1973).

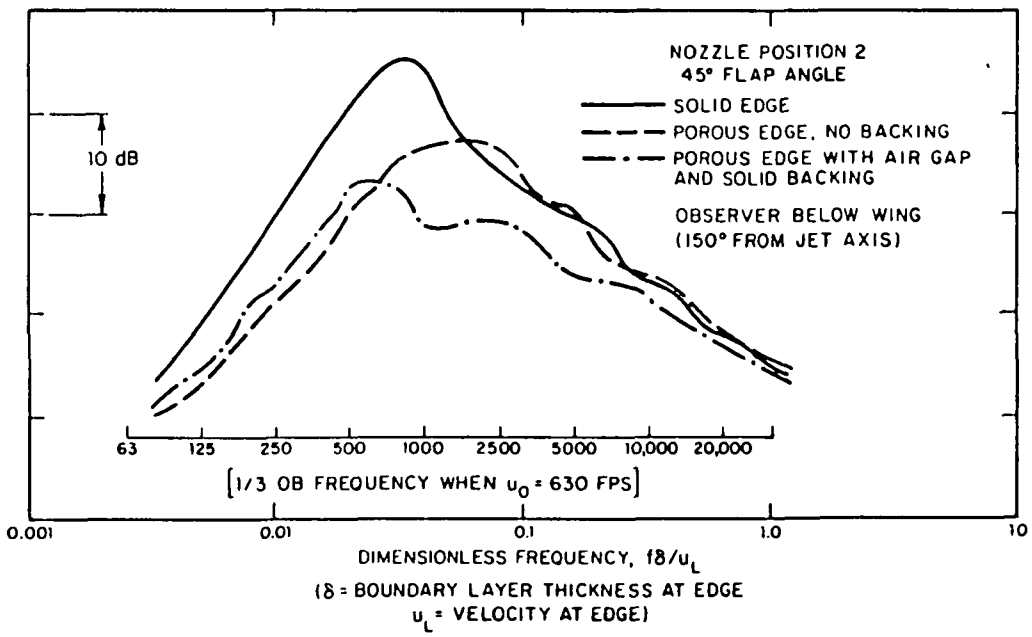

FIG. 2. NOISE REDUCTION ACHIEVED WITH TWO POROUS TRAILING EDGE CONFIGURATIONS (*Ibid*).

The objectives of this study were to obtain a data base on the acoustic and aerodynamic characteristics of a known upper surface blown aircraft configuration with and without a variable impedance (porous) edge flap, and to explore the means of optimization of noise reduction for such configurations by considering which parts and the extent of the flap to be treated, materials, and various designs that may be employed.

The approach to the optimization of the aeroacoustics of a USB flap with porous trailing edge involves first establishing a datum (i.e., noise and aerodynamic performance of a realistic, unmodified flap system), then reproducing earlier results from the smaller scale studies (described above), and finally proceeding with a systematic evaluation of alternate edge configurations.

1.2 Summary of Results from this Study

A part span 1/5 scale model of the NASA Langley Aero Commander USB research aircraft was reproduced and fitted with a removable flap for this study (Fig. 3). This model was chosen since considerable aerodynamic optimization had previously been done, and thus results of this study could be compared with reliable existing data. A 60° flap setting was chosen as a severe test of the ability of porous flaps to achieve acceptable amounts of turning while maintaining desired noise reduction. The model was fitted with various combinations of nozzle deflectors, inboard flow forces, and spanwise flap extensions. All detailed tests on porous flaps were conducted on a configuration consisting of:

- 4:1 AR nozzle with deflector,
- 60° turning flap setting,
- 60° outboard flap setting,
- inboard flow force.

All results quoted are for this configuration unless otherwise noted. Exploratory tests showed comparable static turning performance and efficiency with previous NASA results (Phelps, 1975).

Several fiber metal flap materials were initially investigated, all of which produced significant far field noise reductions over a wide frequency range in exploratory tests. The material which ultimately was selected for continued testing was a steel-screen-reinforced fiber metal having a flow resistance

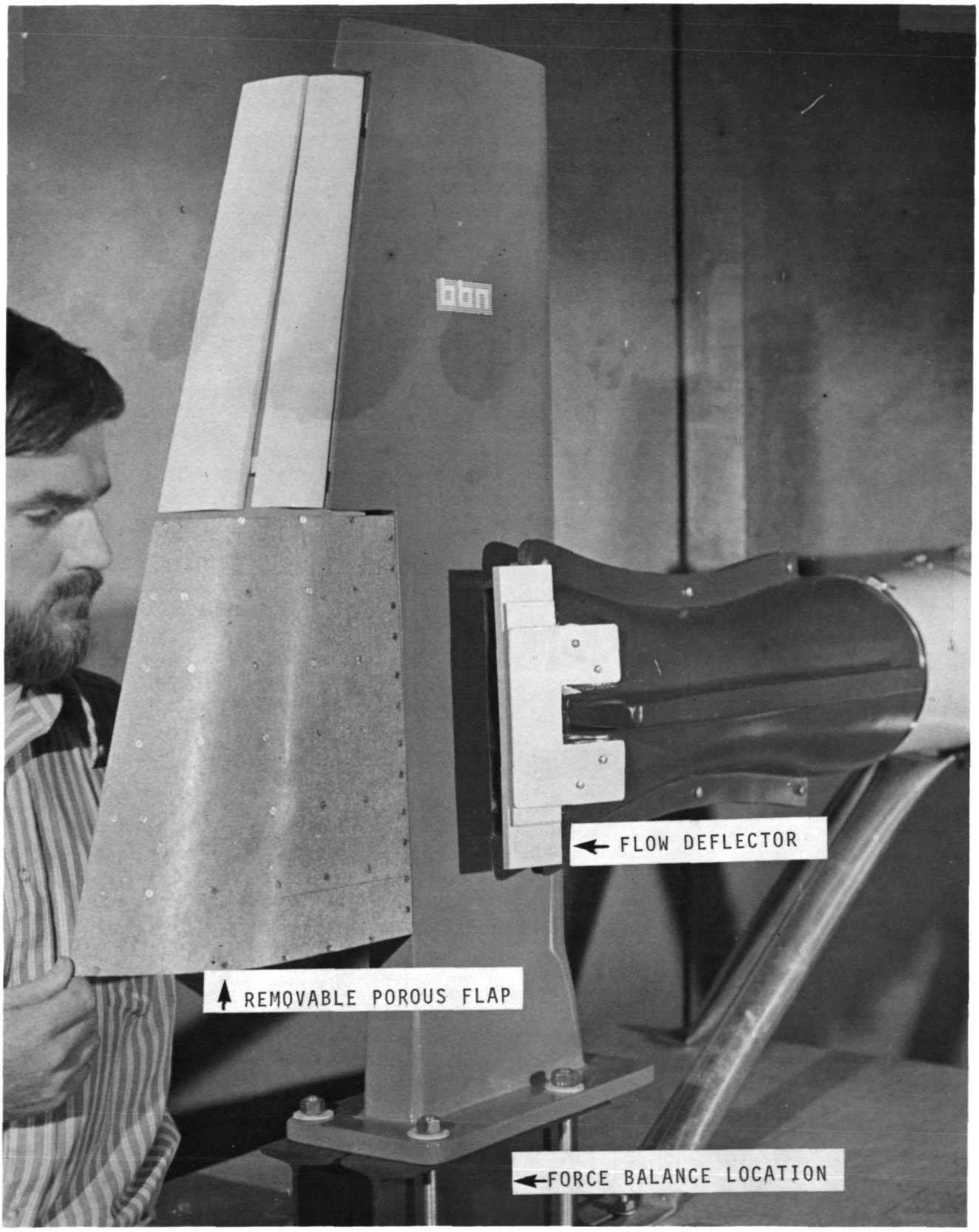

FIG. 3. USB-AERO COMMANDER POROUS FLAP MODEL.

(impedance) of about 0.8 ρc (ρc = acoustic impedance of air), and a tensile strength of about 1.4×10^8 N/m^2 (20 ksi). Other materials had too little flow resistance or deformed under high aerodynamic loads. Mounting techniques, backing configuration, and amount of area treated were varied.

The results of the far field acoustic comparisons with the baseline solid flap configuration showed broadband noise reductions of 3-10 dB at all flyover observation angles and at a sideline position. Typical results are shown in Fig. 4. Fuselage pressure fluctuations were reduced by comparable amounts indicating a potential for lowering interior noise levels by treating the source.

Aerodynamic tests showed that most configurations had comparable turning performance to the baseline flap at low exhaust speeds, and many had comparable turning angle and efficiency at the highest speed tested. Some of the configurations treated over a large portion of the flap experienced flow separation before reaching the design nozzle pressure ratio of 1.265. The static turning performance of all configurations is summarized in Fig. 5.

1.3 Conclusions

The results of this study have indicated that a variable impedance (porous) flap concept can produce significant reductions of far field and interior noise while maintaining good aerodynamic performance. Further reductions appear possible by more detailed optimization studies. A severe flap angle was tested in this study; lower flap angles typical of takeoff settings should be tested. However, it would appear that similar noise reduction can be achieved for lower flap settings, also without aerodynamic penalties.

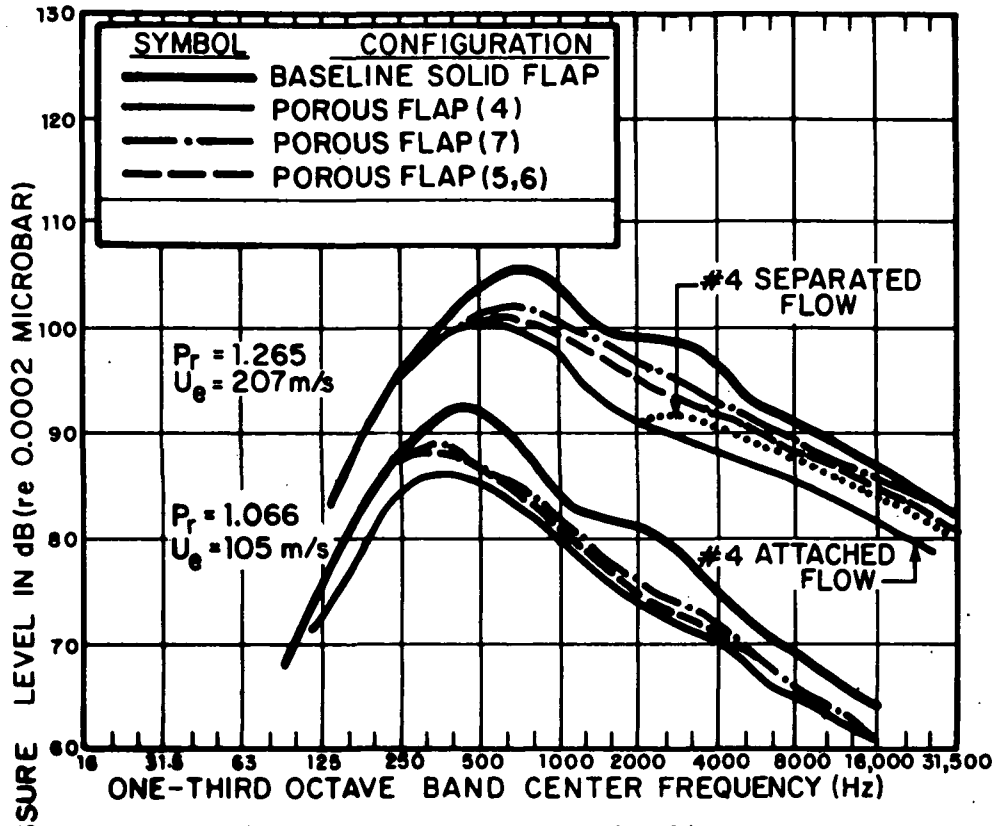

(a) Flyover Position (90°).

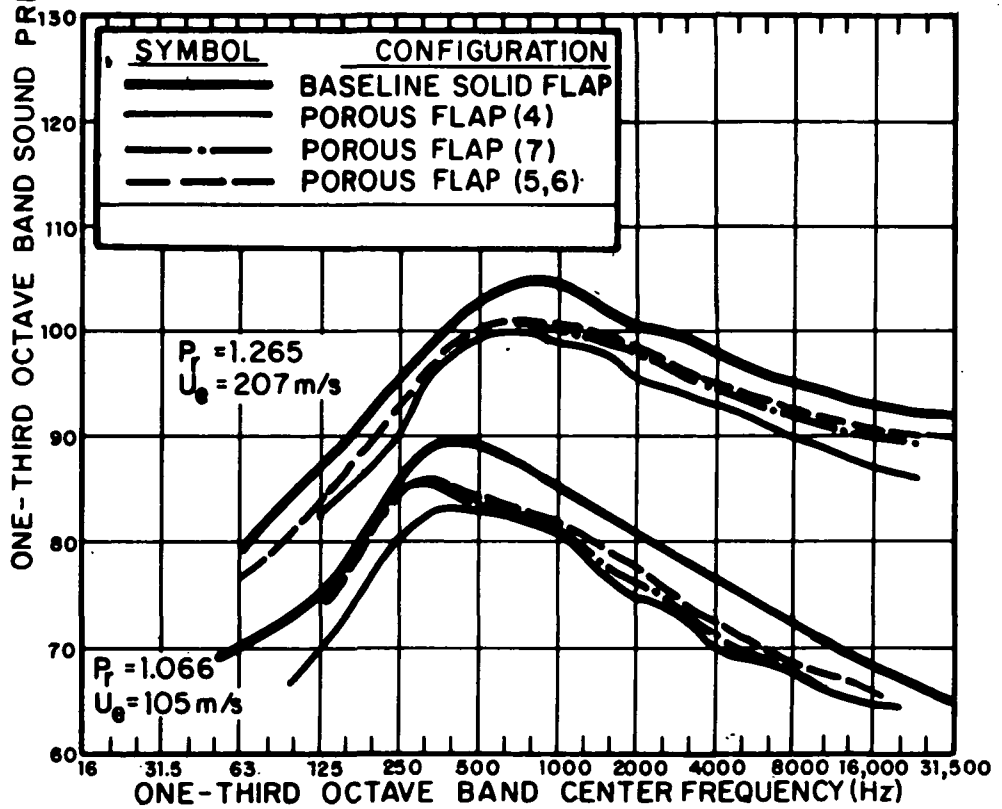

(b) Sideline Position.

FIG. 4. TYPICAL NOISE REDUCTION WITH VARIOUS POROUS FLAP CONFIGURATIONS.

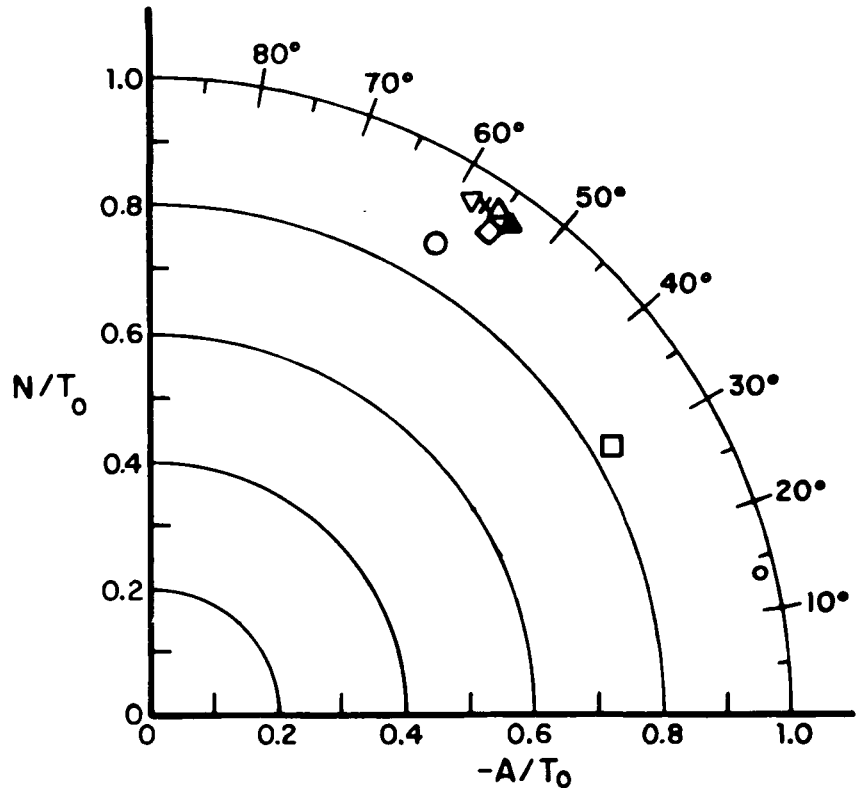

SYMBOL	CONFIGURATION
△	0 AND 1
□	2
○	3
◇	4
▽	5
x	6
▲	7 (BEFORE STALL)

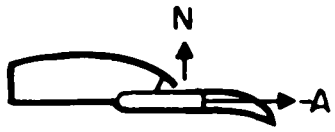

NOTE:
T_0 = CALIBRATION THRUST OF NOZZLE, WITH DEFLECTOR AND WITH FLAP REMOVED.

FIG. 5. SUMMARY OF STATIC TURNING PERFORMANCE OF SEVERAL POROUS FLAP USB CONFIGURATIONS.

SECTION 2

MODEL AND FACILITY LAYOUT

2.1 Description of Model

2.1.1 Configuration selection

The basic purpose of the current study is to establish the feasibility of the variable impedance edge concept for USB systems from both an aerodynamic and acoustic standpoint. Reasonable noise reduction must be achieved while maintaining good aerodynamic performance. Considerable aerodynamic experience with USB systems has been gained over the past few years. At the time of this study, the NASA Langley Aero Commander USB research aircraft was the only operational USB aircraft for which both model and full scale aerodynamic and noise data had been taken. It is presently anticipated that this aircraft configuration will be studied further with improved cruise nozzles, and flap modifications, both for static and forward flight situations. Due to the extensive data base on this configuration, and the considerable NASA experience with this aircraft, it was decided that the present study would be well served by duplicating the nozzle/flap configuration of the Aero Commander USB research aircraft. This would allow direct comparison of the variable impedance flap model tests with past and future tests of the NASA model.

2.1.2 Model geometry

Figure 6 shows three views of the NASA Langley Aero Commander model (from Phelps, 1975); the wing segment modeled for the present static tests is shown by a heavy outline. Pertinent dimensions are listed below, referenced to the original model.

Root chord, cm (in.) 50.80 (20.00)

Sweep of quarter-chord line, deg 3.5

Dihedral, deg 5

Incidence of root chord, deg 3

Airfoil sections ..... NACA 23012

Trailing-edge high-lift devices:

Vane:

Span, cm (in.) 65.53 (25.80)

Root chord at side of fuselage, cm (in.) .. 8.64 (3.40)

Tip chord, cm (in.) 5.97 (2.35)

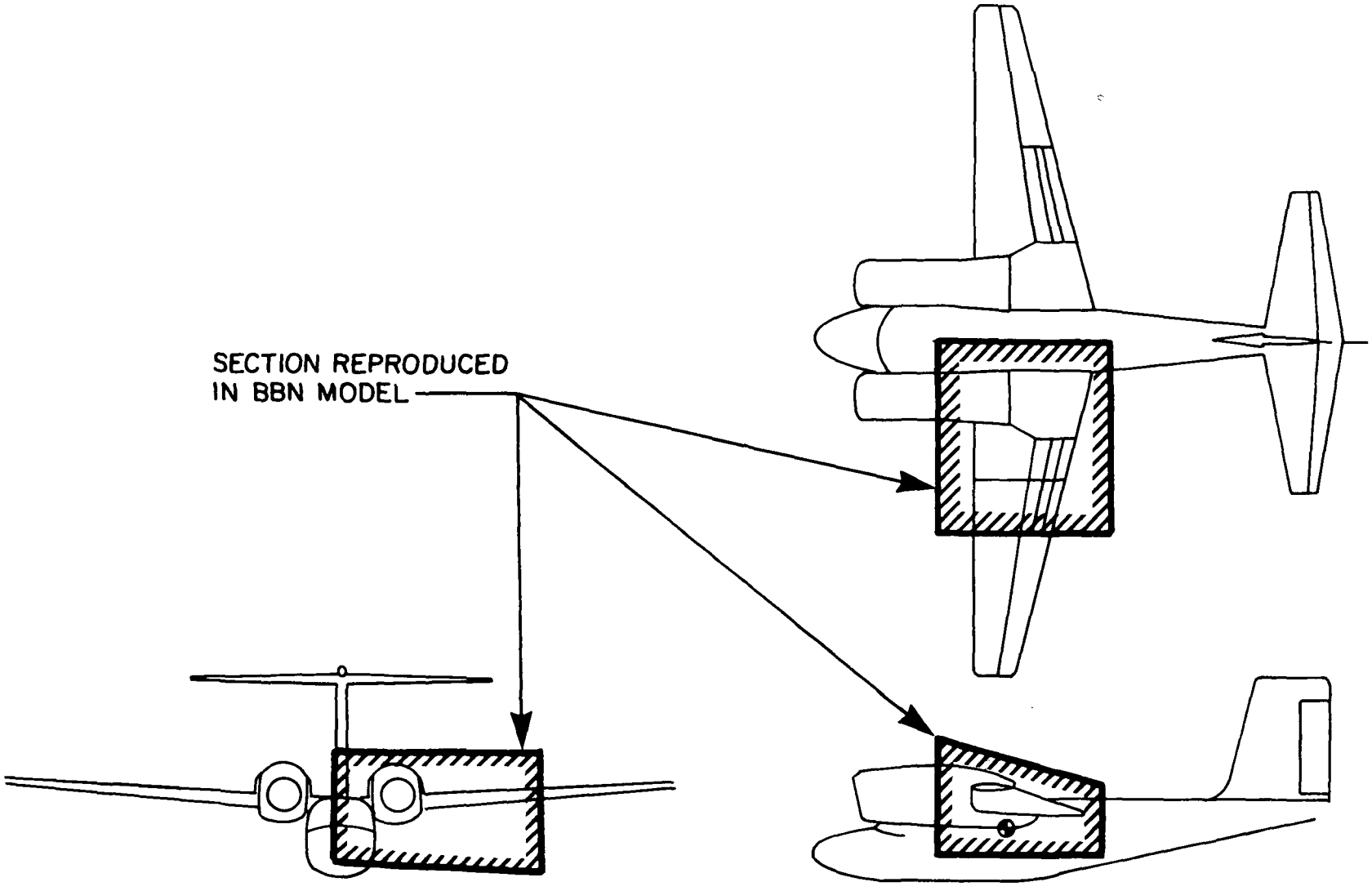

FIG. 6. DRAWINGS OF MODEL USED IN NASA INVESTIGATION. (All linear dimensions are in centimeters [inches]).

Flap:

Span, cm (in.) 65.53 (25.80)

Root chord at side of fuselage, cm (in.) .. 8.36 (3.29)

Tip chord, cm (in.) 5.84 (2.30)

Spanwise station, cm (in.) 22.81 (8.98)

Chordwise position of nozzle esit, percent wing chord . 35.0

Nozzle exit aspect ratio, width/height 4.0

Figure 7 shows schematically the manner in which the NASA nacelle geometry was modified for this application. The deflector plate on the nozzle is removable. Additional details are given in Fig. 8. The turning flap used by NASA was a solid sheet carefully fitted to a smoothly faired envelope of the fully deployed flaps (see Fig. 7). For the model used in this study, the NASA contours were used but the flaps were replaced by a box structure upon which various materials were mounted. This box also can be segmented to allow different cavity depths to be created behind the porous material, and to isolate various regions of the flap aerodynamically thereby preventing a mean through-flow inside the flap. A centerline section of the box appears in Fig. 8 and a photograph of this box is shown in Fig. 9.

The swept wing used introduces spanwise assymetry in the pressure field on the flap (with respect to the nozzle centerline). This leads to a turning of the flow toward the fuselage, especially in the static case. Phelps (1975) used an inboard flow fence to minimize this effect on the NASA model. Figure 10 shows details of this fence, which was also built for the model investigated in the present study.

2.1.3 Materials and mounting

Wing and flaps were made from solid aluminum, cast from masters made in fiberglass and wood. The nacelle and nozzle are fiberglass, laid up on a male mold of the internal contours. The mounting stand allows for a slight separation of nozzle and wing for force tests. However, to allow comparison with NASA and conventional aerodynamic loads presentations, the nozzle was mounted integrally to the wing, and a force isolation link was placed upstream of the nozzle section. The base (root) of the wing segment is integral with the wing and mounts to a six-degree of freedom force balance. The nozzle is mounted to a force isolated, low acoustic noise air supply duct.

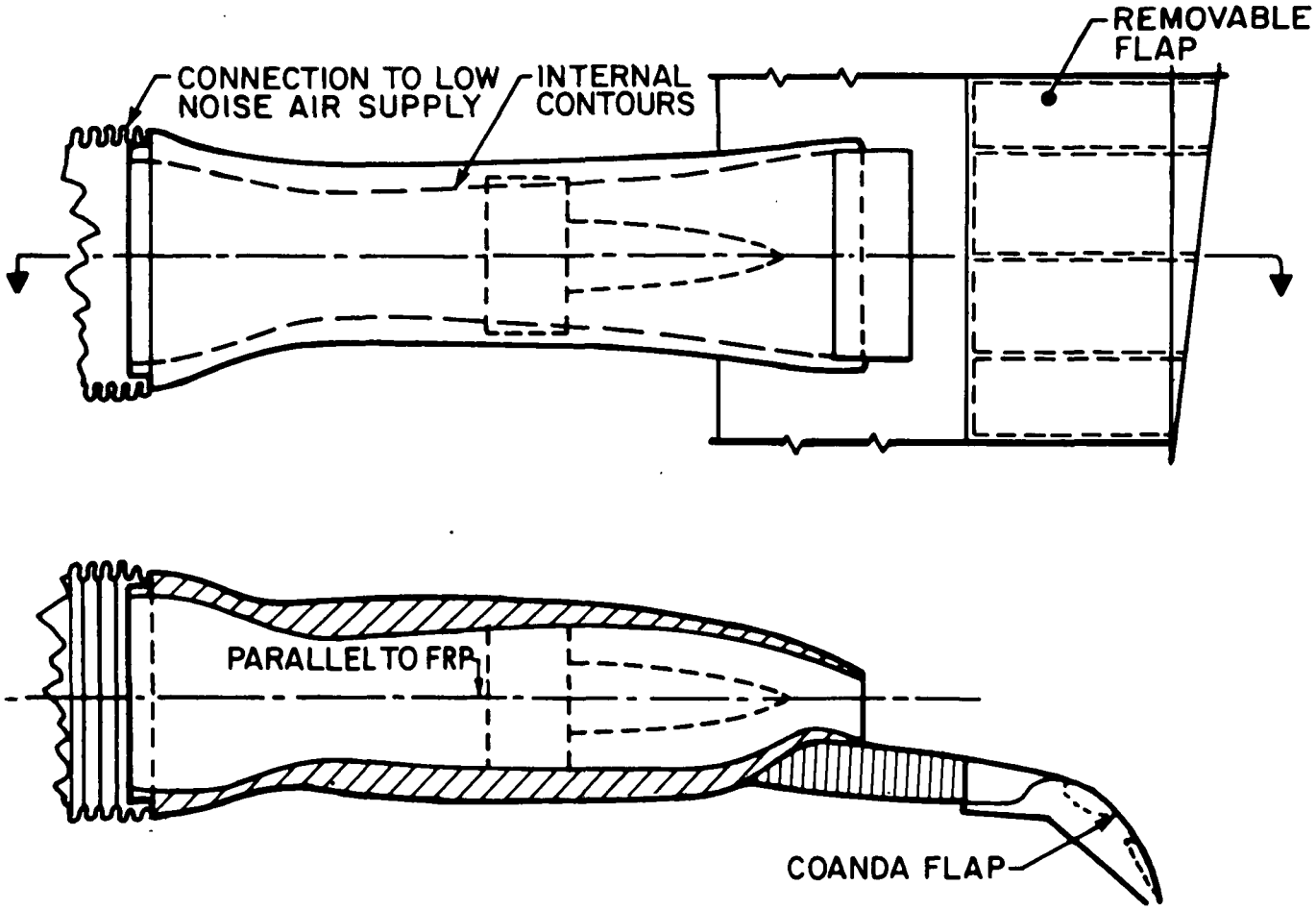

FIG. 7. SECTIONAL VIEWS OF NACELLE AND FLAP CONTOURS.

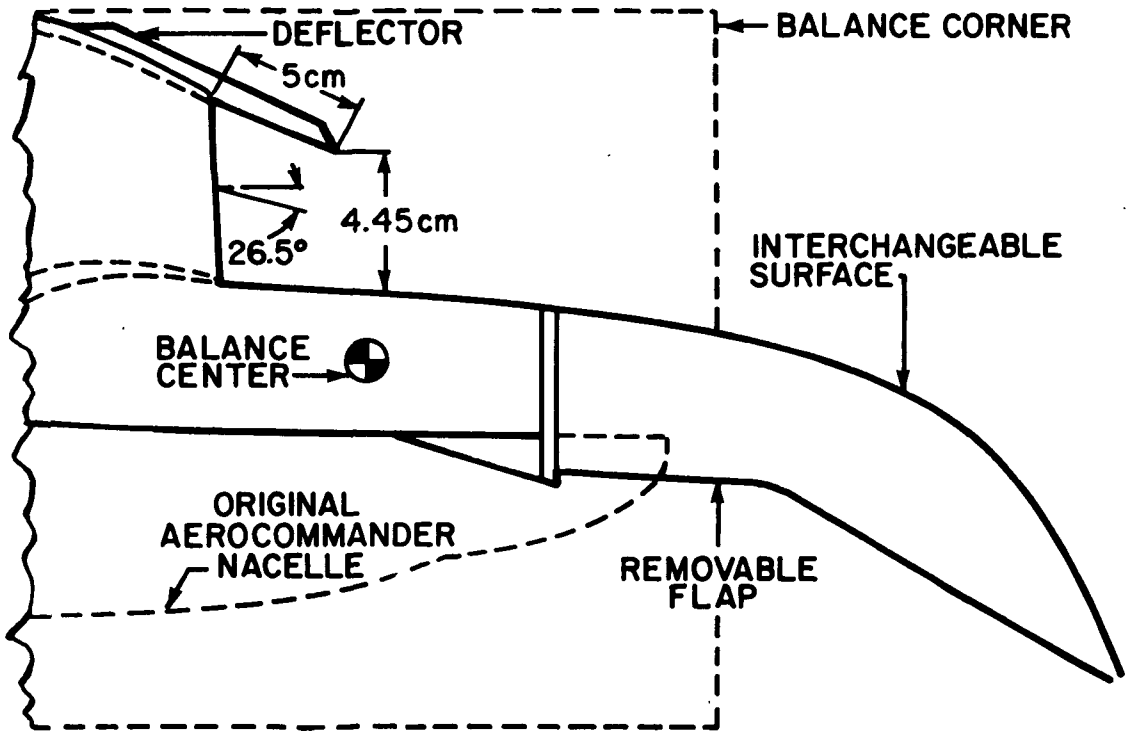

FIG. 8. DETAIL OF NOZZLE AND FLAP ARRANGEMENT, AND FORCE BALANCE LOCATION.

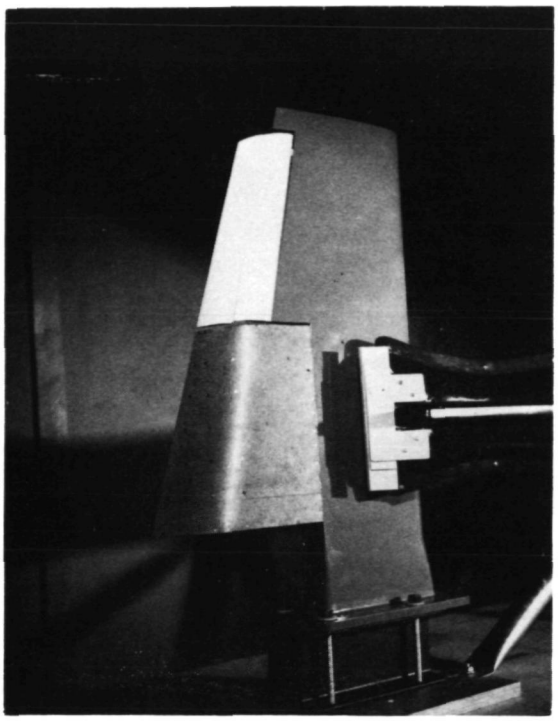

(a) Upper Surface View

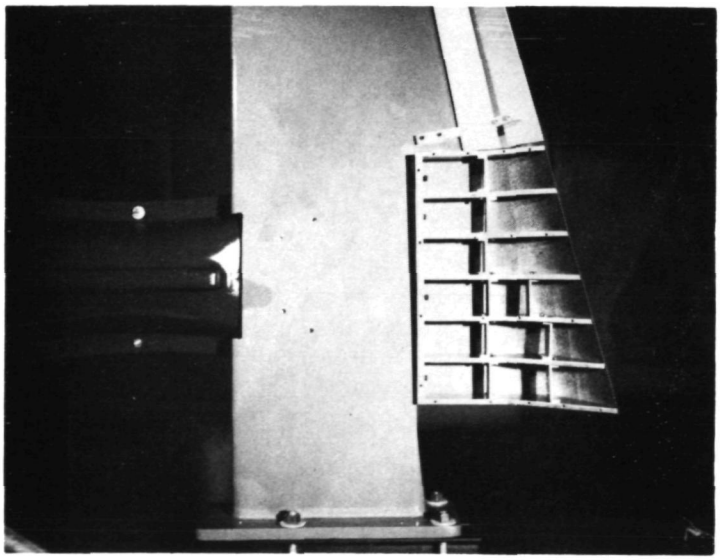

(b) Under the Wing View.

FIG. 9. PHOTOS OF BBN MODEL OF USB WITH REMOVABLE POROUS FLAP.

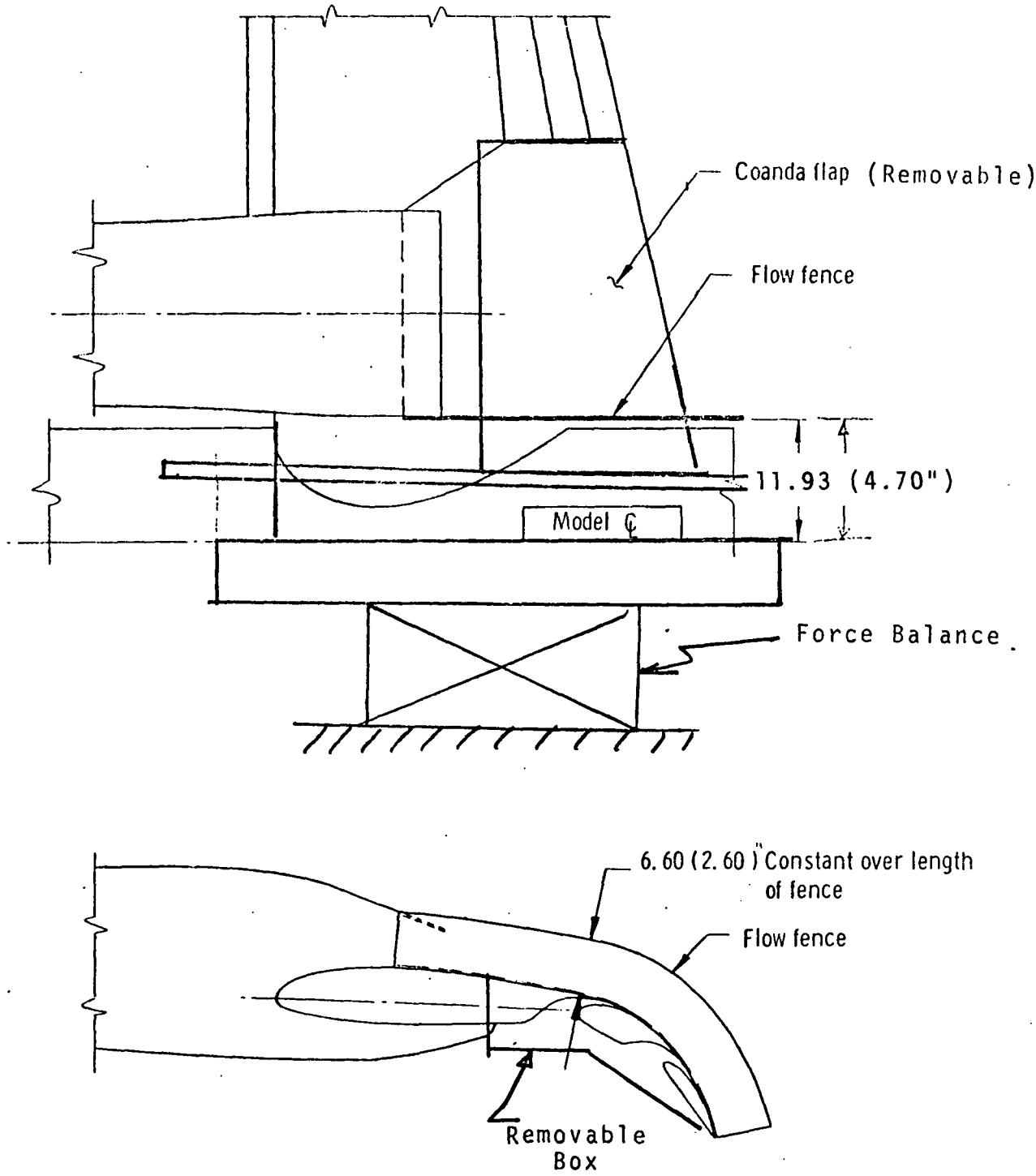

[NOTE: Dimensions in cm (inches in parenthesis).]

FIG. 10. DETAILS OF FLOW FENCE USED FOR ALL DETAILED STATIC TESTS.

The interchangeable flap device is made from aluminum and can be mounted rigidly to the main wing structure. This device is slotted on the mounting plate to permit height adjustments when materials of various thicknesses are used.

The flap materials used were Brunswick fiber metal products, the characteristics of which are discussed in Section 3.

2.1.4 Instrumentation

Flow instrumentation used included nozzle total pressure taps and, for some cases, total pressure rakes for velocity surveys. The wing is mounted on a BBN-built six-degree of freedom force system which measures the net F_T (thrust force), F_N (normal force), and M_Y (pitching moment) on the wing.

In the diagnostic study, an array of BBN Model 376 and 377 dynamic pressure sensors was used in the solid flap. These sensors are correlated with the far field acoustic instrumentation, B&K 1/4-inch microphones.

2.2 Facility Layout and Definition of Coordinates, and Acoustic Measurement Points

The aerodynamic and acoustic measurements were made in the BBN Acoustic Wind Tunnel Facility, which is shown in Fig. 11, operated in an anechoic condition. No forward speed tests were performed in this study.

The far field measurement positions were a constant 2.134 (7.0 ft) radius from the flap trailing edge. The sideline position was 36° below the plane of the wing at approximately 90° from the "engine" inlet axis. The coordinate system is shown in Fig. 12.

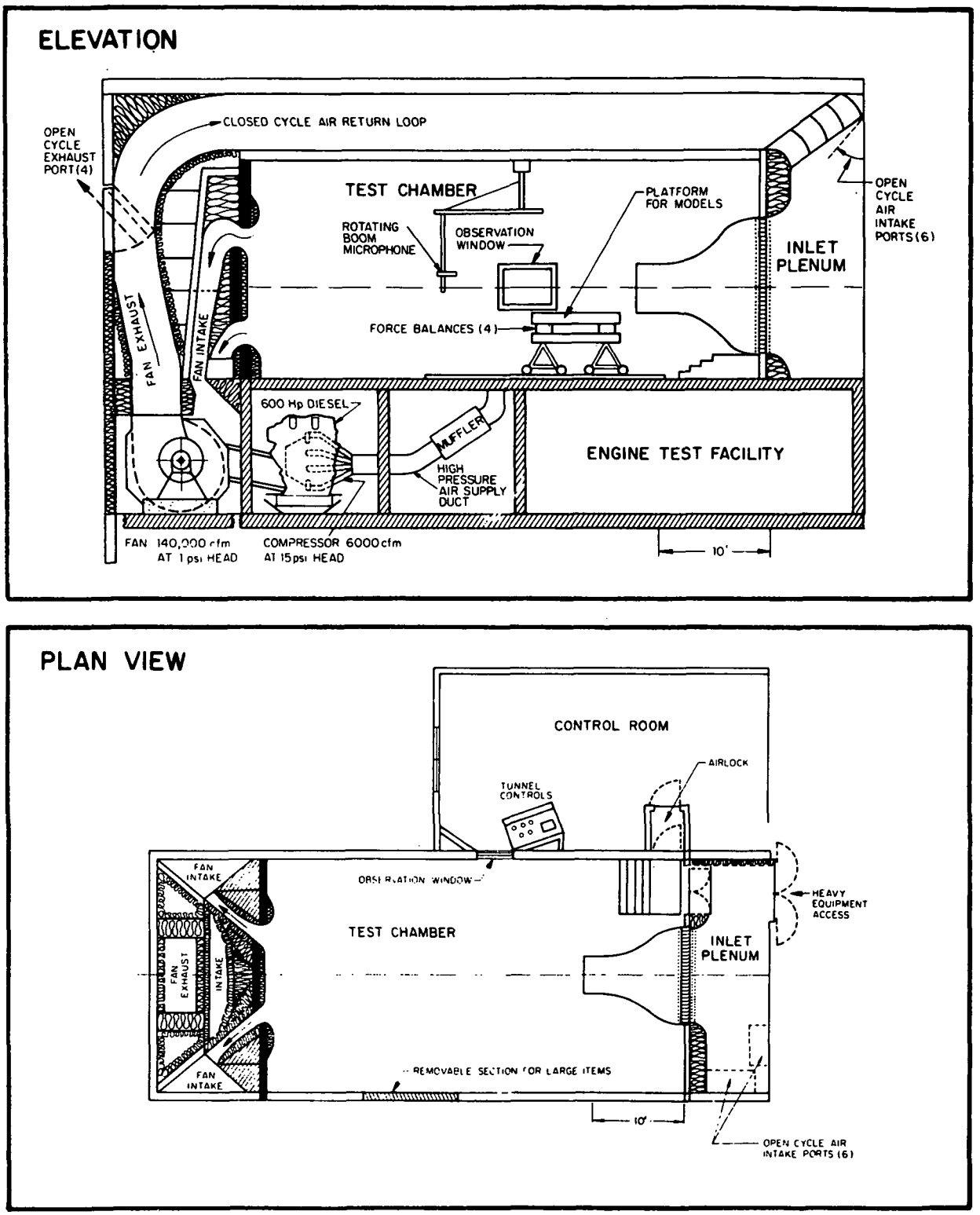

FIG. 11. HIGH-SPEED WIND TUNNEL.

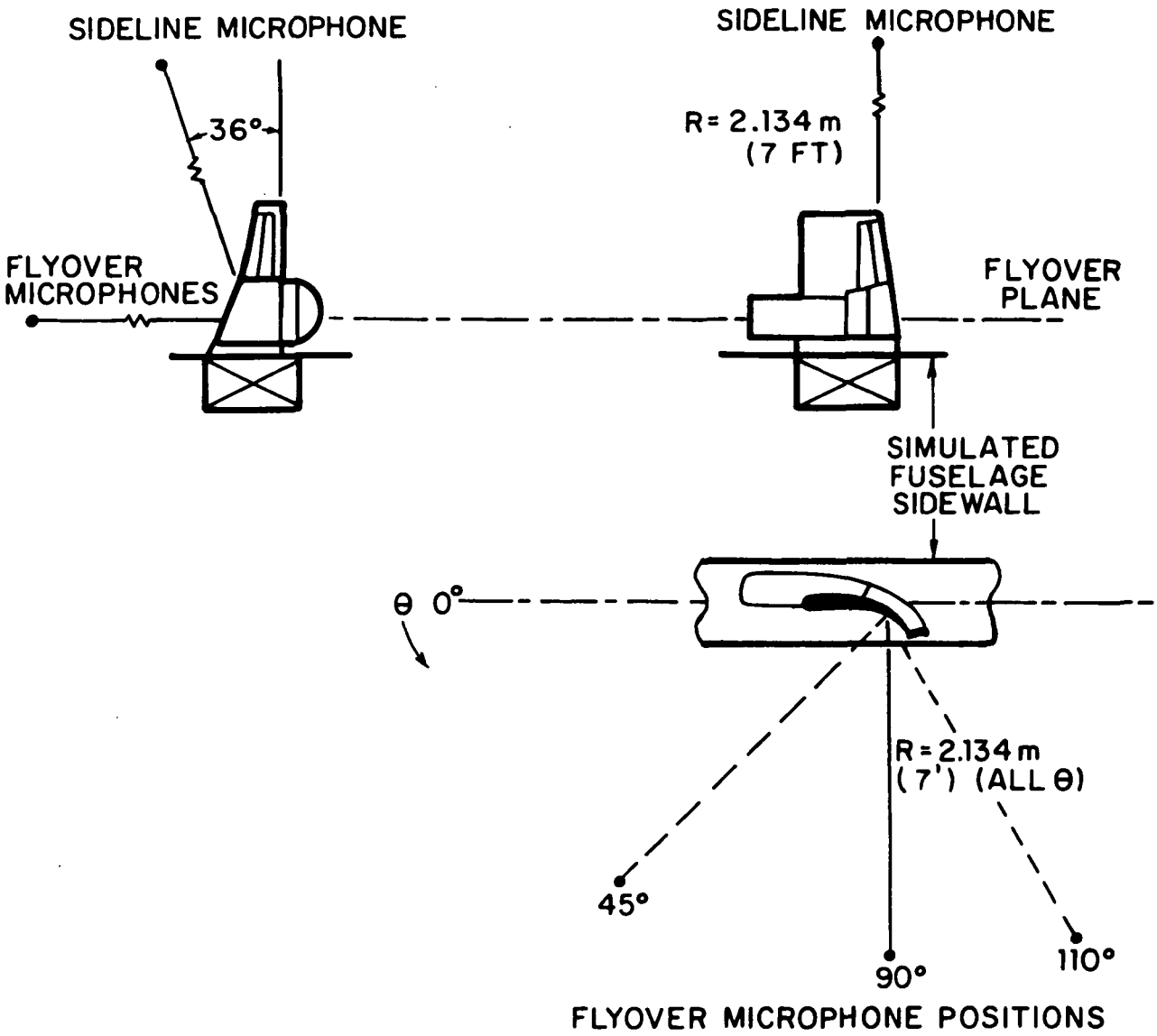

FIG. 12. COORDINATES OF SIDELINE AND FLYOVER MICROPHONE ARRANGEMENT.

SECTION 3

ACOUSTIC CHARACTERISTICS

The sound generation by USB systems has an impact in both the far field and the near field. In the far field, community noise is of concern while in the near field, the acoustic and flow excitation of the fuselage structure creates high interior noise levels and poses structural fatigue problems.

The sound spectra from USB systems exhibit a pronounced low frequency peak which is due to the intense shear layers interacting with the flap surface. This peak may occur at 40-100 Hz in full scale aircraft, and thus will be a distinctive characteristic of USB aircraft in the powered lift mode of operation. The effect of such low frequency noise on community response has not yet been evaluated. However, the effect of such a peak on cabin noise levels can be readily assessed by comparison with conventional jet aircraft. Wilby and Scharton (1974) have shown that for USB aircraft, low frequency noise levels (at frequencies below 200 Hz) will be 10-30 dB above levels in current jet aircraft. Reduction of low frequency cabin noise must be achieved at the source, since the ability of conventional airframe structures to reduce low frequency sound transmission is limited to about 15-25 dB in 1/3 octave bands.

In this study, we examined the effect of porous surfaces on both community noise and interior noise. The ensuing discussion is divided into two major sections, one on far field (community) noise, and one on near field (interior) noise.

3.1 Far-Field Noise

3.1.1 Baseline characteristics of the Aero Commander USB model

The Aero Commander USB has been optimized by NASA to produce high turning angles and high turning efficiencies. To achieve such desirable aerodynamic performance, spreading of the nozzle flow over as much of the span as possible is necessary. Achieving spreading involves a combination of a high aspect ratio nozzle (4:1), a substantial "kickdown" angle of flow impingement on the surface, and, for further improvement, a spreader extension to the nozzle. The basic Aero Commander USB configuration incorporates the 4:1 AR nozzle with a mean kickdown angle of about 25°, while the flow spreader is removable. Also removable is an inboard fence which reduces the tendency toward a net inboard turning of the flow, which results from the "negative" sweep angle of the wing (i.e., in the forward direction).

These flow spreaders and control devices also have an effect on the noise-generating flow parameters (boundary layer thickness at the trailing edge, turbulence intensity scale, and mean shear profiles, wetted span of the trailing edge, and location of maximum fluctuating pressures). Thus, it would be expected that the far field sound spectra could be affected by these configuration variables. Figure 13 (a-c) shows that, in fact, these variations have a considerable effect on the sound field. Figure 13a shows radiated spectra somewhat forward of the wing (θ = 60°) for three nozzle and flow fence configurations for a typical takeoff flap setting (60°). The baseline configuration is the kicked 4:1 AR nozzle without inboard fence or deflector. Addition of an inboard fence impedes the spanwise flow and actually increases acoustic levels in frequency bands near the Strouhal peak. The further addition of a deflector extension to the nozzle causes greater spanwise flow spreading in the outboard direction and a greater spanwise extent of well-attached flow at the trailing edge. The acoustic consequences shown in Fig. 13a are to reduce the characteristic low frequency peak and increase the levels in higher frequency bands. Figure 13b shows the same comparison of configuration effects at a position directly below the wing (θ = 90°); the same trends in the spectra as were seen at θ = 60° for configuration changes are seen at θ = 90°. Figure 13c shows the same comparisons of configuration effects at an azimuthal position (θ = 110°) nearly aligned with the deflected flap angle. The acoustic effects at the peak show a strong effect of the nozzle spreader, but little effect of the fence. At higher frequencies, the spectral level variations are not a strong function of configuration. At all observation angles under the wing, the low frequency peak is the greatest when the deflector is off and the inboard fence is on, while the levels in high frequency regime are the greatest for the aerodynamically-optimized system (which has the lowest level at the Strouhal number of the spectral peak).

For a given configuration, the levels do not vary rapidly with azimuthal position, as is shown in Fig. 14. The directivity pattern exhibits the characteristic null in the direction of the resultant flow turning angle.

For the evaluation of noise reduction potential porous surface treatments, the optimized configuration was chosen as the baseline. The change in sound radiation will be compared with the sound radiation from this baseline configuration at various observation angles at a nozzle pressure ratio of 1.235, which gives an exit velocity of 207 m/s (680 fps). This pressure ratio falls in the range currently being considered for new-generation

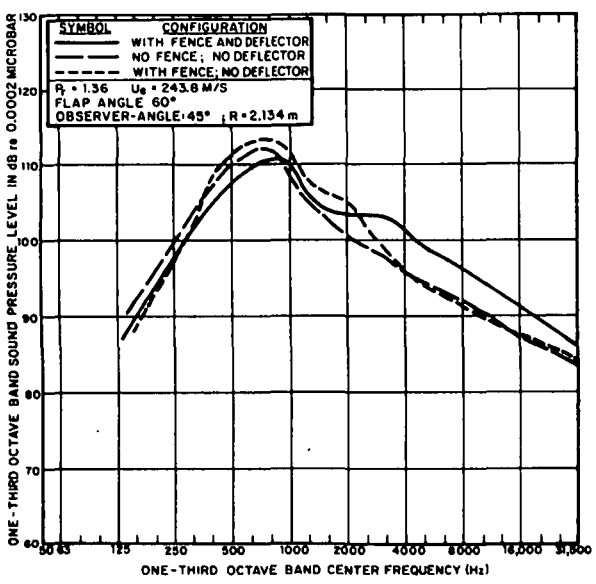

(a) Flyover; θ = 45°.

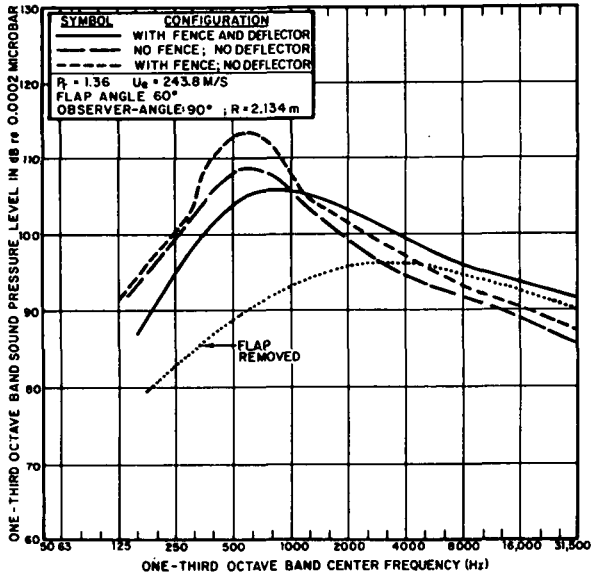

(b) Flyover; θ = 90°.

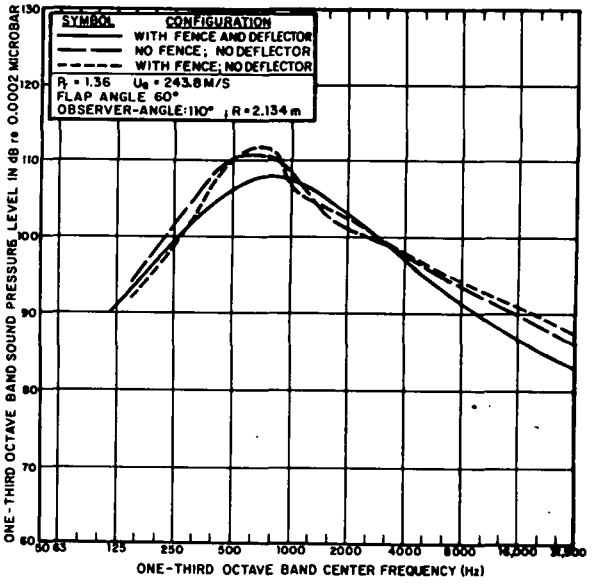

(c) Flyover; θ = 110°.

FIG. 13. FARFIELD ACOUSTIC CHARACTERISTICS OF USB SYSTEM WITH NOZZLE AND FENCE VARIATIONS.

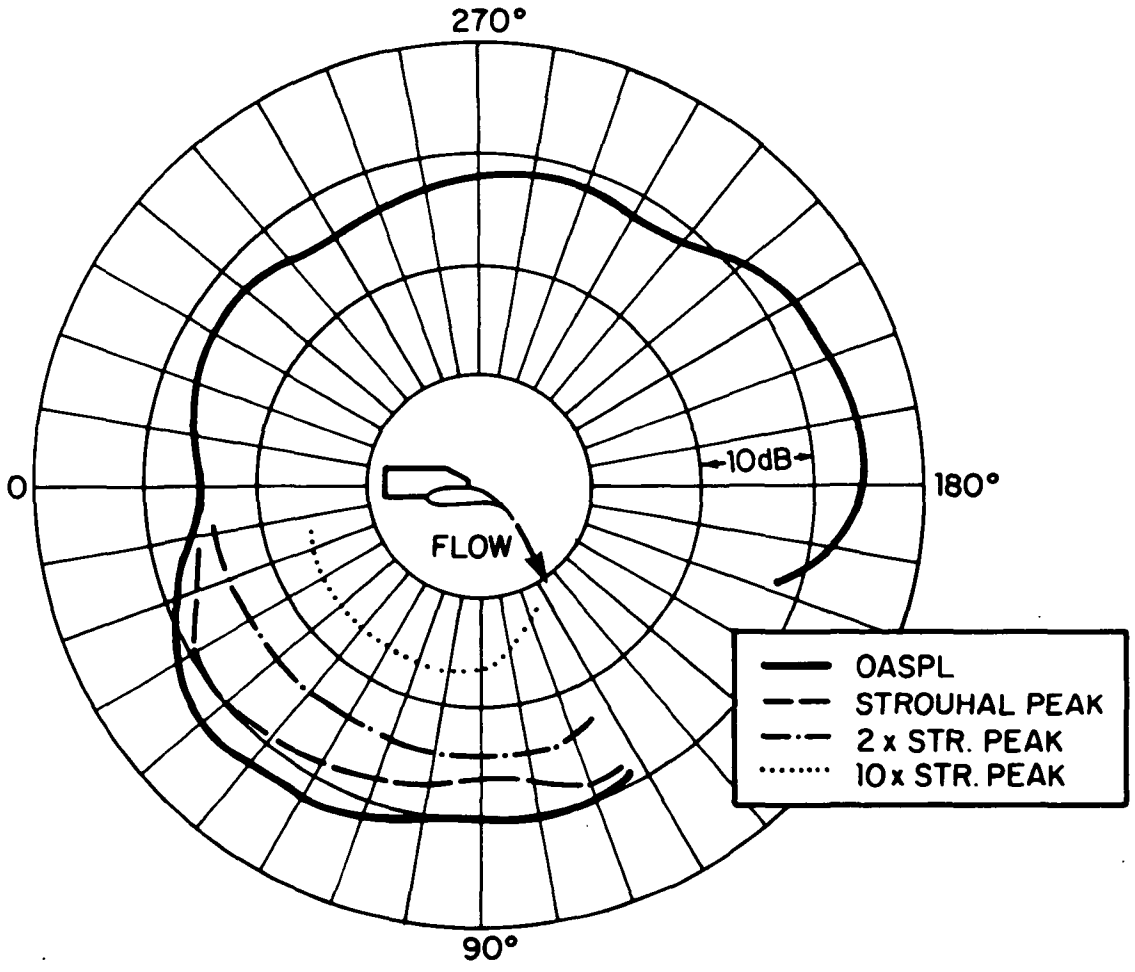

FIG. 14. TYPICAL DIRECTIVITY IN FLYOVER PLANE; (60° Flap with Deflector and Fence).

engines for quiet propulsive lift aircraft. As is discussed in more detail later, some of the flap configurations were unable to maintain high lift performance up to this pressure, so noise reductions were evaluated at lower exhaust speeds. This led to some interesting observations regarding scaling of the acoustic spectra which are briefly summarized below.

It is now well-established that propulsive lift systems may have a number of inter-related flow and acoustic phenomena occurring simultaneously. For instance, the large scale turbulence in the attached wall jet shear layer creates a "whole body" dipole mechanism. Since the wavelength of the sound is comparable to the wing chord, this dipole may not radiate as efficiently as a point dipole force fluctuation source, whose wavelength is much longer than the source dimensions. Thus, the whole body mechanism on the USB, which is inherently associated with the lift concept, may obey a speed scaling relationship of U^4 to U^6 (Hayden *et al*, 1972b; Hayden, 1973).* The attached flow adjacent to the flap surface consists of small scale turbulence which, when encountering the trailing edge regime, creates a line of incoherent, partially-baffled dipole sources. These radiate as U^6 when the source characteristics (intensity and scale) are independent of speed. Finally, the free shear layer, above the flap and in the wake of the flap, produces jet-like mixing noise which radiates as U^8. In the following figures, the results of speed variation tests on the basic solid flap configuration (with spreader and fence) are summarized. On each figure, the noise at the respective observation points measured with the flap removed is given for reference. The flap-removed case may not be dominated by jet noise, since about 20% of the wing chord exists between the jet exit and the point where the flow truly becomes free, as can be seen in Fig. 15. Thus, the "no-flap" noise can include lip noise from the spreader and trailing edge noise from the wing box edge, in addition to mixing noise of the free jet.

Figure 16a shows that at the 45° position, the radiated sound spectra may be decomposed into Strouhal number regimes with radiation at constant Strouhal number varying from U^5 to U^6. At the 90° position, which corresponds to a direct flyover position, this is also the case, except at very high frequencies where some mixing noise contribution becomes evident (Fig. 16b). In both cases, the no-flap noise is well below the "flap-on" noise, except at high Strouhal numbers. It should be noted that the 90° position is 30° off the axis of the turned flow, and thus is the position at which one expects to observe a maximum contribution of mixing noise.

---

*U and V are used interchangeably; both refer to mean velocity of a flow stream.

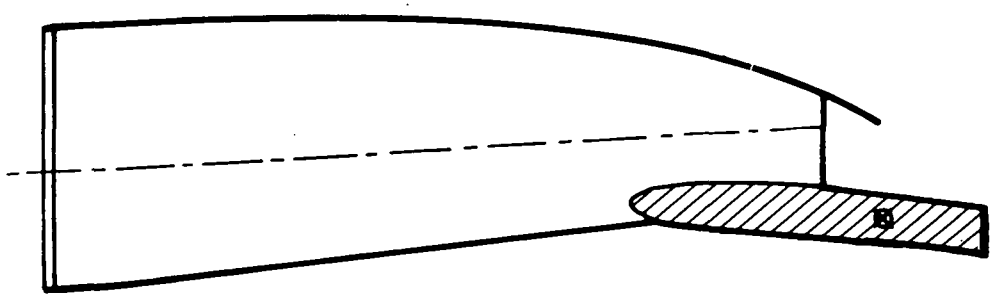

FIG. 15. CONFIGURATION FOR FLAP-REMOVED TESTS.

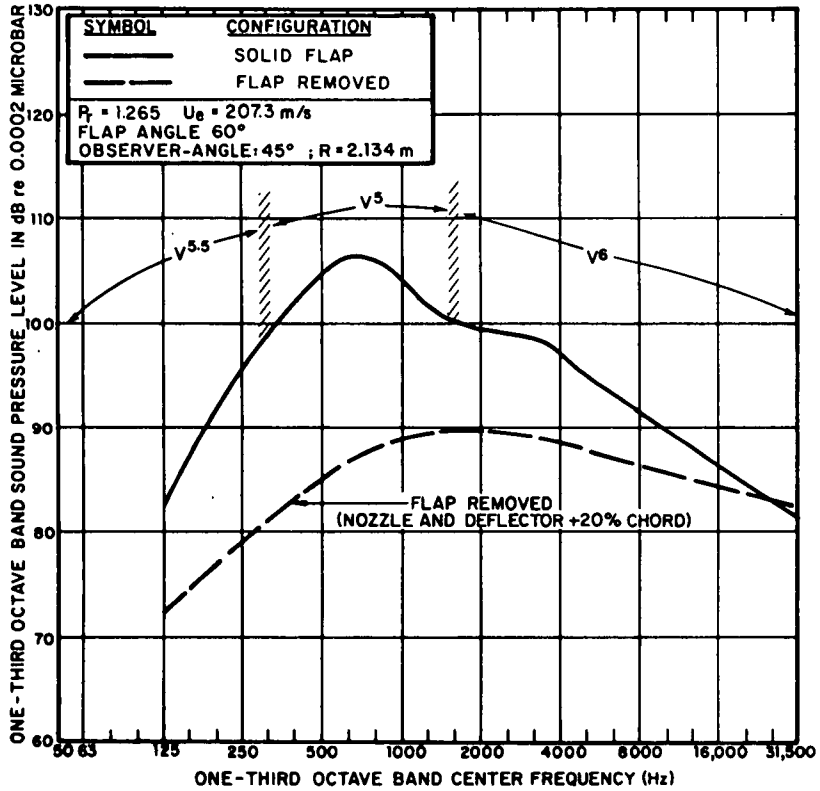

(a) Flyover Position; θ = 45°.

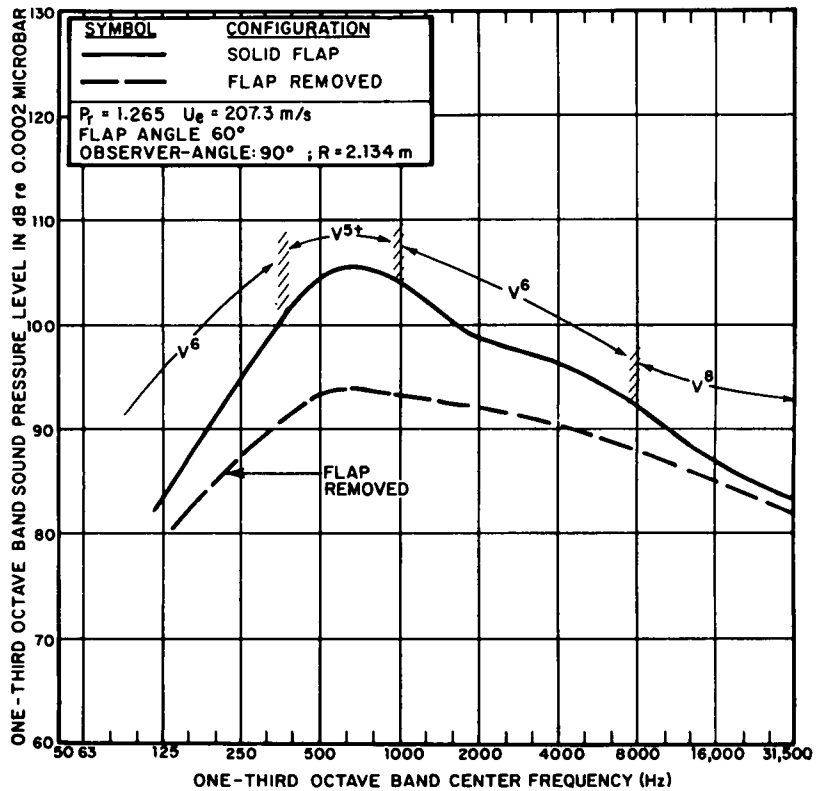

(b) Flyover Position; θ = 90°.

FIG. 16. RESULTS OF VELOCITY SCALING OF FARFIELD NOISE RADIATED BY BASELINE USB CONFIGURATION (Scaled to U_e = 207 m/s).

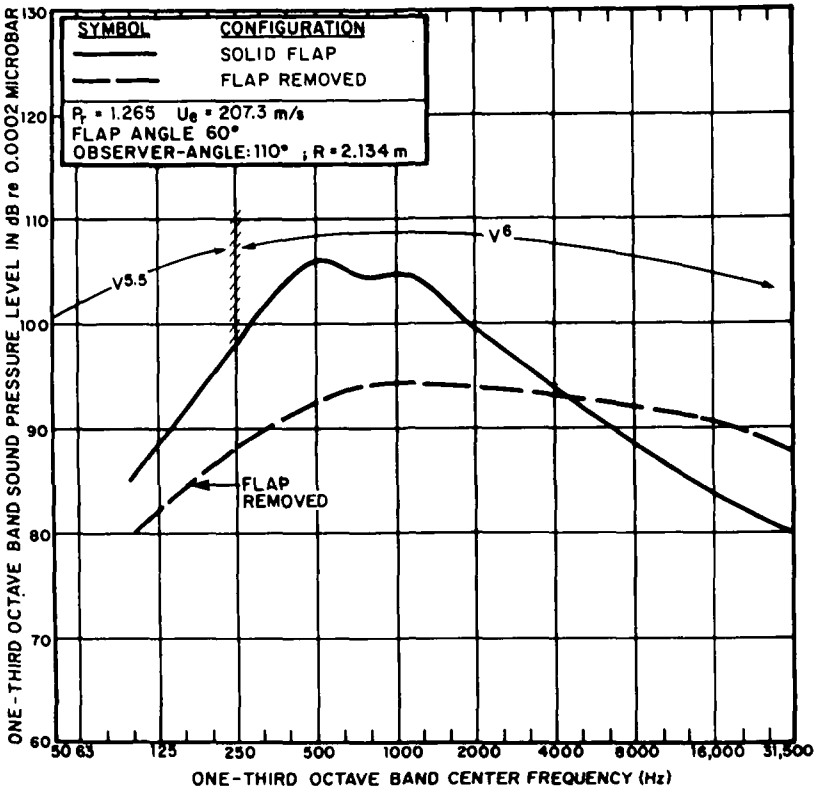

(c) Flyover Position; $\theta \approx 110°$.

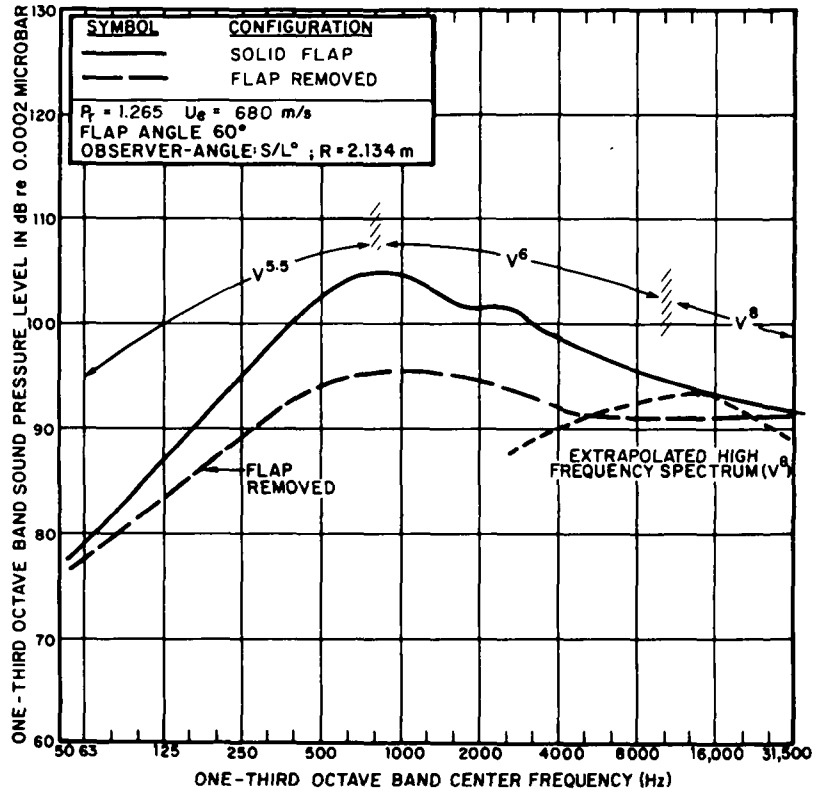

(d) Flyover Position; $\theta \approx 90°$.

FIG. 16. (Continued).

The 110° position is a location which is approximately 10° off the axis of the turned flow. Figure 16c gives the result that the "flap-on" spectra scale nearly as U^6 at all Strouhal numbers. The no-flap case shows substantial high frequency noise. However, when recalling the geometry of the no-flap measurement (Fig. 15), this result is not too surprising since the 110° position corresponds to a 60-70° off-axis location with respect to the unturned jet, and thus is in a region where the jet directivity is near its maximum value.

The sideline noise spectra (Fig. 16d), behave much like the 110° spectra except that a significant mixing noise contribution is found at high frequencies. The sideline spectrum level is similar to that at the 90° position under the wing, except for increased noise levels at high frequencies.

The comparisons of treated flaps with baselines will be made at two exit velocities (nozzle pressure ratios) of 105.2 m/s (345 fps) and 207.3 m/s (680 fps) (P_r = 1.067 and 1.265, since some flap configurations produced good aerodynamics at low speeds but encountered flow separation at higher speeds. Thus, the comparisons at both speeds give an indication of the potential noise reduction for unstalled conditions. Figure 17 gives the baseline far field noise spectra at four representative observation points for an exit velocity of 207.3 m/s (680 fps).

3.2 Noise Reduction Materials and Structures

3.2.1 Materials

A variety of candidate materials is available for use in applications where reduction of edge-generated noise is desired. However, for this particular study, which is an attempt at optimizing noise reduction versus aerodynamic and other considerations, the list of materials shrinks. The materials for application to USB aircraft should satisfy the following general criteria:

- Flow Resistance Range: 0.3 - 1.0 ρc,
  The flow resistance range has been prescribed in Hayden and Chanaud (1973; 1974) for successful application of the concept to any edge configuration. (See Hayden [1976] for further discussion.)
- Spatially-Continuous Porosity of the surface (i.e., no perforated plates),
- Stiffness: No significant deformation under full aerodynamic load,

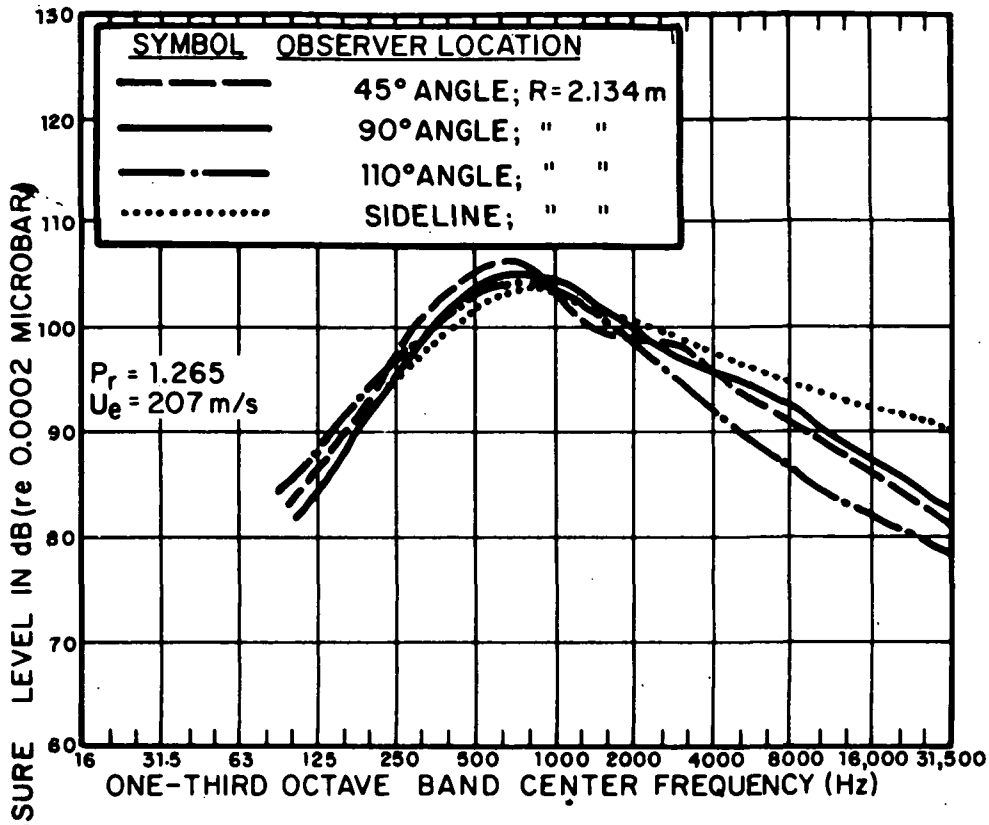

(a) 60° Flap at U_e = 207 m/s.

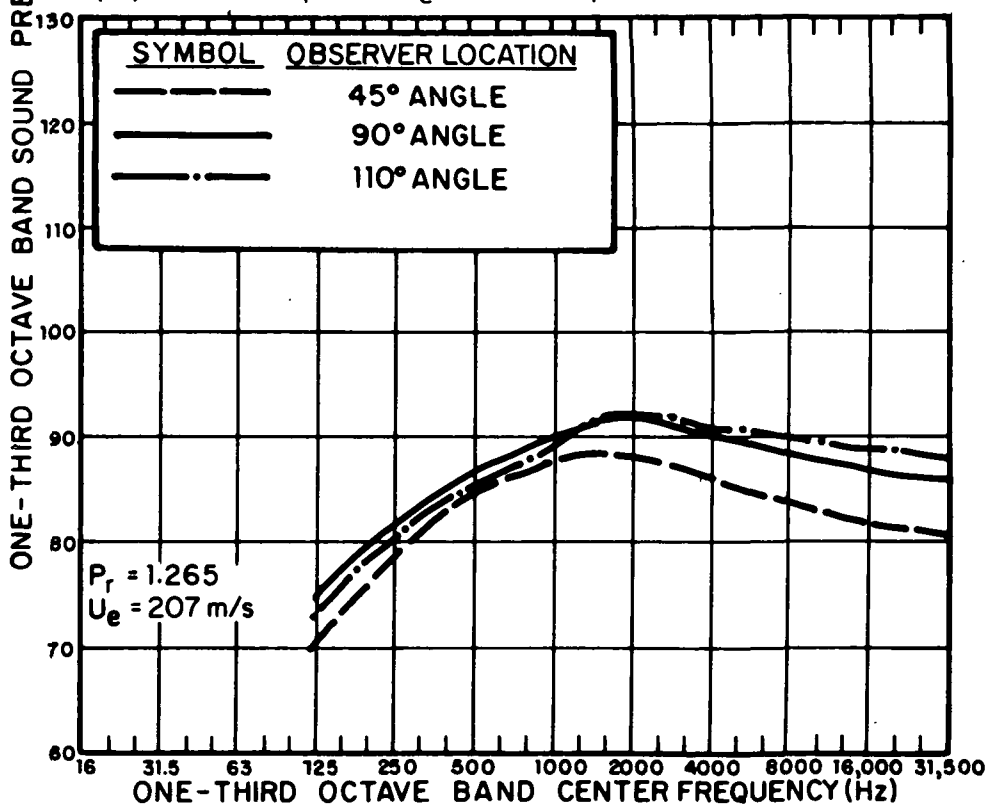

(b) Flap - Removed Case (U_e = 207 m/s).

FIG. 17. SUMMARY OF BASELINE FARFIELD SPECTRA.

- Thickness Range: Comparable to conventional airframe structures (not considered a stringent acoustic requirement).

Based upon the previous study (1972), outlined in Sec. 1, a series of fibermetal products was selected for initial consideration. The properties of these materials as quoted by the manufacturer is given in Table 1; the steady flow resistance of the actual samples used was measured and is also shown in Table 1. The impedance was then evaluated as a function of frequency using standard impedance tube techniques. The procedures, and an a analytical model for converting these data to complex impedance for cavity-backed porous materials is given in Appendix A. The results of the measurements are given in Fig. 18.

The results of these tests led to preliminary survey tests on the porous flap. These acoustic and aerodynamic tests led to the selection of FM 134 material (which is a steel-screen-reinforced fibermetal, consisting of relatively coarse stainless steel metal fibers) for further aeroacoustic optimization studies. As shown in Table 1 and Fig. 18, the impedance of FM 134 is nearly $\rho_0 c_0$ at all frequencies of interest, and the material exhibits a relatively high tensile strength which is needed for this application.

3.2.2 Flap structures

Section 2 described a removable flap section which allows interchangeable flap surfaces and which has compartments which may be sealed, blocked, or filled to vary the spatial distribution of impedance "seen" by the flow on the surface. After diagnostic studies to locate the strongest sound-producing regions as a function of Strouhal number, eight configurations were developed which were tested for noise reduction and aerodynamic performance.

Figures 19a through 19h show these configurations in detail. The configurations are described below, and summarized in Table 2 for later reference. In all cases, the surface material was a single layer of FM 134 Fibermetal. Also, reference to a "closed cavity" means that the lower surface of the cavity is sealed with a rigid backing.

Figure 19a defines the compartments, dimensions, etc. and is the "baseline" configuration (surface solid)
tion "0"

TABLE 1. PROPERTIES OF FIBERMETAL SPECIMENS TESTED.

Mfg's Reference	Steady Flow Resistance θ** (rayls/$\rho_0 c_0$)		Weight kg/m^2 (lbs/ft^2)	Thickness cm (inches) ±20%	Typical Tensile Strength N/m^2 (ksi)
	Mfg's Specs*	Measured			
FM 185	.24	.20	.017 (.40)	.051 (.020) ±20%	1.17×10^8 (17.)
347-10-30 -AC3A-A	.24	.37	.0097 (.23)	.076 (.030) ±20%	4.5×10^7 (6.5)
FM 134	.83	.78	.032 (.77)	.089 (0.35) ±15%	1.38×10^8 (20.)
FM 1307	.21	.25	.044 (1.04)	.318 (.125) ±5%	7.6×10^6 (1.1)

* From Brunswick Bulletin No. M-2004, issued 9/1/72.

** At 3000 SCFH/ft^2; $\rho_0 c_0$ = acoustic resistance of air at standard day conditions = 42 cgs rayls.

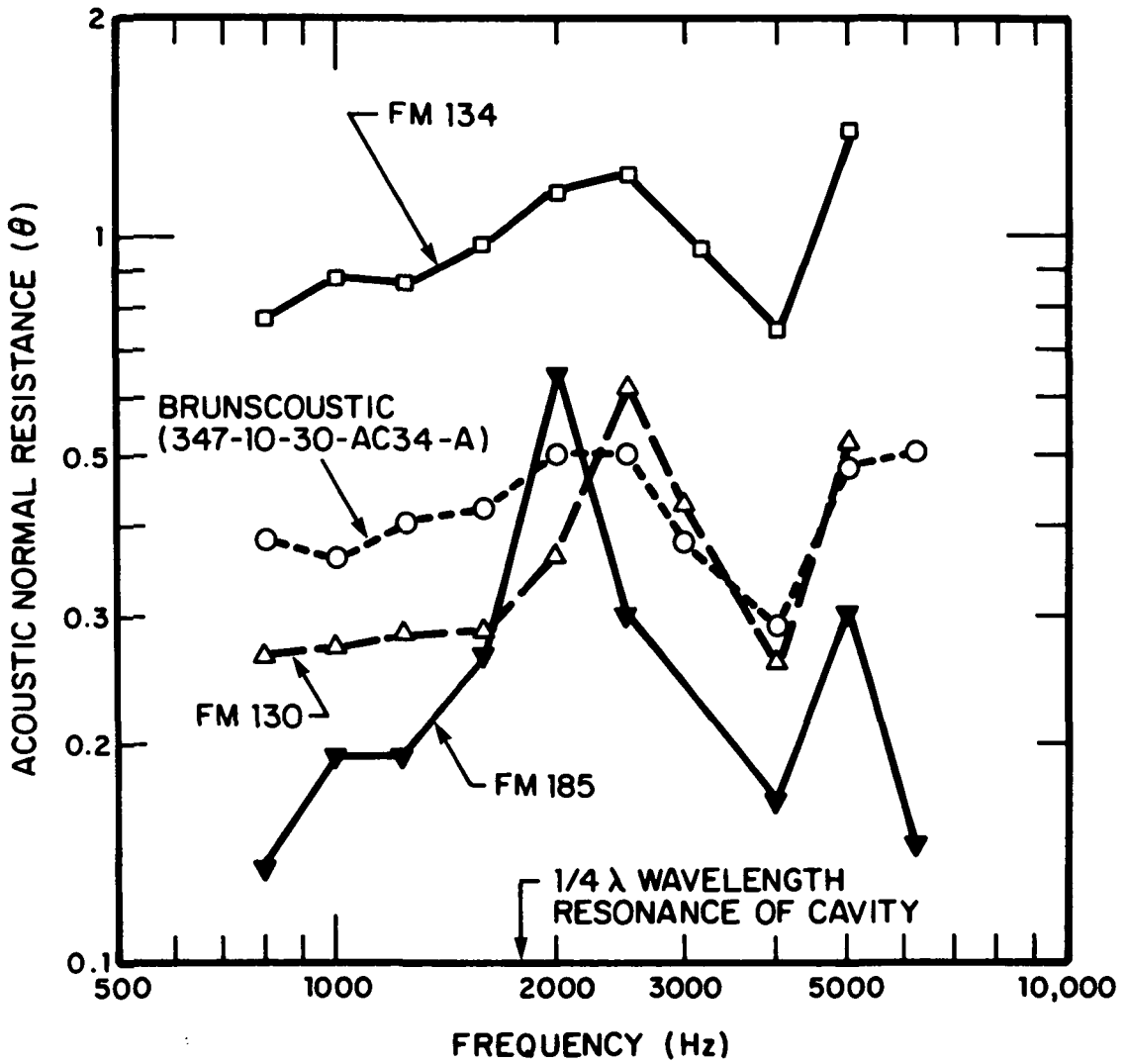

FIG. 18. MEASURED ACOUSTIC RESISTANCE OF SELECTED POROUS SHEETS.

TABLE 2. SUMMARY OF FLAP CONFIGURATIONS TESTED.

Configuration Number	Description	Diagram in Figure No.
0	Baseline Solid Flap	19a
1	Fully Porous Surface; Solid Backing	19b
2	Fully Porous Surface; No Backing	19c
3	Fully Porous Surface; Empty Cavity Backing	19d
4	Fully Porous Surface; Cavities Foam Filled	19e
5	Aft 30% of Flap Porous; Cavities Foam Filled	19f
6	Aft 30% of Flap Porous; Cavities Empty	19g
7	Aft 30% Chord, 60% Span Treated; Cavities Open	19h

The first step in developing a porous flap test matrix was to replace the solid surface with a porous surface and back the porous surface with impervious material. This was done in all compartments, as shown in Fig. 19b. This configuration, called Configuration 1 ("Porous Surface with Solid Backing"), was tested to explore any possible effects of surface roughness in generating high frequency noise, and to see if the non-zero aerodynamic slip condition at the boundary had any effect on the sound generation.

The next step in the sequence was to make the flap fully porous with no cavities and no seals to prevent through-flow. The solid backing behind the porous surface was removed. This configuration, #2, is a "Fully Porous" flap, as shown in Fig. 19c, and constitutes one limiting case - full porosity over the entire flap surface area.

Following the "Fully Porous" configuration is the addition of a solid lower surface to the support structure to form "cavities" beneath the flap surface (Fig. 19d). This configuration

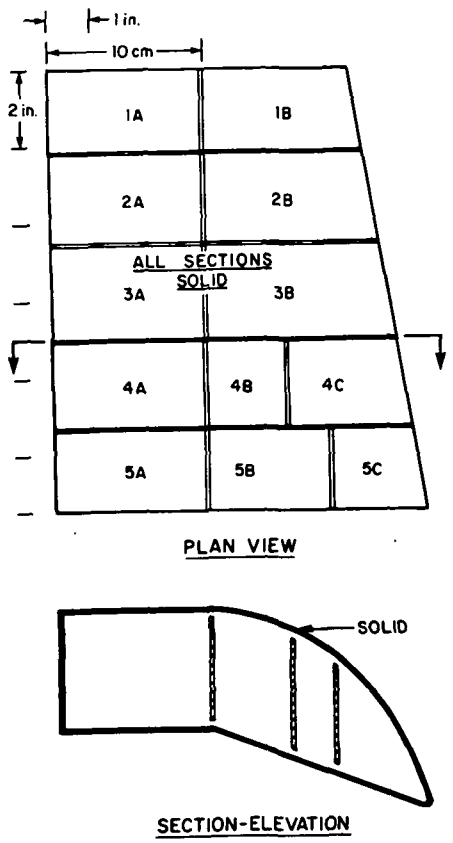

19a. Baseline Solid Flap; (Configuration 0).

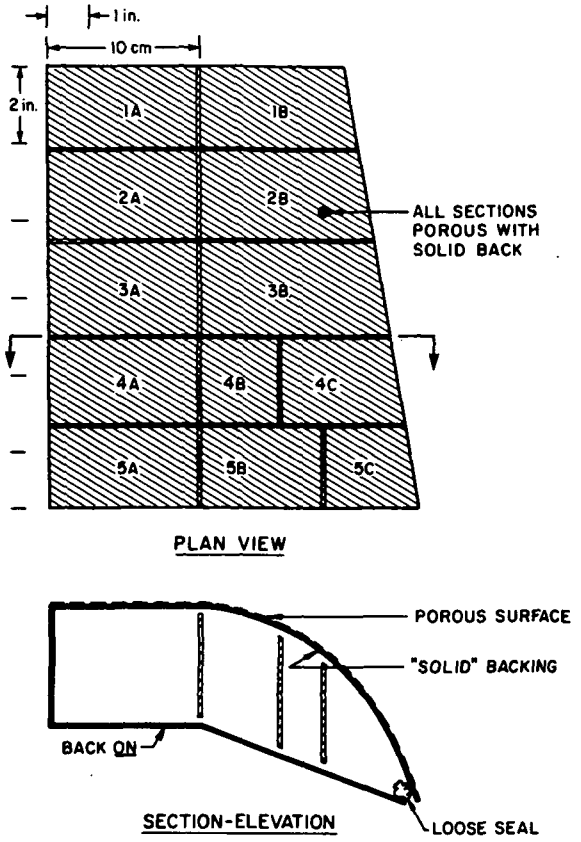

19b. Fully Porous Flap; Solid Backing; (Configuration 1).

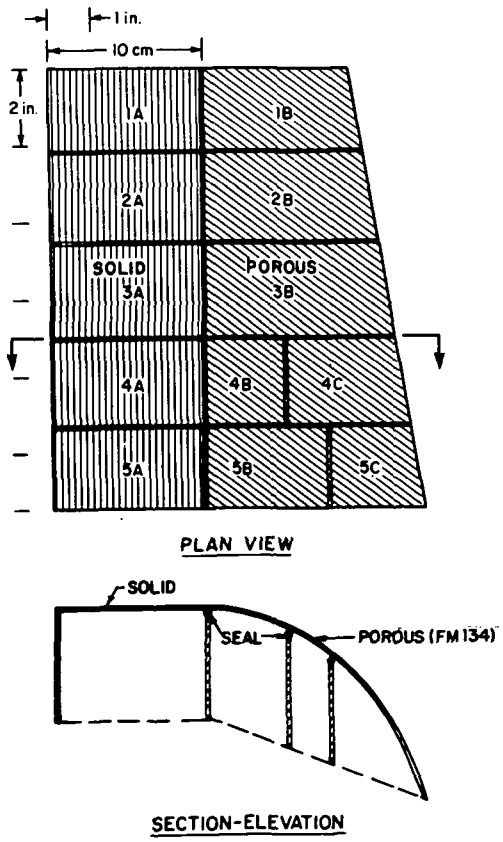

19c. Fully Porous Flap; No Backing; (Configuration 2).

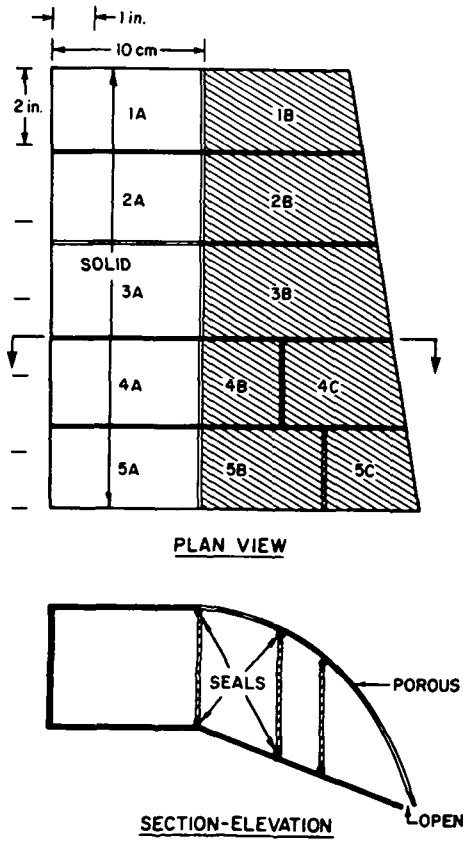

19d. Fully Porous Surface with Cavities; (Configuration 3).

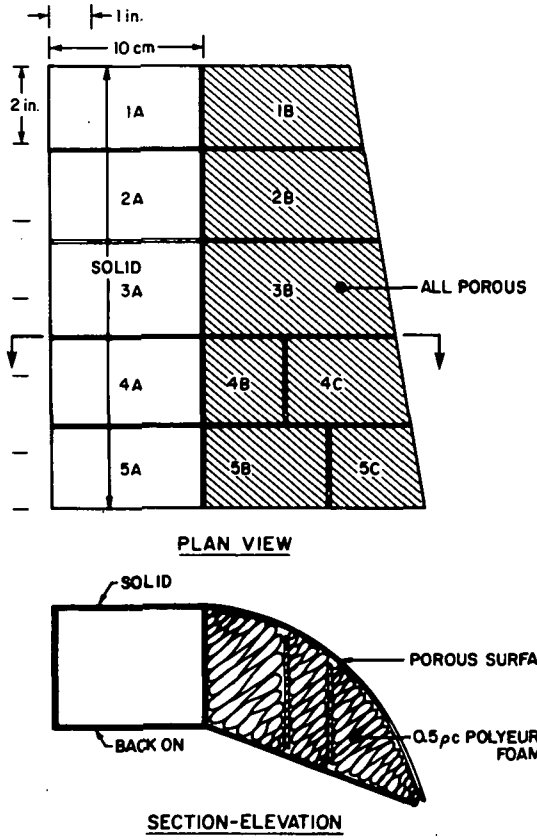

19e. Porous Surface; Cavities Foam Filled (Configuration 4).

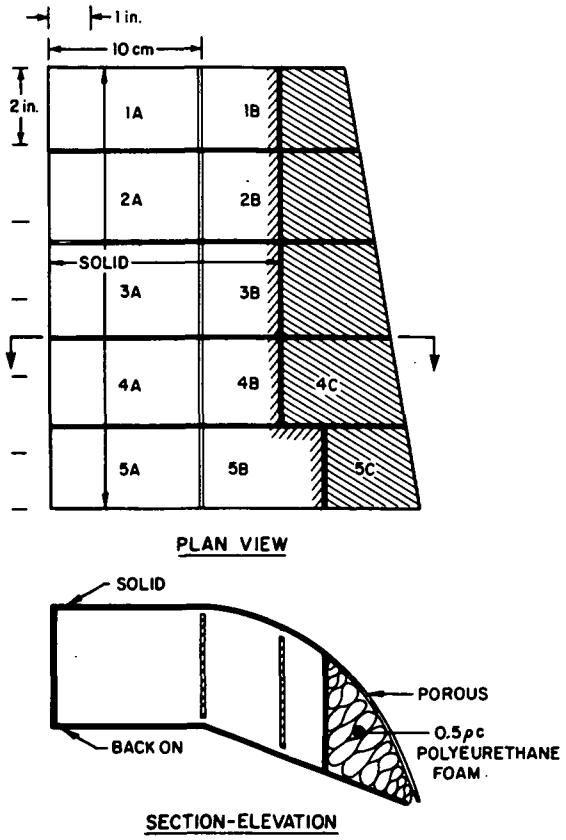

19f. Aft 30% Flap Porous; Cavities Foam Filled (Configuration 5).

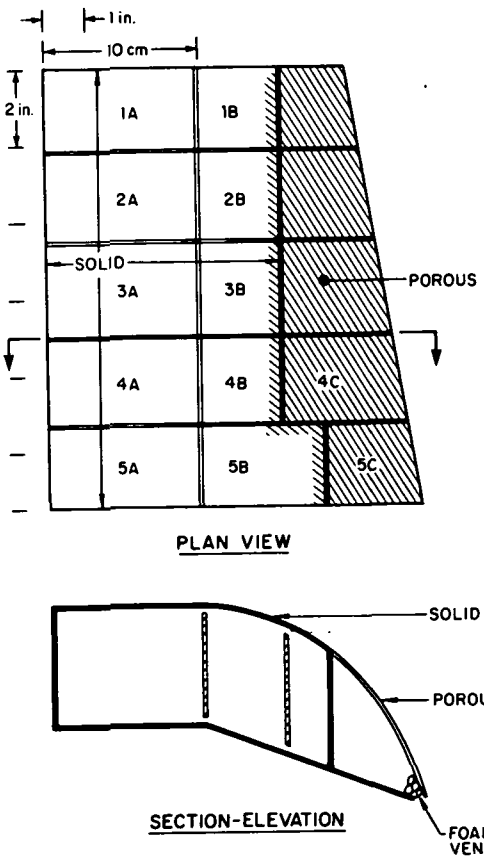

19g. Aft 30% Porous; Cavities Empty (Configuration 6).

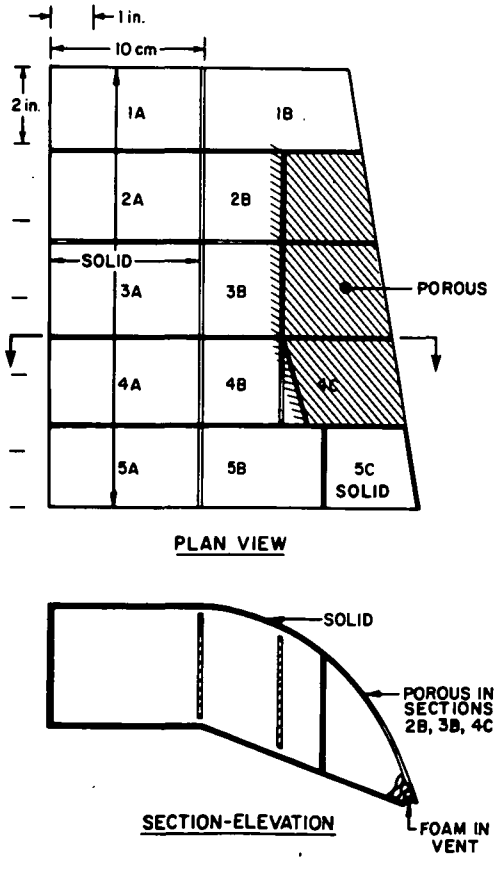

19h. Aft 30% Chord, 60% Span Treated; (Configuration 7).

can be grossly expected to reduce aerodynamic "through flow," although internal flows were not inhibited. Further, some shielding of high frequency sound generated at the solid/porous interface where the wing and flap join was expected from a previous result. This closed cavity-backed surface is Configuration #2 (Fully Porous Surface with Empty Cavity Backing).

A modification of the simple empty cavity configuration is one in which the internal flow is restricted by filling the cavities with a low flow resistance foam. This is Configuration #4, (Fully Porous Surface; Cavities Foam Filled) and is shown in Fig. 19e.

So far, the test configurations have dealt with treatment of the full flap surface area. The next configuration, #5, Fig. 19f, reduced the amount of treated surface to approximately 5 cm (2 inches) from the trailing edge (≈15% of the basic wing chord and about 30% of the total flap chord). Again, foam was kept in the cavity to restrict internal flow, as well as providing some damping of internal acoustic modes. Configuration 5 is called "Aft 30% of Flap Porous; Foam in Cavities."

An alternate configuration to 5 was one in which the foam was removed except along the vent at the trailing edge. This configuration, #6, is shown in Fig. 19g, and is called "Aft 30% of Flap Porous; Cavities Empty."

Diagnostic studies had shown that the high frequency noise generation was stronger in the center of the flap where the flow was well attached than at the edges. Thus, a configuration was devised to restrict the trailing edge treatment to the center 60% of the flap. This configuration, #7, is called "Last 30% Chord, 60% Span Treated; Cavities Open," and is shown in Fig. 19h. These configurations are summarized in Table 2.

3.3 Far Field Noise Reduction Results

For each of the configurations described above, the sound radiated to the far field stations was measured at nozzle exit velocities of 105, 152 and 207 m/s (345, 500, and 680 fps). The results are presented for the lowest and highest speeds at 45°, 90°, and 110° from the "engine" inlet axis, and at a sideline position 30° below the wing midchord line (i.e., at a 90° position from the inlet axis). All results are normalized to a distance of 2.134 m (7 ft) from the flap centerline, with the origin taken to be abour 7.6 cm (3 in. (≈20% chord) from the trailing edge.

3.3.1 Flyover plane: 45° position

Figure 20 presents the measured noise reduction at the 45° position in the flyover plane. The simple porous surface with a (nominally) solid backing, "Configuration 1" surprisingly shows significant noise reduction at the Strouhal peak (630 Hz); no increase in high frequency noise is observed thus ruling at any significant noise generation by the rough surface. The fully porous unbacked flap (Configuration 2) shows noise reductions of 9-10 dB over a wide range of frequencies. At the highest speed, the reductions at highest frequencies in the spectrum are reduced, presumably because of the significant role of jet noise in this region, which was earlier shown to contribute into the total spectrum at high speeds (>200 m/s).

Addition of backing to the fully porous flap (Configuration 3) detracts from the noise reduction at lower speeds but does not have a major detrimental effect at the high speed. When the cavities are filled with foam, Configuration 4, some improvement in the noise reduction at the peak is found. At higher speeds, the foam-filled configuration experienced separated flow, which had an interesting effect on the high frequency sound radiation. At speeds just below the velocity at which separation occurred, the high frequency noise reduction of Configuration 4 was 5-6 dB below the baseline configuration. After separation, the noise reduction at frequencies below 2000 Hz was unaffected, but a broad band high frequency noise increase of about 3 dB was observed. The shape and level of this increased high frequency spectrum matches closely the no-flap noise spectra, suggesting that a free jet has developed over part of the flap span. This hypothesis was strongly supported by observations of the flow field, and comparison of the "flap off" noise with the high frequency spectrum in Fig. 20 for Configuration 4.

Configurations 5, 6, and 7 in which the last 5 cm (2 in) of the flap were treated, showed reductions of 5-6 dB at the spectral peak and around 2 kHz where a second spectral peak occurred. At high frequencies, the reductions were only 1-3 dB.

3.3.2 Flyover plane: 90° position

The trends observed at the 45° position were found to be similar at the 90° position, as illustrated in Fig. 21. Again, the fully porous surface backed up with an impervious material Configuration 1, shows the surprising reduction of levels near the spectral peak, and the lack of increased high frequency noise levels, which again indicates that flow over the porous surface does not cause an important noise source in the frequency range of interest.

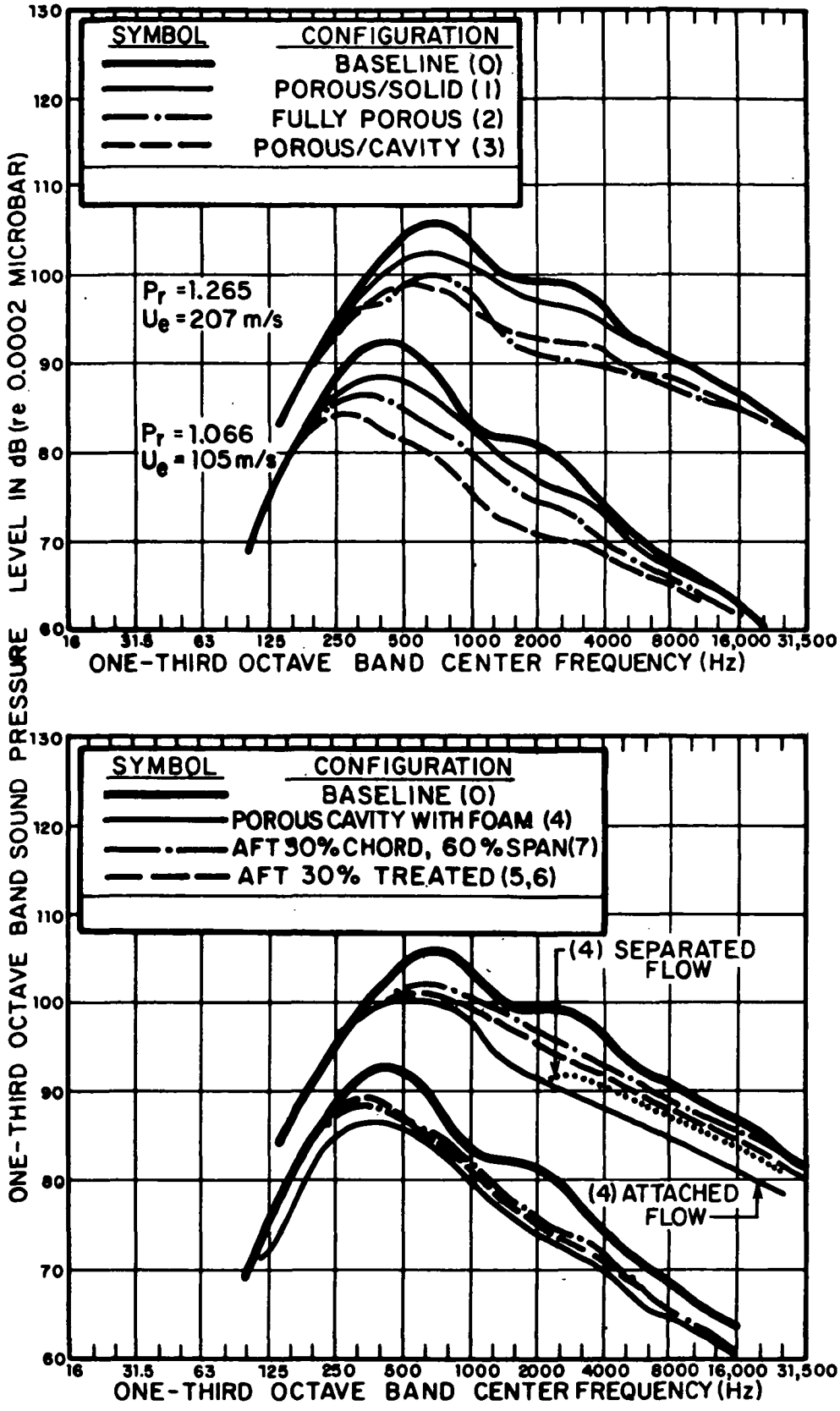

FIG. 20. NOISE REDUCTION AT 45° POSITION.

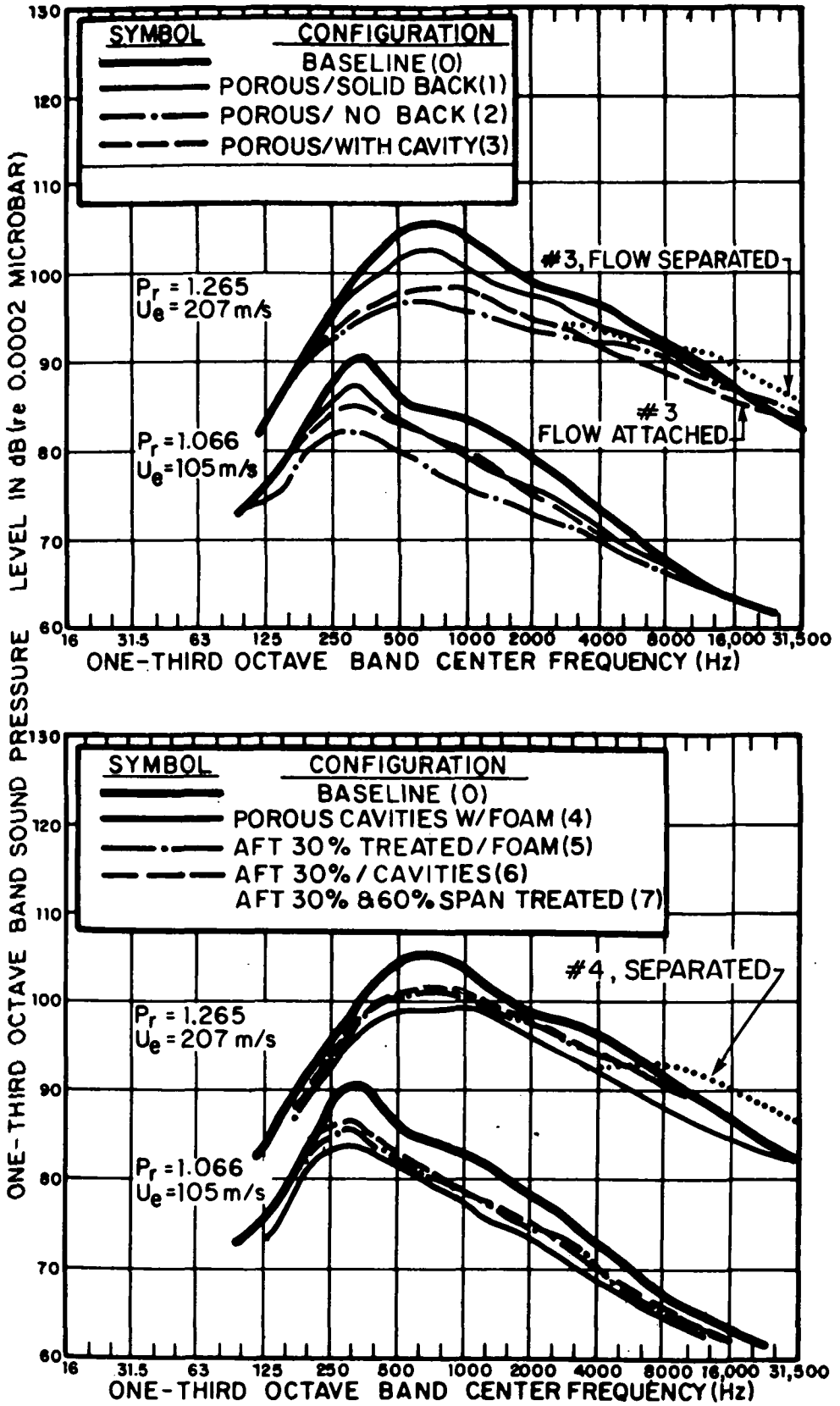

FIG. 21. NOISE REDUCTION AT 90° POSITION.

All other configurations produce a reduction of 5-9 dB at the Strouhal peak and 3-5 dB in the frequency range 2-3 octaves above the peak. The influence of separation was again found to cause a jet-like spectrum at frequencies above 5 kHz which, for the two configurations which experienced separation, increased levels by 2-4 dB above the baseline at frequencies above 8 kHz.

3.3.3 Flyover plane: 110° position

Figure 22 shows that the trends observed at 45° and 90° were repeated at the 110° position in the flyover plane. This position is 10° forward of the flap setting angle which, for most configurations was only slightly greater than the resultant turning angle of the flow. Thus, jet noise mechanisms were strong when flow separated (Configurations 2, 3 and 4) at the highest pressure ratios.

Reductions of 3-10 dB were observed at the peak Strouhal number, and reductions of 3-5 dB at high frequencies were common to most configurations.

3.3.4 Sideline position 30° below plane of wing

At the sideline position, the same trends were found as for the flyover positions, except that the high frequency noise increase did *not* occur for those configurations which experienced flow separation at high pressure ratios (Fig. 23).

An encouraging aspect of the sideline measurement is that those configurations involving the least treatment (Configurations 5, 6 and 7) had more noise reduction over a broad frequency range than those configurations with extensive treatment (Configurations 2, 3 and 4). As shown in Sec. 4, the configurations with trailing edge treatment only (Configurations 5, 6 and 7) had aerodynamic performance equal to the baseline configuration; thus these noise comparisons are at "equal performance."

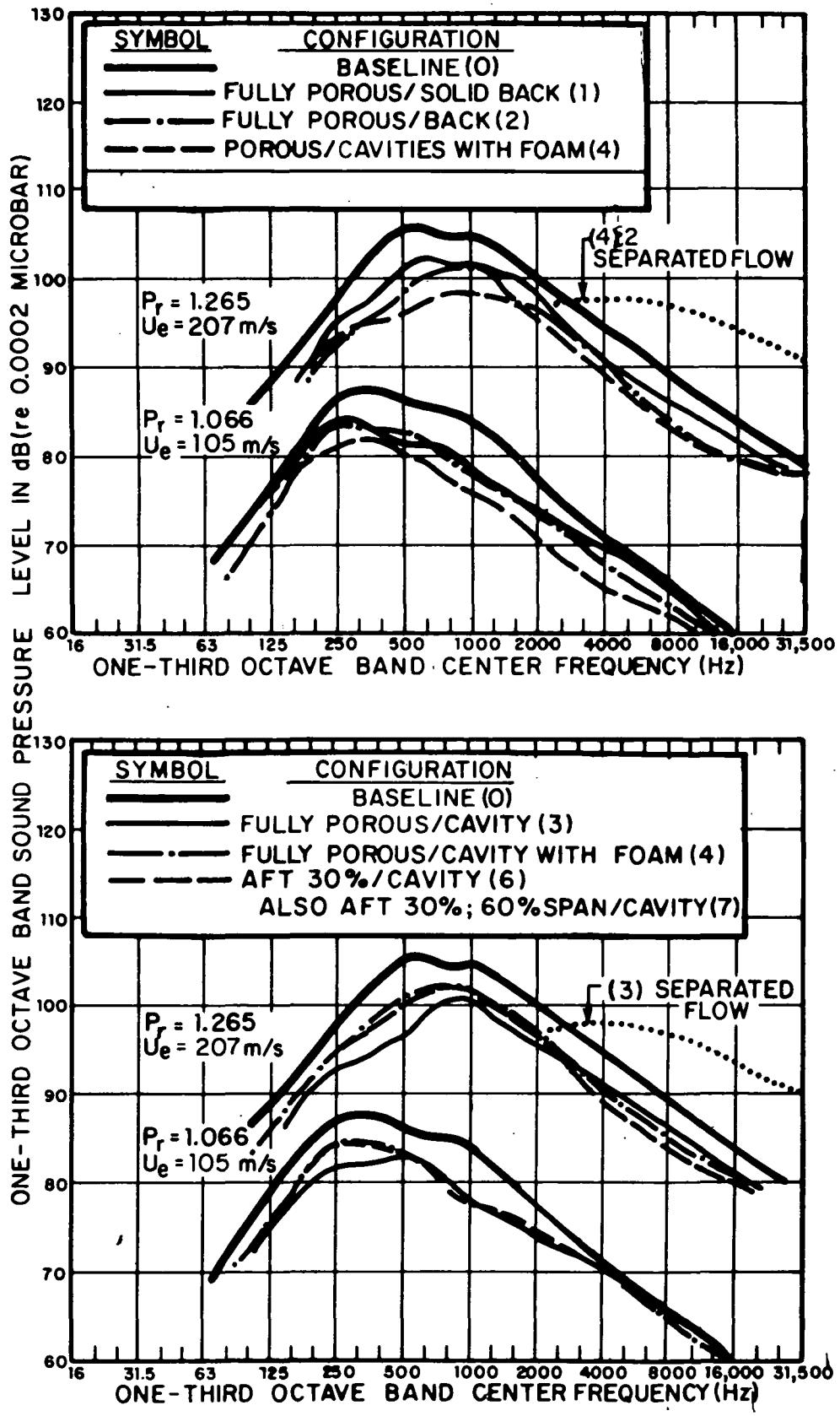

FIG. 22. NOISE REDUCTION AT 110° POSITION.

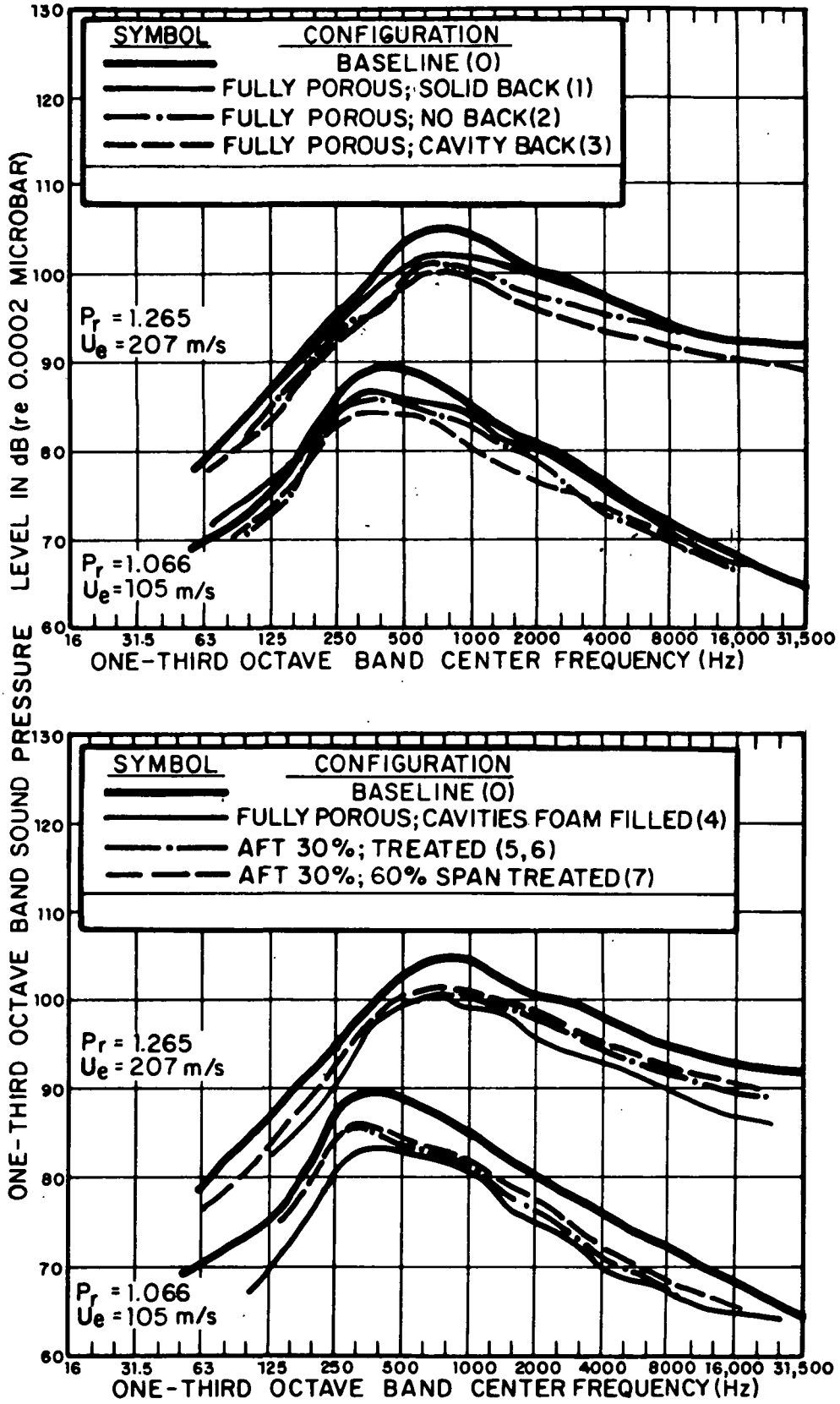

FIG. 23. NOISE REDUCTION AT SIDELINE POSITION.

3.4 Near Field Noise on Fuselage Wall

3.4.1 Areas of concern

Propulsive lift aircraft are vulnerable to two near field "noise" problems which do not typically exist in modern jet aircraft:

(1) High levels of low frequency interior noise during powered lift mode operations,

(2) Structural fatigue due to flow and low frequency sound impingement on the fuselage.

Wilby and Scharton (1974) appear to be the first to have identified and made order-of-magnitude estimates of this particular problem as it pertains to propulsive lift aircraft. The basic problem relates to the low transmission loss of fuselage structures at low frequencies. Figure 24 gives measured values from current generation aircraft along with an analytical prediction developed by Wilby and Scharton. Below 250 Hz, full scale aircraft structures achieve less than 20 dB reduction (in 1/3 octave bands) of acoustic noise, as measured on the exterior surface. Wilby and Scharton estimated that the low frequency asymptote is about 10 dB above this for typical jet type flow impingement, with the two T.L. (transmission loss) curves merging at 500 Hz, and being similar above 500 Hz.

Wilby and Scharton estimated interior noise for a USB aircraft with "state-of-the-art" fuselage construction for two cases of USB flap noise acoustic excitation, and for flow impingement. These estimates were based on far field acoustic data and on-flap pressures from a small scale model (Hayden *et al.*, 1972b) to illustrate that USB interior noise levels may be significantly higher than levels inside jet aircraft in the current commercial fleet. If this is the case, USB powered lift aircraft would have some difficulty competing for passengers who would surely object to the high levels of exposure. Wilby and Scharton noted significant increases in low frequency levels (below 250 Hz) as compared with CTOL.

In the following section, data taken on a simulated fuselage wall on the 1/5 scale model are summarized, and then used to obtain a refined estimate of USB cabin noise levels.

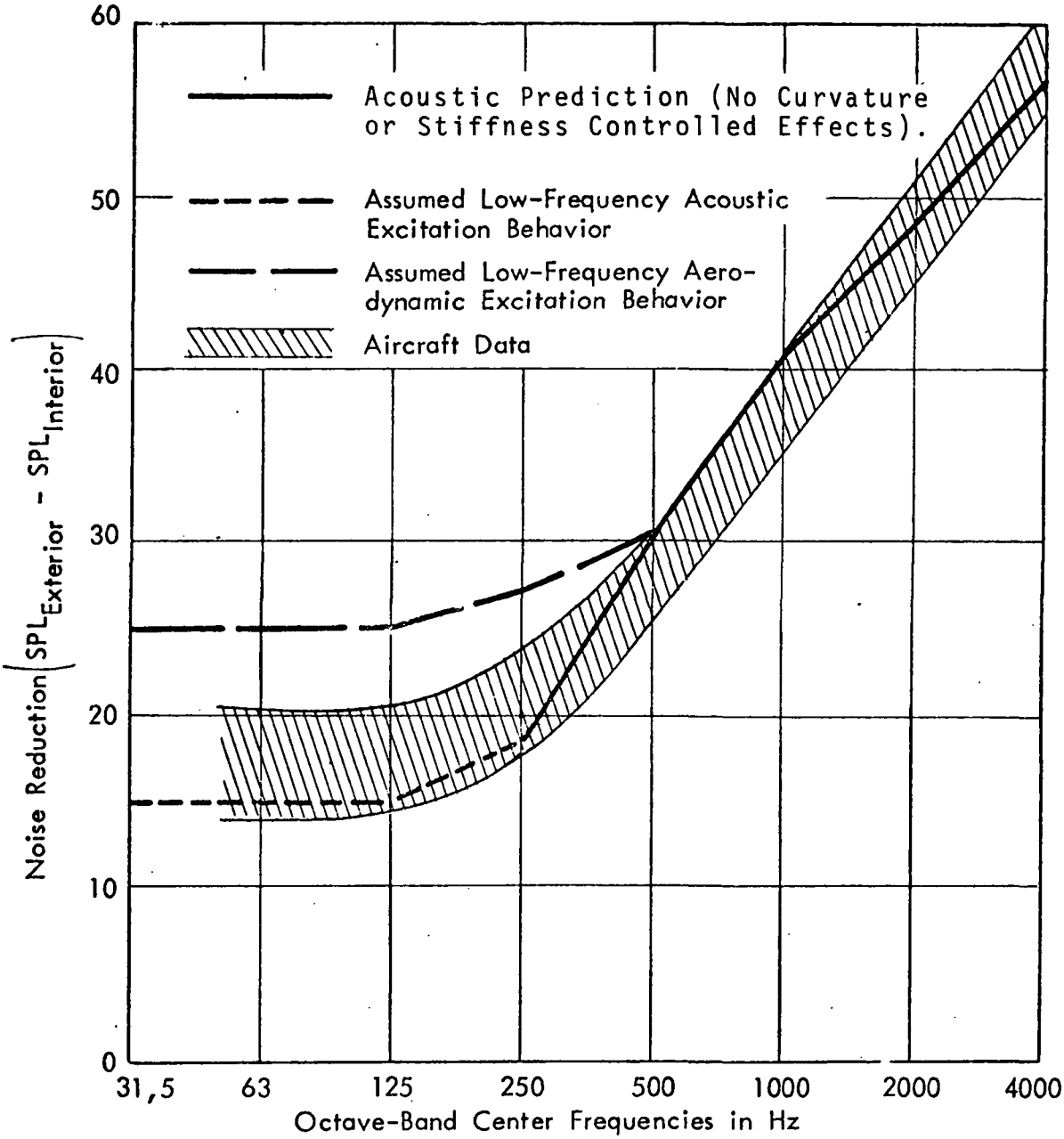

FIG. 24. FUSELAGE NOISE REDUCTION FOR DIFFERENT EXCITATION MECHANISMS, (Wilby and Scharton; 1972).

3.4.2 Baseline data on Aero Commander model

A flat plate fuselage was constructed and instrumented with flush-mounted pressure sensors (BBN Model 376 1/4" Dynamic Pressure Sensors) at several representative positions in the vicinity of the flap. Figure 25 illustrates these locations with respect to the mid-chord geometry of the nozzle/flap system. The fuselage plane was 7.62 cm (3 in.) inboard of the nozzle inner boundary.

The 1/3 octave spectra were taken over a speed range from 105 m/s (250 fps) to 207 m/s (680 fps). Significant variations in level and spectrum shape were observed at different locations. Also, the spectra were found to decompose into separable peaks with varying scaling laws. Figures 26a through 26e show how parts of these spectra vary with speed.

Data from various speeds have been scaled to form composite spectra at 207 m/s (680 fps) exit speed. The U^4 behavior at low Strouhal numbers (for model frequencies <250 Hz) may be attributable to flow impingement. The peaks around 800 Hz (model frequency) appear to be acoustic radiation, as determined by inspection of the far field spectra. Above 8000 Hz (model frequency), free jet noise is evident at some positions (see Figs.

The range of fuselage pressures which may occur is summarized in Fig. 27. To assess the implications on a full scale vehicle, the frequencies of the spectra in Fig. 27 should be shifted down by a factor of 5* and the levels kept unchanged. Applying the transmission loss curves of Fig. 25 to these shifted levels will provide an estimate of the expected interior noise levels in a full scale USB Aero Commander. Figure 28 illustrates such a calculation. Very high low frequency levels are indicated as was indicated by Wilby's earlier estimate. The jet-alone levels (flap removed) are nearly 20 dB lower below 250 Hz. As compared with existing levels in CTOL jet aircraft, the USB interior levels of USB aircraft are significantly higher in the low frequency regime (Fig. 29). It thus appears that the magnitude of the interior noise problem is very severe, and must be reduced if USB aircraft are to be acceptable to commercial passengers.

3.4.3 Interior noise reduction by variable impedance flap treatment

At each fuselage pressure sensor position, spectra were recorded at various exit speeds for the same porous flap treatments described above for the far field measurements.

---

*Frequency shift for 1/5 scale Aero Commander; a frequency shift greater than 5 is appropriate for larger aircraft.

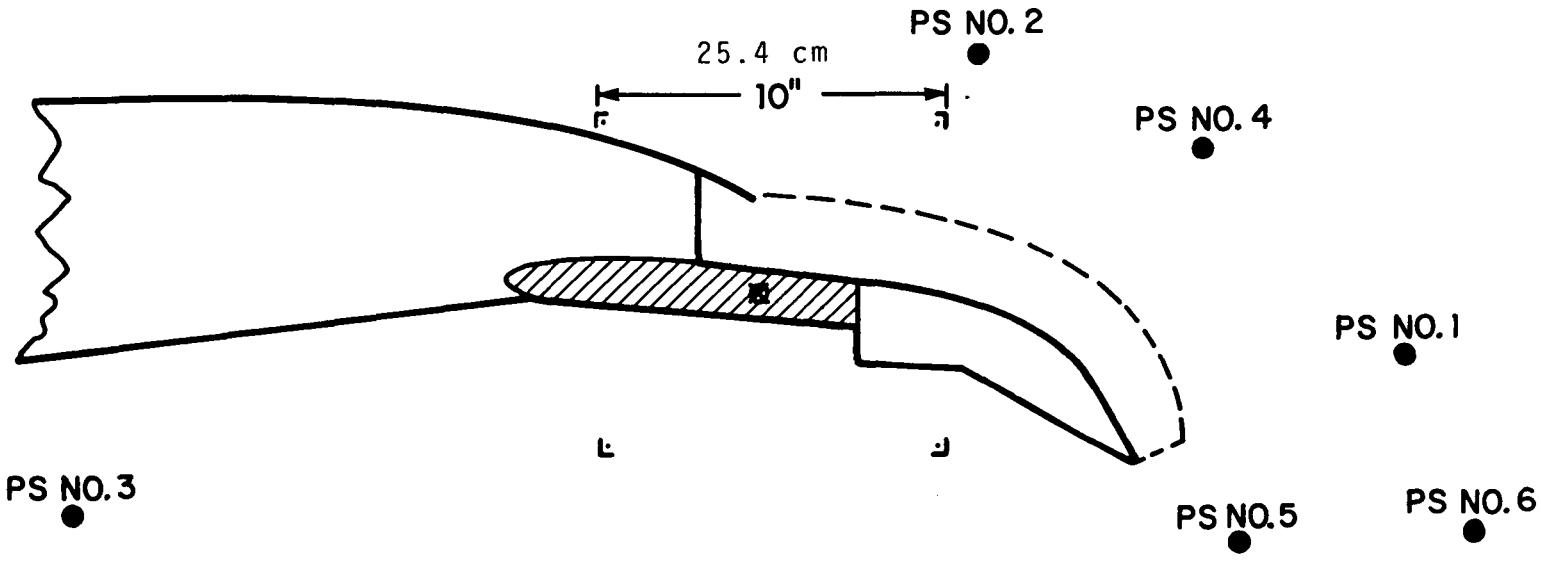

FIG. 25. LOCATION OF FUSELAGE MICROPHONES WITH RESPECT TO CENTERLINE SECTION OF MODEL FLAP.

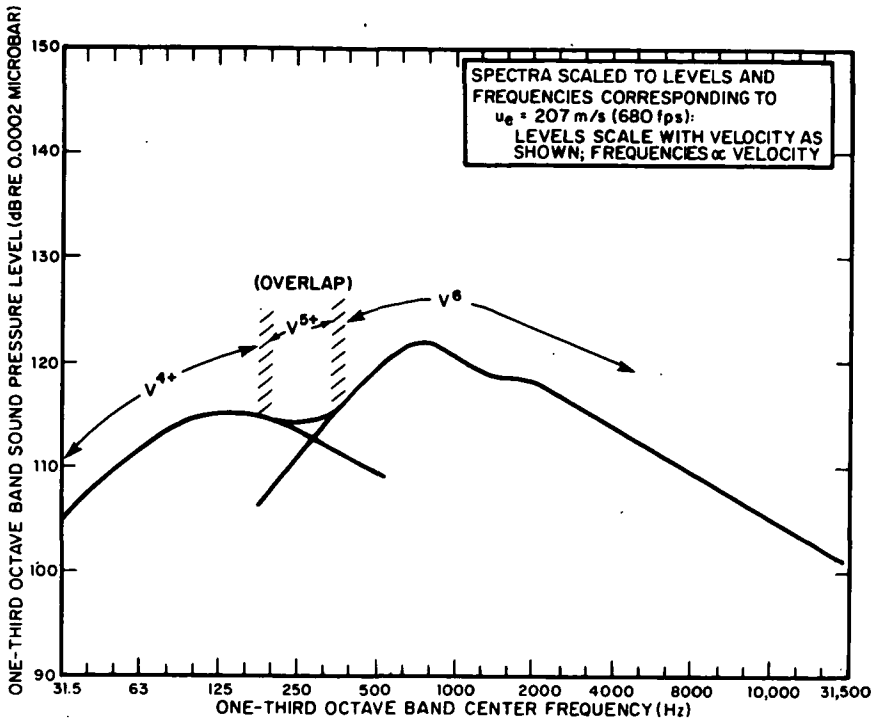

(a) Sensor Location 1.

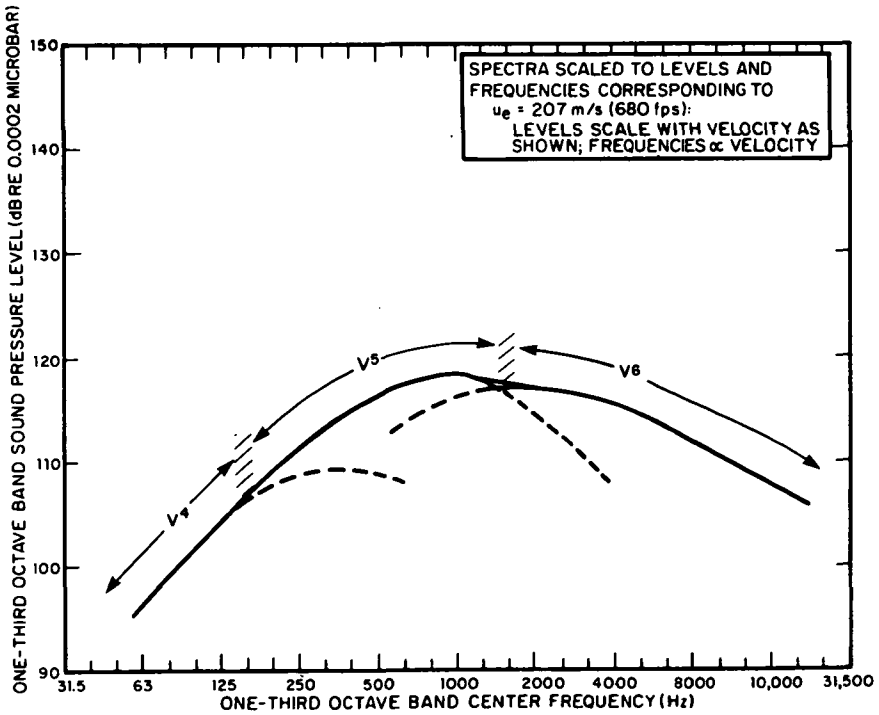

(b) Sensor Location 2.

FIG. 26. RESULTS OF VELOCITY SCALING OF FUSELAGE PRESSURES (Scaled to U_e = 207 m/s).

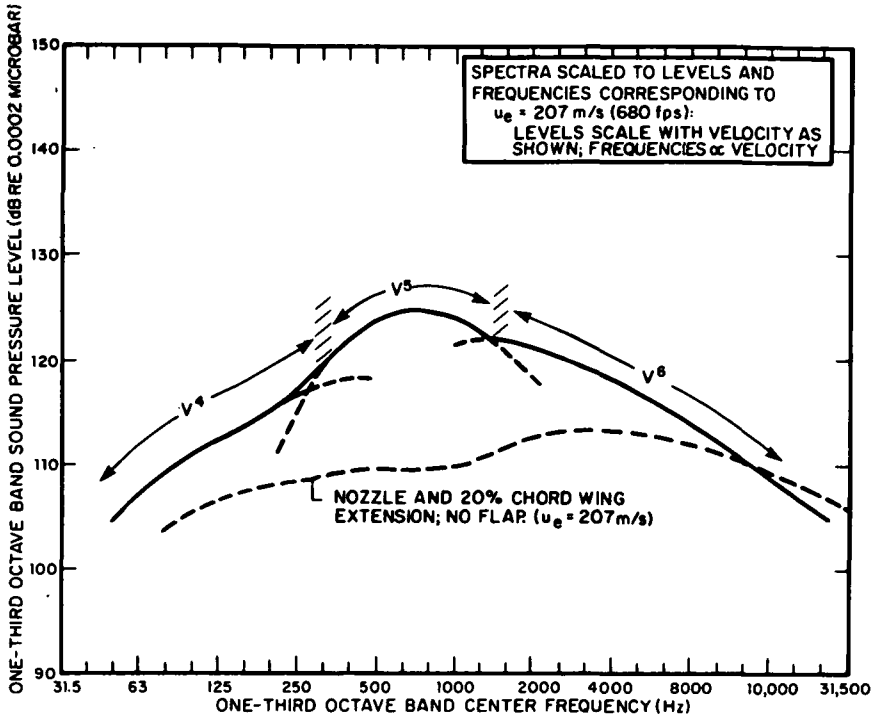

(c) Sensor Location 4.

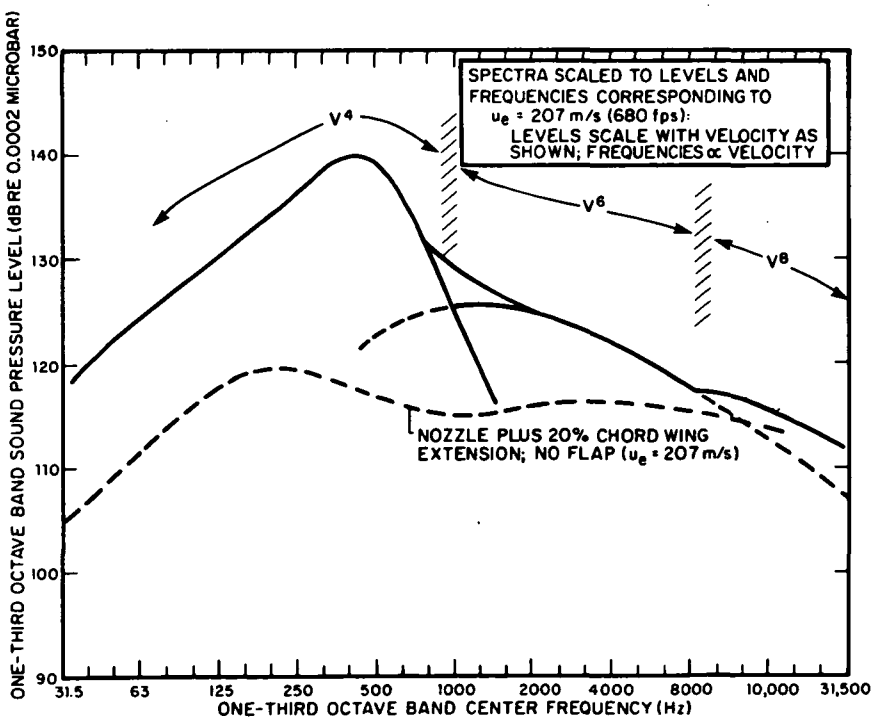

(d) Sensor Location 5.

FIG. 26. (Continued).

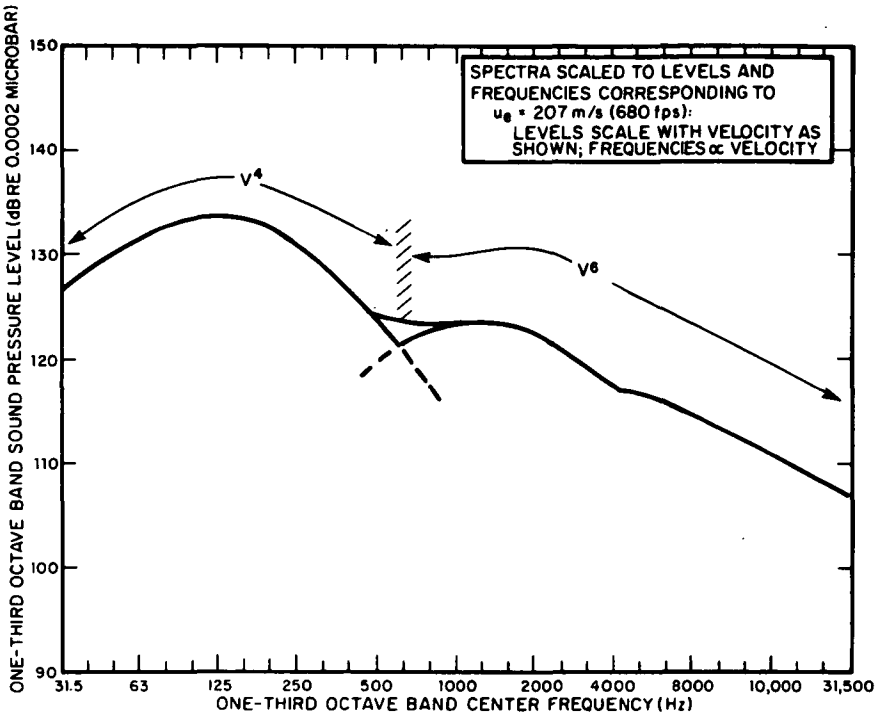

(e) Sensor Location 6.

FIG. 26. (Continued).

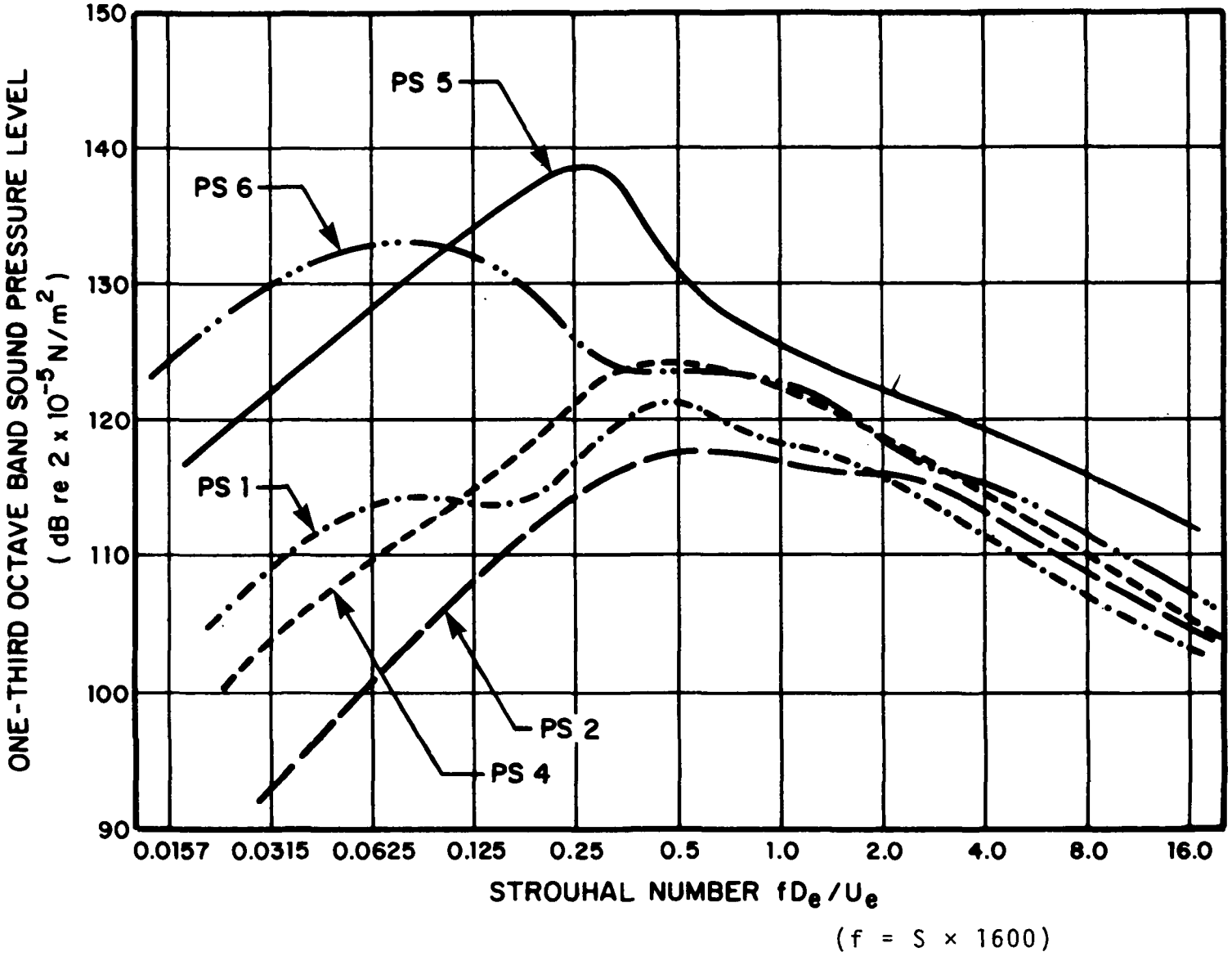

FIG. 27. NEARFIELD NOISE LEVELS ON USB MODEL FUSELAGE SIDEWALL AT 207 m/s (680 fps) JET VELOCITY.

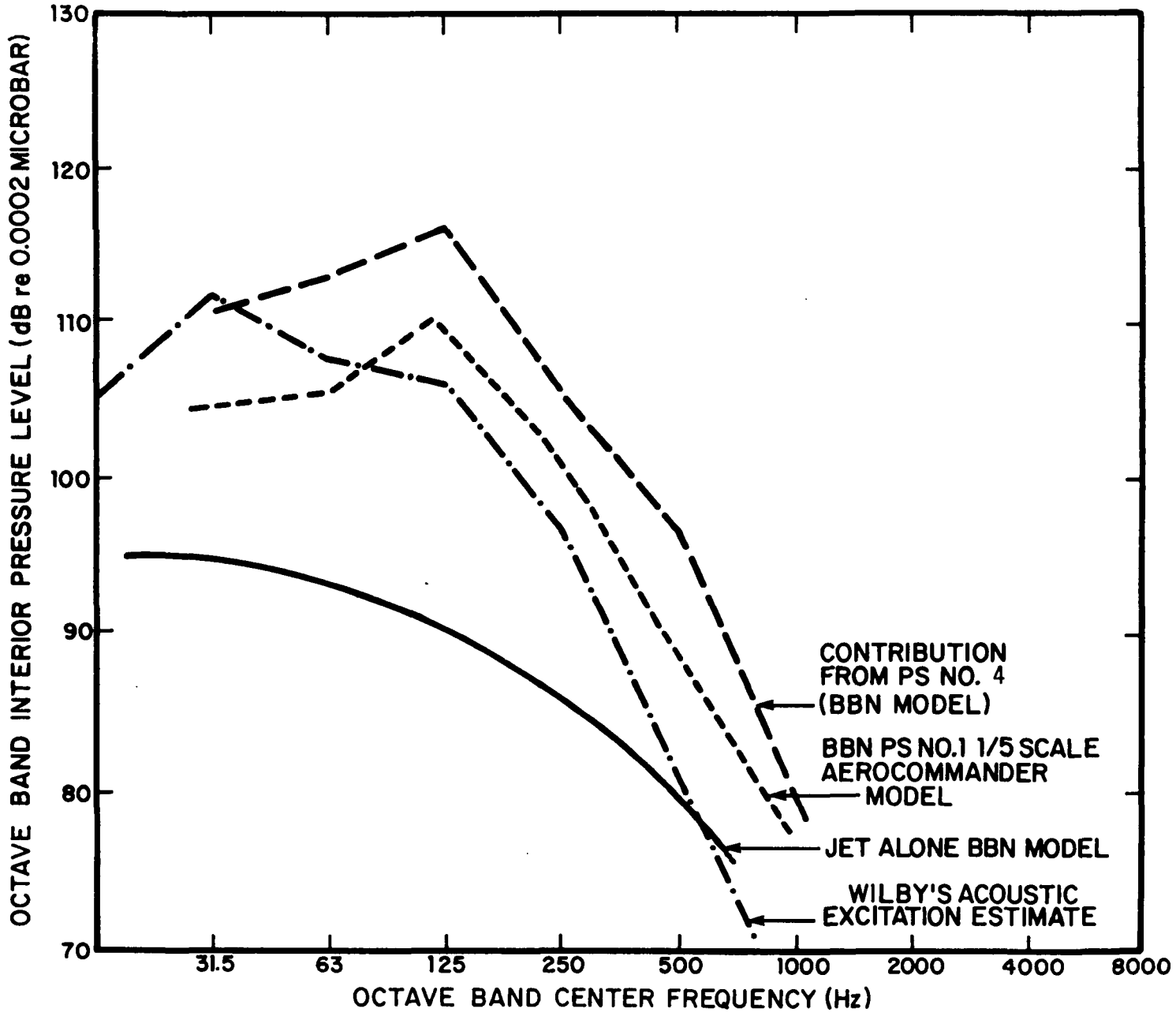

FIG. 28. ESTIMATED USB INTERIOR NOISE FROM VARIOUS EXCITATION SOURCES.

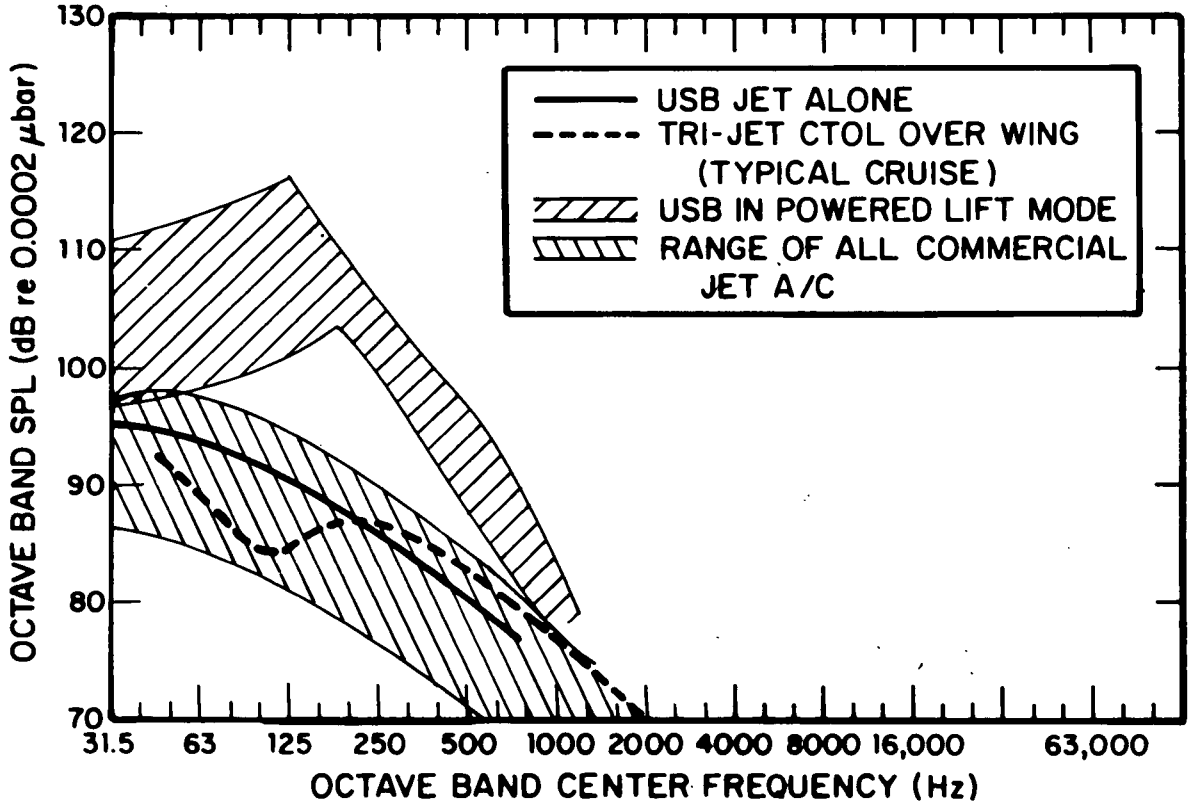

FIG. 29. COMPARISON OF OWB AIRCRAFT INTERIOR NOISE ESTIMATES WITH DATA FOR CURRENT JET AIRCRAFT, (Wilby and Scharton; 1974).

In the particular flap configuration tested, the trailing edge of the fence and an outboard section of flap which was added were not treated. The latter modification to the model improved the flow attachment and total turning, and was observed to have significant flow velocities over it. Thus, some additional reduction could be expected by treating these elements of the configuration.

Figures 30 through 34 show that noise reductions on the fuselage were achieved with all porous treatments. In some cases, such as Position 5 (Fig. 33), very large reductions of the low frequency peak occurred, indicating that the flow impingement on the fuselage may have been eliminated for those cases, possibly as a result of a new trajectory of the jet, which could occur from varying flap pressure distributions or separation.

The 4-8 dB reduction of the very low frequency noise, Figs. 33 and 34, raises a question as to the mechanism responsible for those peaks. It seems likely that those peaks are due to flow impingement, in which case the reduced levels observed when porous treatment is used implies that the intensity of the fluctuations in the free shear layer is somehow reduced. The resolution of this question must be left to future studies.

3.5 Conclusions

The data presented in this section provide the basis for optimism regarding the potential for noise reduction of USB propulsive systems through the use of porous flap treatment. Broad-band reductions of about 6 dB were achieved at all observation angles using a fibermetal flap treatment having a flow impedance of 30-50 cgs rays (~1.0 $\rho_0 c_0$) applied to a relatively localized section of the flap. The spectral variation of the noise reductions had some dependence on speed, but the broad-band results generally were nearly the same for all speeds and all angles for a given porous flap configuration.

Significant reductions (~6 dB) of cabin noise can also be achieved using the porous flap treatments. However, the cabin noise problem will not be fully solved by a broad-band reduction of 6 dB. More attention must be given to this problem, with special emphasis on aerodynamic design details which prevent flow impingement on the fuselage.

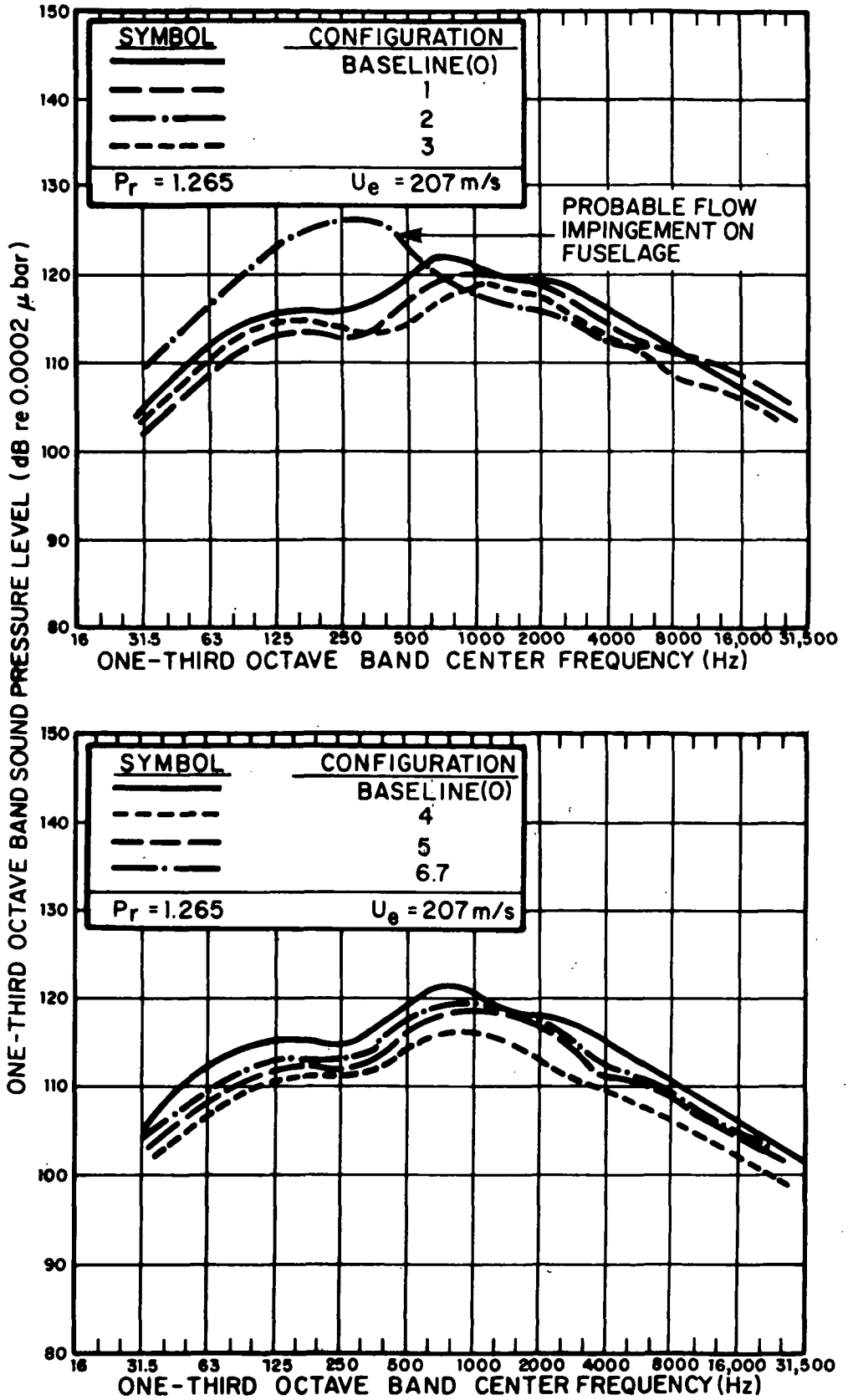

FIG. 30. FUSELAGE SIDEWALL PRESSURE REDUCTION WITH POROUS FLAP CONFIGURATIONS. SENSOR LOCATION #1.

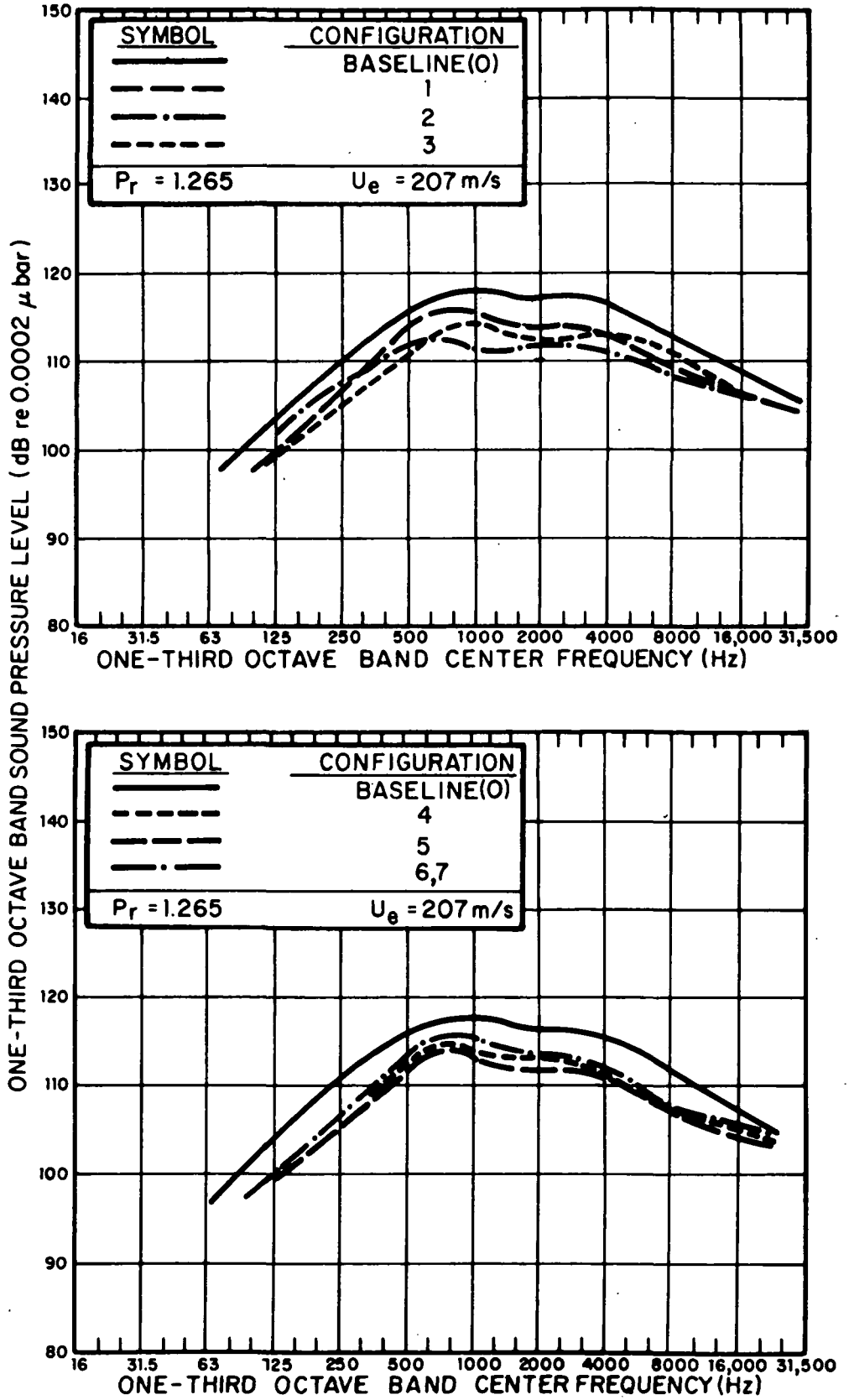

FIG. 31. FUSELAGE SIDEWALL PRESSURE REDUCTION WITH POROUS FLAP CONFIGURATIONS. SENSOR LOCATION #2.

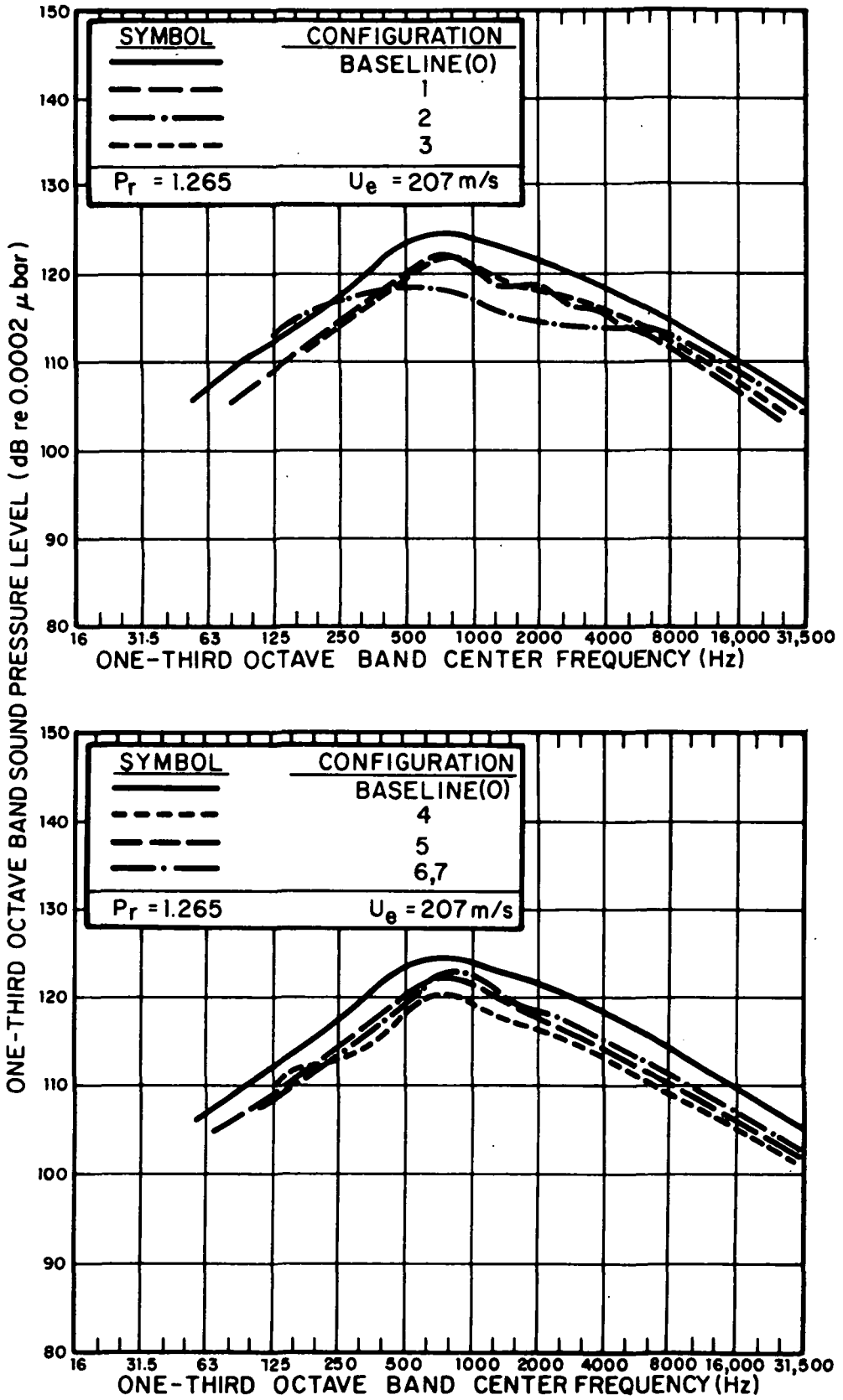

FIG. 32. FUSELAGE SIDEWALL PRESSURE REDUCTION WITH POROUS FLAP CONFIGURATIONS. SENSOR LOCATION #4.

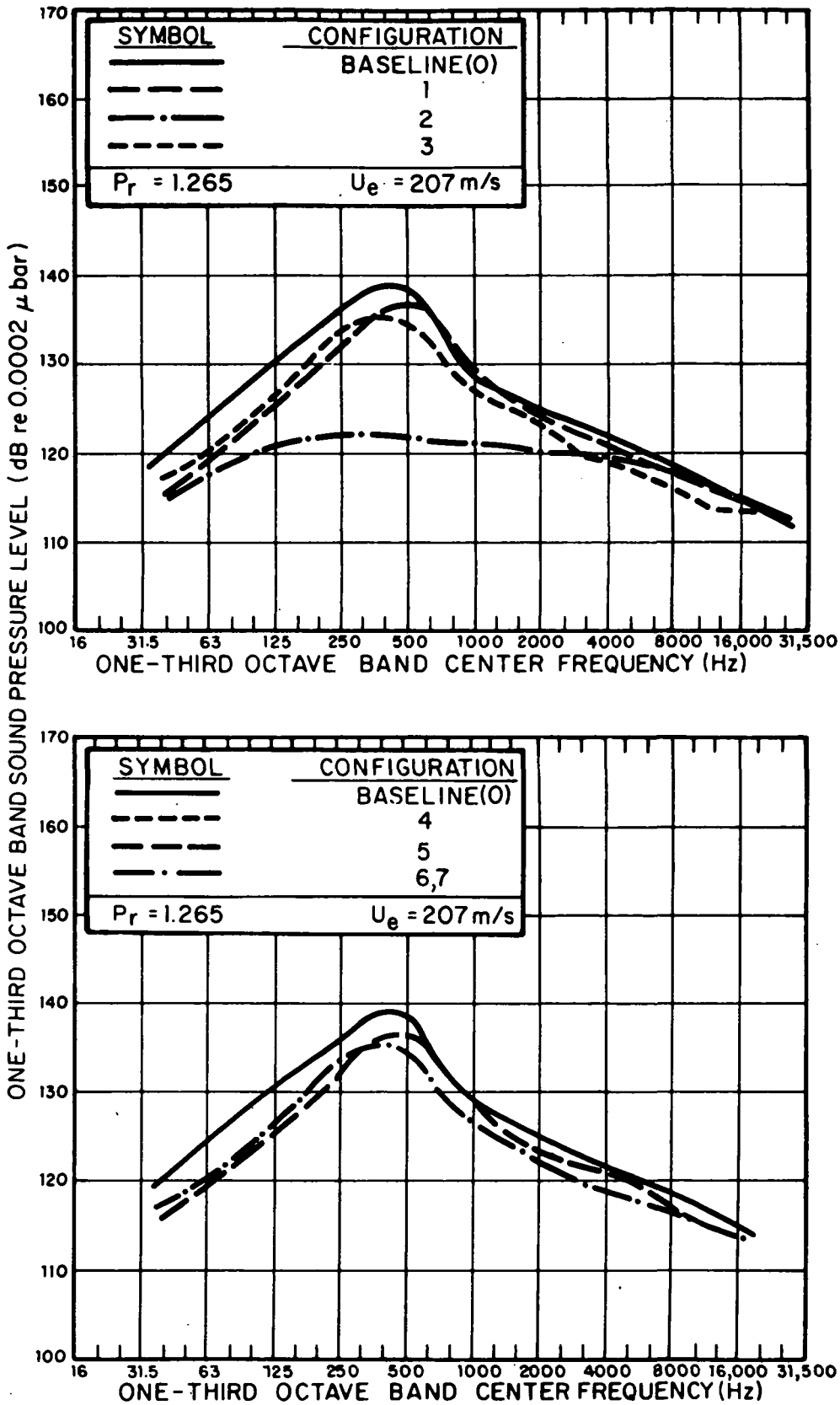

FIG. 33. FUSELAGE SIDEWALL PRESSURE REDUCTION WITH POROUS FLAP CONFIGURATIONS. SENSOR LOCATION #5.

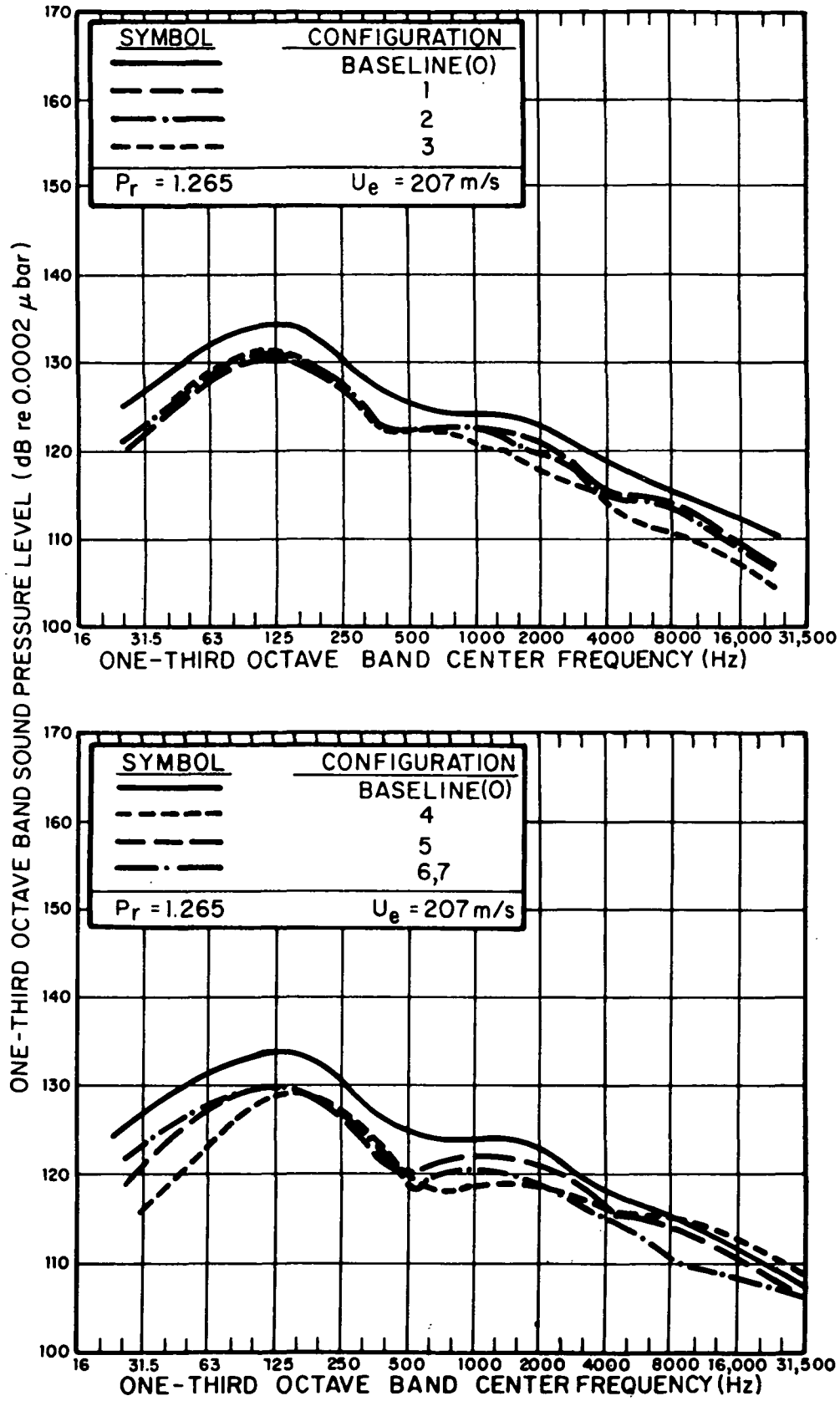

FIG. 34. FUSELAGE SIDEWALL PRESSURE REDUCTION WITH POROUS FLAP CONFIGURATIONS. SENSOR LOCATION #6.

SECTION 4

AERODYNAMIC PERFORMANCE

4.1 USB Systems

Upper surface blown systems are attractive when compared to under-the-wing EBF configurations due to their more efficient turning at high flap angles. The USB can achieve up to 65° of static turning without separation of the flow. (See, for example, NASA SP-320 (1972) and NASA SP-406 (1976). In this range of turning angles, the thrust recovery is about 90% versus about 75% for the EBF. Various nozzle/flap configurations have been investigated over the past few years, with considerable variation in both static turning and level-flight powered lift performance.

For this study, it was desired to observe the variations in aerodynamic performance caused by flaps having varying amounts of porous treatment. A baseline flap configuration was chosen which had been optimized by NASA to produce very high thrust recovery and good static turning. This system was a model of the Aero Commander USB Research Vehicle, which is shown in Fig. 35. The static turning characteristics have been studied in detail and reported by Phelps (1975). The baseline nozzle was a nominal 4:1 aspect ratio and had a mean kickdown angle of 25°. Phelps found that a nozzle deflector and inboard fence produced the best performance. The inboard fence also helped keep flow off the fuselage. For forward speed powered lift mode operations, the inboard fence did not affect the performance and the flow impingement on the fuselage was not as severe as in the static case. The NASA static turning results are given in Fig. 36.

4.2 Baseline Conditions of Part-Span Model

The part-span 1/5 scale model described earlier was placed on a 6-degree of freedom force balance as shown in Fig. 37. The air supply was isolated through a flexible coupling which was calibrated as a function of static pressure and found to be very linear with pressure and highly repeatable (to within 3-4%). This isolation was necessary if a low-noise air supply was to be used in lieu of a noisy model fan, such as the commonly-used tip-turbine air-driven fans. The isolation joint assures that all downstream forces will be measured by the balance, along with the force across the isolation joint itself. Typically, the force across the joint was about 20% of the total axial force.

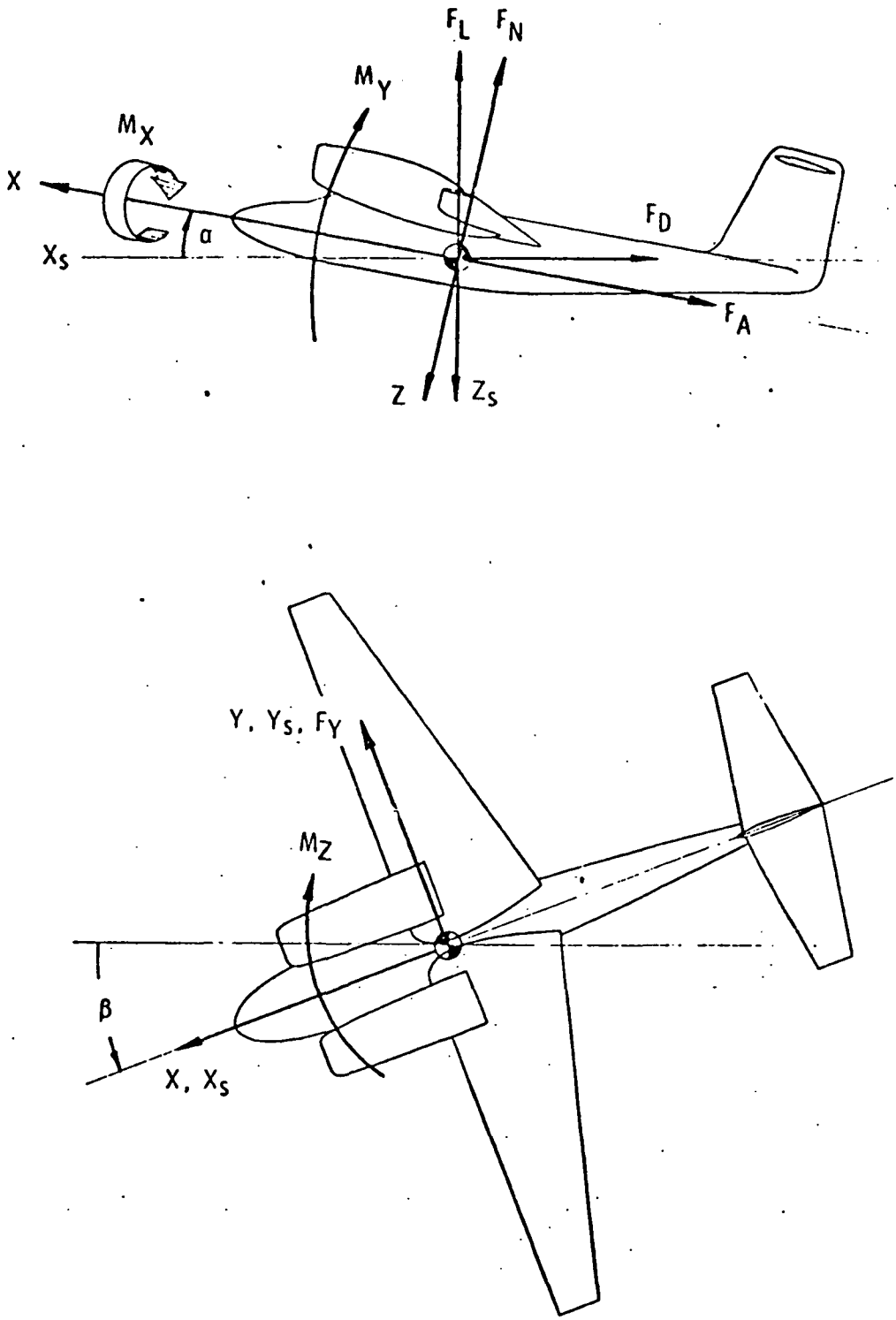

FIG. 35. AXIS SYSTEMS USED IN PRESENTATION OF DATA. ARROWS INDICATE POSITIVE DIRECTION OF FORCES, MOMENTS, AXES, AND ANGLES.

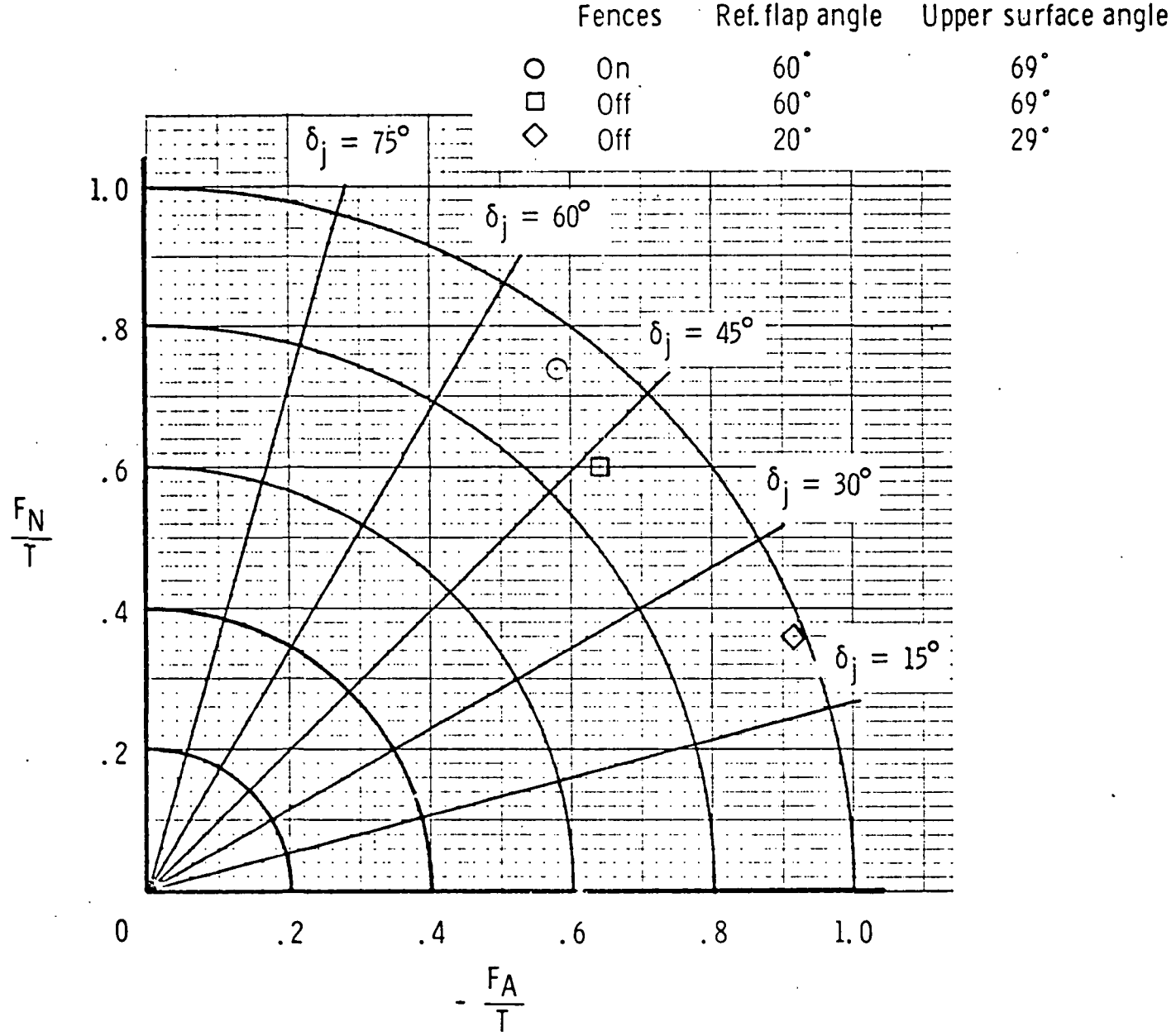

FIG. 36. SUMMARY OF FLAP TURNING EFFICIENCY AND TURNING ANGLE; FULL POWER, (Phelps, 1975).

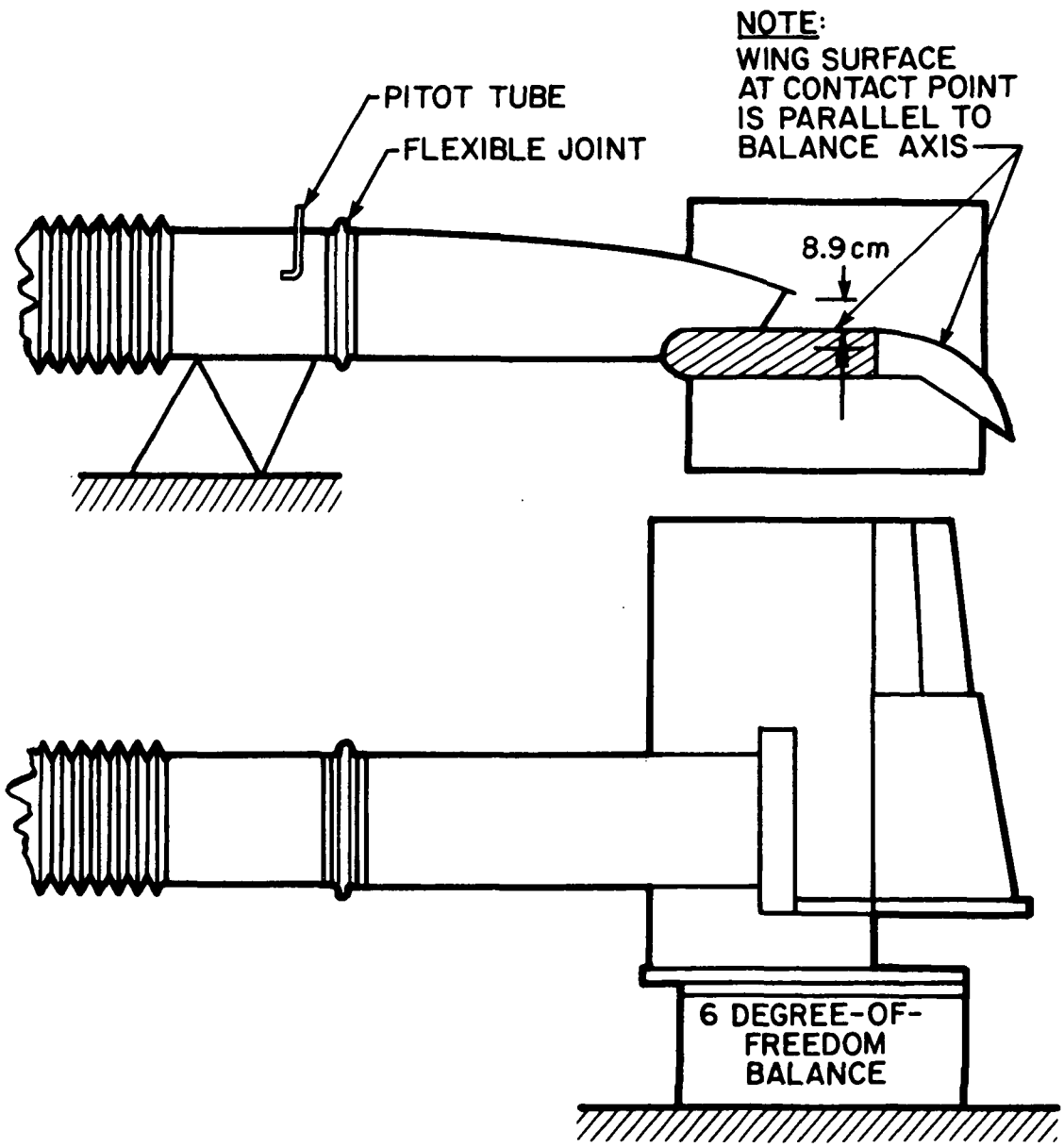

FIG. 37. SCHEMATIC OF MEASUREMENT SET UP.

The configuration of the air supply to the model nozzle necessitates conversion of the measured thrust forces to an "equivalent" system where the inlet duct "sees" ambient pressure and velocity; i.e., an internal power source accelerates the air and pressurizes the nozzle. The basic problem is outlined in Fig. 38.

For the first case, the net force on the system is

$$\Sigma F_x = \dot{m} U_e$$

where there is no relative velocity between the nozzle system, and the medium.

For the second case, which is the case relevant to the present tests, the net force is approximately

$$\Sigma F_x = -p_1 A_1 + \dot{m} (U_e - U_1) + J$$

where J is the force across the isolation joint. The force which we wish to know from the total force (ΣF_x) measured on the system is $\dot{m} U_e$ minus losses, or the recovered thrust, F_A. Therefore, from the measured data we must add the following

$$p_1 A_1, \dot{m} U_1, J$$

or

$$F_A = \Sigma F_{x_{meas}} + p_1 A_1 + \dot{m} U_1 - J$$

The raw net force (ΣF_x, ΣF_y) data was obtained as a function of pressure ratio to detect any effects of Mach number, and to detect separation. Figure 39 illustrates such data for four baseline configurations.

- Basic nozzle, no deflector, no flap (wing included)
- Basic nozzle with deflector; no flap
- Deflector nozzle with rigid, smooth flap surface and fence (configuration 0)
- Deflector nozzle with porous FM 134 flap surface backed with solid material; fence included (configuration 1).

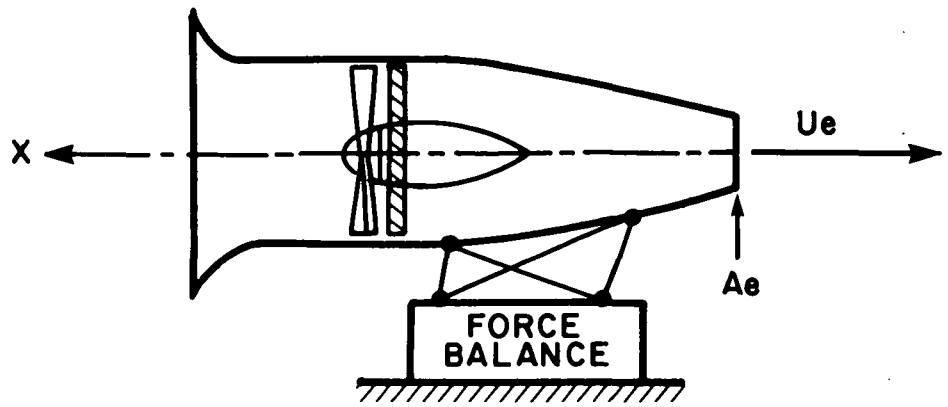

(a) ENGINE INTERNAL; "FREE" SYSTEM

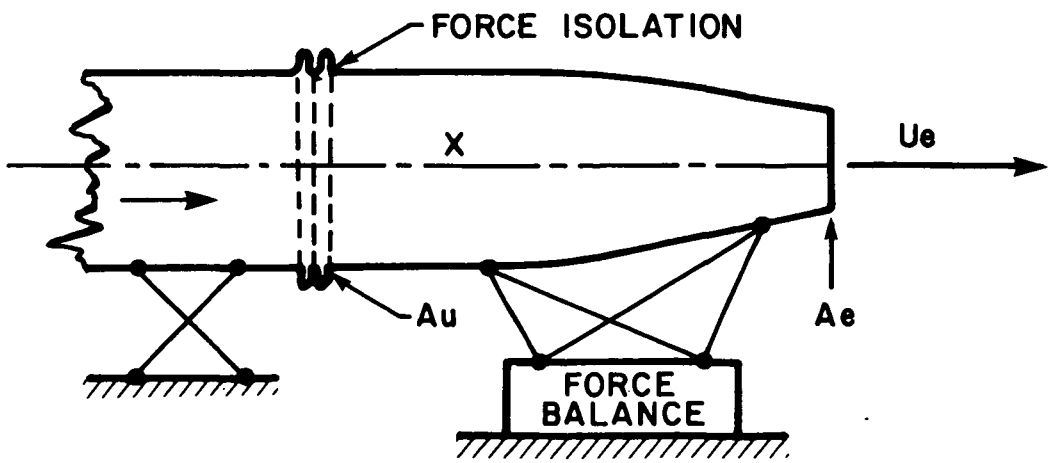

(b) DUCTED AIR SUPPLY

FIG. 38. SCHEMATIC OF CONFIGURATIONS FOR CONVERSION OF FORCES MEASURED IN A DUCTED AIR SUPPLY TO EQUIVALENT "FREE" SYSTEM.

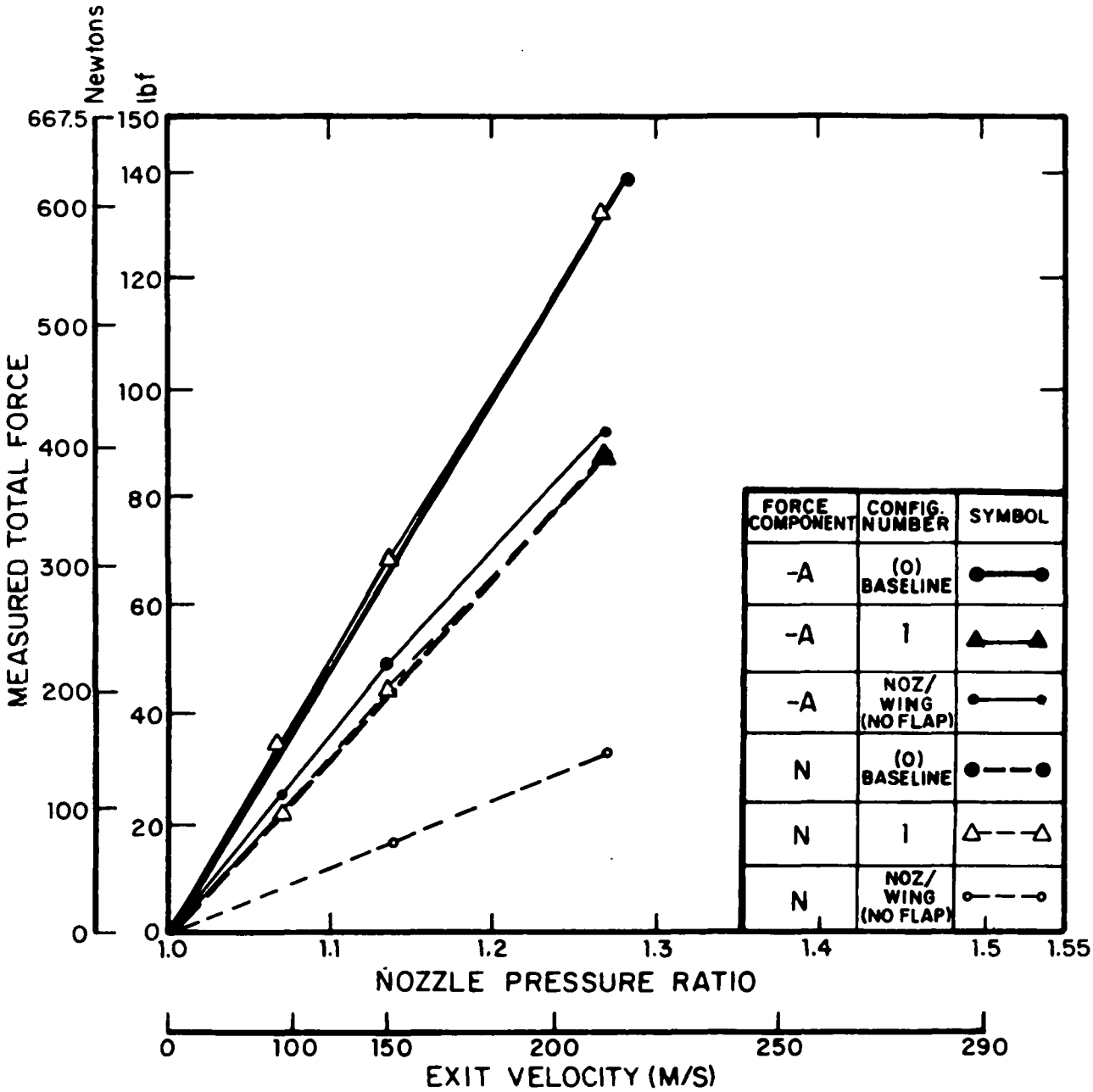

FIG. 39. STATIC FORCES vs. NOZZLE PRESSURE RATIO – BASELINE NOZZLE AND FLAP CONFIGURATIONS.

Using the above-described correction procedures, the following results were obtained for the baseline nozzles and flaps (with and without deflector) at a pressure ratio of 1.265 (U_e = 207 m/s):

1. Basic nozzle, no deflector:

F_A = 529.5 N (119 lb_f)

F_N = 98.8 N (22.2 lb_f)

$T_R = \sqrt{F_{A^2} + F_{N^2}}$ = 538.5 N (121 lb_f)

$\frac{F_A}{T_R}$ = 0.98

$\frac{F_N}{T_R}$ = 0.183

The ideal thrust calculated for this nozzle, $\dot{m}\, U_e$, at the same conditions is 552.7 (124.2 lb_f). Since the measured forces included "scrubbing" and spreading losses, the measured resultant force seems quite believable.

2. Basic nozzle with deflector

F_A = 429.8 N (96.6 lb_f)

F_N = 103.24 N (23.2 lb_f)

T_R = 455.7 N (102.4 lb_f)

$\frac{F_A}{T_R}$ = .94

$\frac{F_N}{T_R}$ = .226

This nozzle configuration produced substantial spreading of the flow laterally, thus, much of the axial momentum was converted into non-axial momentum, as reflected by the reduced total resultant thrust.

3. Baseline solid flap (nozzle with deflector, and inboard fence); configuration 0:

F_A = 247.42 N (55.6 lb_f)

F_N = 364.9 N (82. lb_f)

T_R [from (2)] = 552.7 N (102.4 lb_f)

$\frac{F_A}{T_R}$ = .54

$\frac{F_N}{T_R}$ = .79

4. Porous surface flap (configuration 1) with rigid backing (nozzle with deflector, and inboard fence)

F_A = 251.9 N (56.6 lb_f)

F_N = 356. N (80. lb_f)

T_R [from (2)] = 552.7 N (102.4 lb_f)

$\frac{F_A}{T_R}$ = .55

$\frac{F_N}{T_R}$ = .78

The turning angle and efficiency are plotted in Fig. 40 for all these baseline cases. Comparing these results with those of Phelps (1975) Fig. 36 on the nominally-identical model, it is noted that the baseline solid flap performs virtually identically to the full span model studied by Phelps.

It is interesting and significant to note that the porous surface has a negligible effect on the turning angle and efficiency although a very slight reduction of both were measured. Further understanding of porous surface aerodynamics could improve these minor deficiencies.

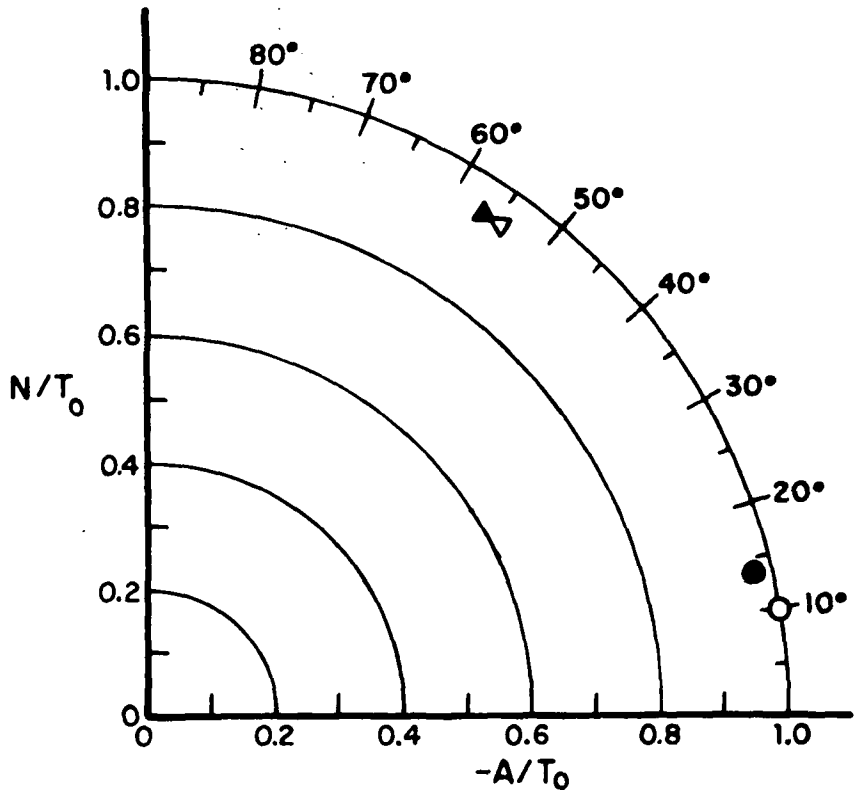

SYMBOL	CONFIGURATION
○	BASIC NOZZLE WITHOUT DEFLECTOR
●	BASIC NOZZLE WITH DEFLECTOR
▲	DEFLECTOR NOZZLE WITH SOLID FLAP AND FENCE
▽	DEFLECTOR NOZZLE WITH POROUS SURFACE/ SOLID BACKED FLAP AND FENCE. (CONFIGURATION)

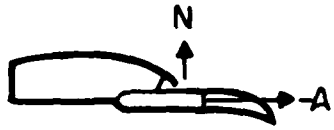

NOTE:
T_0 = CALIBRATION THRUST OF NOZZLE, WITH DEFLECTOR AND WITH FLAP REMOVED.

FIG. 40. BASELINE FLAP AND NOZZLE EFFICIENCIES AND TURNING ANGLES.

In the remainder of this section, other porous flap configurations will be compared with these baseline configurations using the same approach to the data presentation.

4.3 Aerodynamic Performance Results for Porous Flaps

Several flap configurations which were found acoustically advantageous were tested for their aerodynamic performance. As mentioned in Section 3, the flap material used had an impedance of approximately 0.8 $\rho_0 c_0$, (Brunswick FM 134). This was chosen after preliminary surveys indicated that this material and impedance gave the best acoustic results when all frequencies and observation angles were considered. During the aerodynamic tests, some "fine tuning" of the spatial variation of the porous treatment, and of the cavity-backing, was carried out.

The results presented below are the gross forces versus pressure ratio, and a summary curve of turning efficiency and turning angle at a pressure ratio of 1.235 (U_e = 207 m/s). The following configurations are presented (refer to Table 2 and Figs. 19a through 19h for details).

Configuration Number	Reference Fig. No.	Brief Description
1	19b	Porous Surface with Solid Backing
2	19c	Full Area of Flap Porous; No Backing
3	19d	Full Flap Porous; with Back; T.E.* Vented
4	19e	Full Flap Porous; with Back; .5 $\rho_0 c_0$ Foam in Cavity
5	19f	T.E. Region Porous; Full Span; .5 $\rho_0 c_0$ Foam in Cavity
6	19g	T.E. Region Porous; Full Span; .5 $\rho_0 c_0$ Seal at T.E. only
7	19h	T.E. Region of Center Span Porous; Outer Bays Solid; .5 $\rho_0 c_0$ Seal at T.E. only

*T.E. = Trailing Edge.

Figure 41 shows the variation in total axial and normal forces with pressure ratio for the fully porous flap with no backing (configuration 2), as compared with the baseline solid flap (configuration 0). This configuration clearly demonstrates that a fully porous flap has inferior lifting (N) capability, and that the drag force is less (-A) than for the baseline solid flap. Flow separated from the particular flap at a nozzle total pressure of about 1.2. Thus, the dramatic noise reduction achieved with this flap is offset by the poor aerodynamic performance.

The next obvious step in evolving an aerodynamically statisfactory flap is to place a backing plate on the lower surface structure supporting the porous surface, thus creating a substantial cavity below the surface. Crudely speaking, placement of such a backing plate blocks the mean flow through the flap. However, the trailing edge is vented for acoustic reasons, thus allowing air to enter the cavity and bleed through the flap. Also, some gross aerodynamic flow can occur within the cavity due to the spatially non-uniform distribution of near aerodynamic pressure on the flap surface. Figure 42 shows that this configuration (3) has *superior* turning capabilities at low exhaust speeds, but flow separates at a pressure ratio of about 1.2 ($U_e \approx 180$ m/s). Note that the separation began at the inboard trailing edge location. However, the good low speed performance is an encouraging trend, which leads to the next logical step which is to try to restrict the internal airflow without changing the impedance presented to the flow pressure fluctuations above the flap surface.

Figure 43 shows that the attempt at restriction of internal airflow with .5 $\rho_0 c_0$ impedance foam did not substantially change the aerodynamic performance of the flap configuration with the entire surface porous, and a backing plate creating cavities beneath the surface.

The background diagnostic studies of source location had shown that the region of the flap most responsible for sound generation was the region 5 cm (2 in.) (≈15% chord) or less from the trailing edge. The next step is to take this observation into account by reducing the amount of flap treatment to the last 5 cm. Configuration 5 has the trailing edge region porous across the entire flap span for a distance of about 5 cm upstream of the edge. The cavity created behind the flap with the backing plate was filled with foam to restrict internal airflow. The aerodynamic effect was extremely favorable, as shown in Fig. 44. No separation occurred, and the axial (-A) and normal (N) gross forces appear to be nearly equivalent to the baseline solid flap.

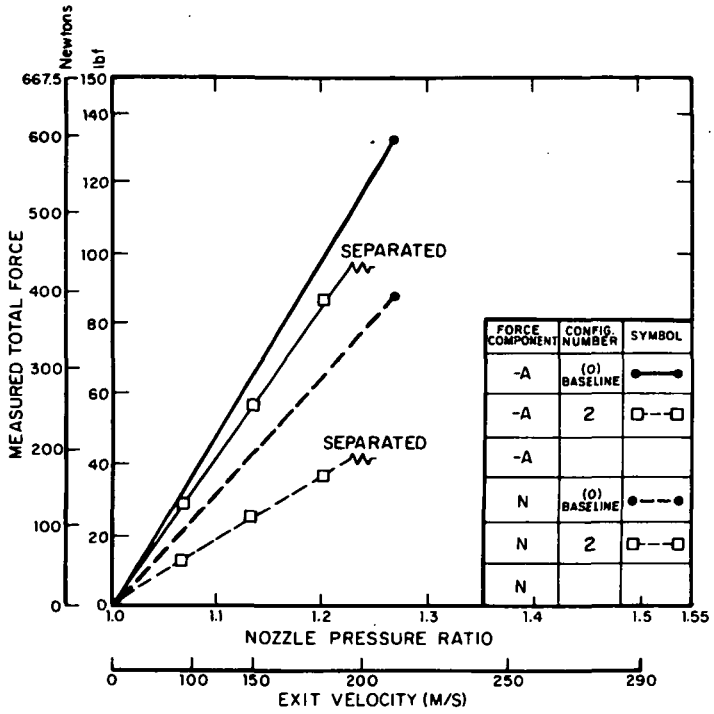

FIG. 41. STATIC FORCES vs. NOZZLE PRESSURE RATIO — CONFIGURATION 2.

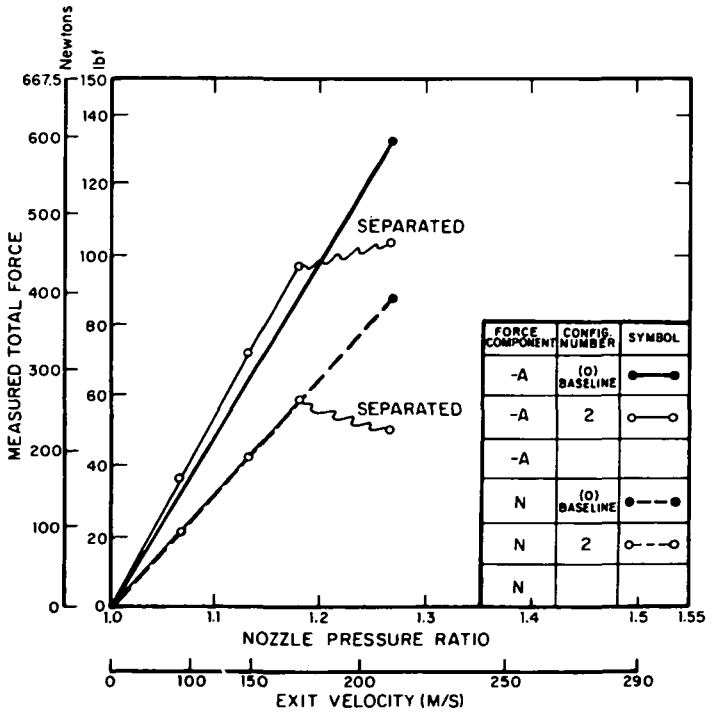

FIG. 42. STATIC FORCES vs. NOZZLE PRESSURE RATIO — CONFIGURATION 3.

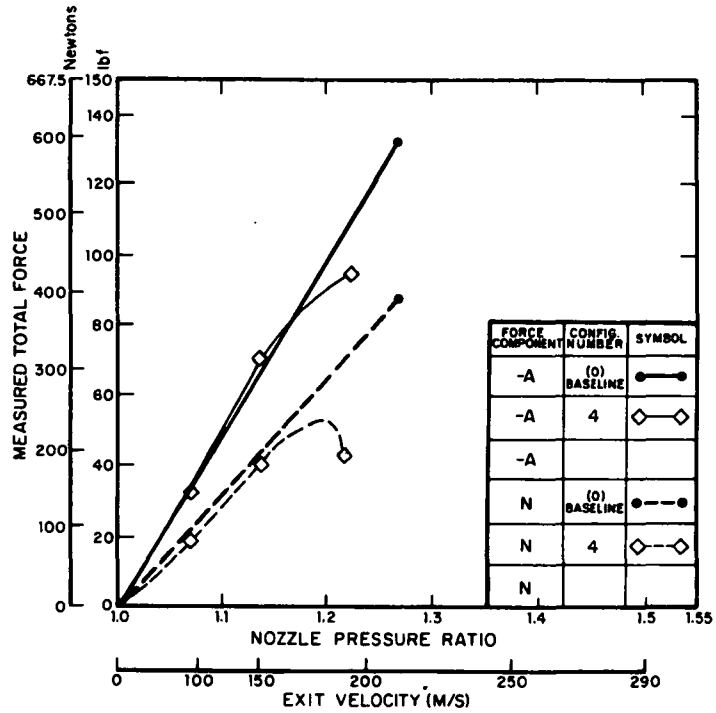

FIG. 43. STATIC FORCES vs. NOZZLE PRESSURE RATIO — CONFIGURATION 4.

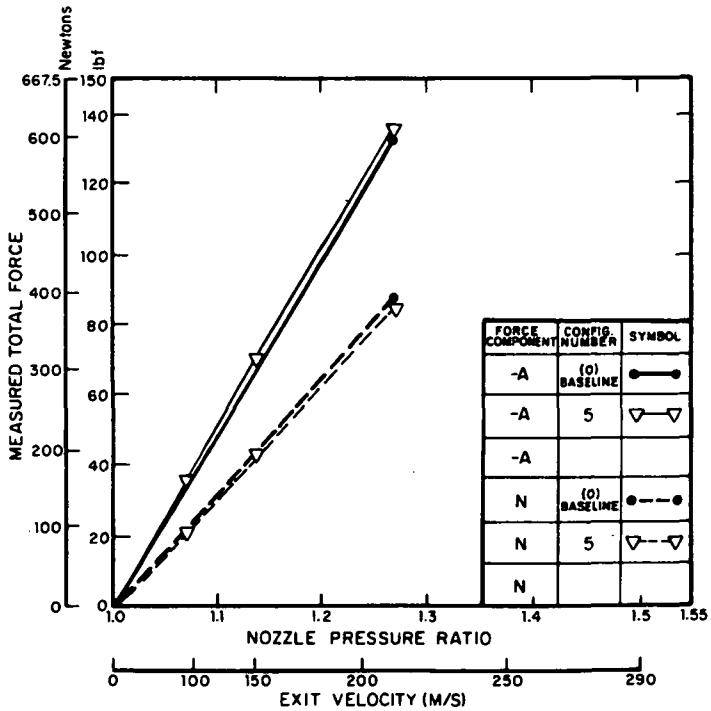

FIG. 44. STATIC FORCES vs. NOZZLE PRESSURE RATIO — CONFIGURATION 5.

Removal of the foam from the cavity did not change this result, as shown in Fig. 45. In this configuration, the trailing edge vent was filled with .5 $\rho_0 c_0$ foam to minimize the circulation of air through the flap from the lower surface.

A final step was to restrict the span of the treated trailing edge region to about 60% of the turning flap in the center region (outer edges of the turning flap were made solid). In this case (configuration 7), the aerodynamic performance appears to be virtually identical to the baseline configuration (Fig. 46).

Turning Angle and Efficiency:

Using the conversion procedures described above (Sec. 4.2), the results of the porous flap aerodynamic studies can be summarized in terms of turning angle and efficiency. Figure 47 compares the turning angle and efficiency of the above-described flap configurations (at their unstalled pressure ratios). Note that configurations 3 and 4 stalled before reaching the maximum pressure ratio of 1.265. Data for all others is taken at P_r = 1.265. The results indicate that several configurations turn the flow as well as or slightly better than the baseline flap, and that comparable efficiencies are possible. The fully porous configuration with no backing (2) turns poorly. By reviewing the previous figures, it will be noted that the stalled flaps reach similar values of A and N to that of the fully porous configuration at a pressure ratio of 1.265. However, in their unstalled condition, most of the porous flaps have satisfactory turning performance.

The challenge for further development of this concept is to extend the stall point for those configurations which stalled at low pressure ratios, but which had exceptional noise reductions. To do so, more detailed information on the dynamics of the flow on a curved porous surface is needed, as well as an indication of internal flow within the flap. A detailed surface pressure map would undoubtedly give further insight into the redistribution of surface pressures for porous surfaces. From this information, and diagnostic acoustic measurements, the tailoring of local surface impedance to the aerodynamic and acoustic requirements could be further developed.

4.4 Conclusions

A number of porous flap configurations have been tested on a USB system previously optimized for efficient powered lift aerodynamic performance. A severe turning condition (60° nominal

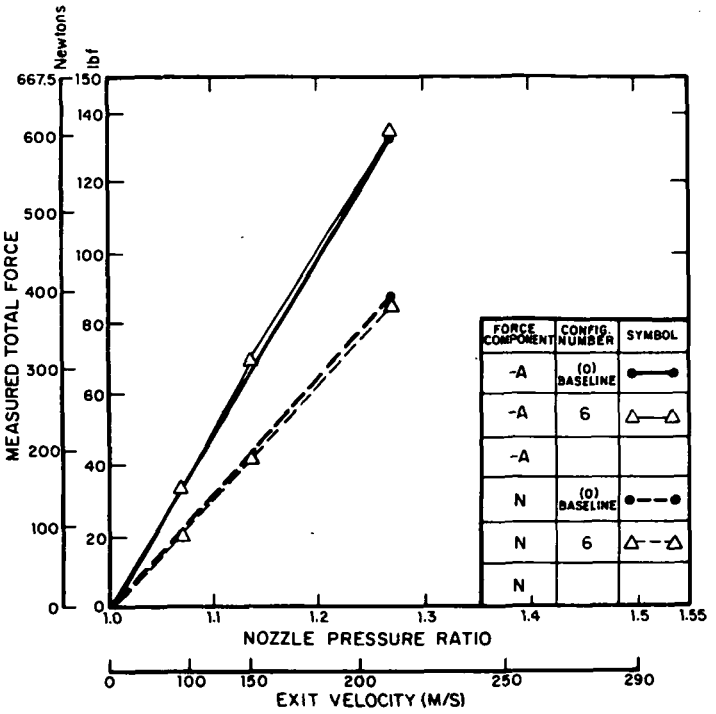

FIG. 45. STATIC FORCES vs. NOZZLE PRESSURE RATIO — CONFIGURATION 6.

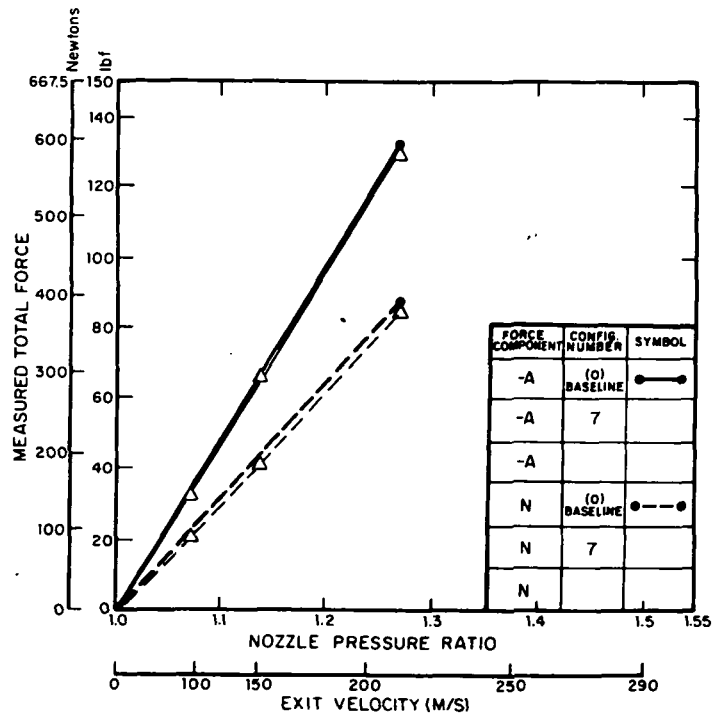

FIG. 46. STATIC FORCES vs. NOZZLE PRESSURE RATIO — CONFIGURATION 7.

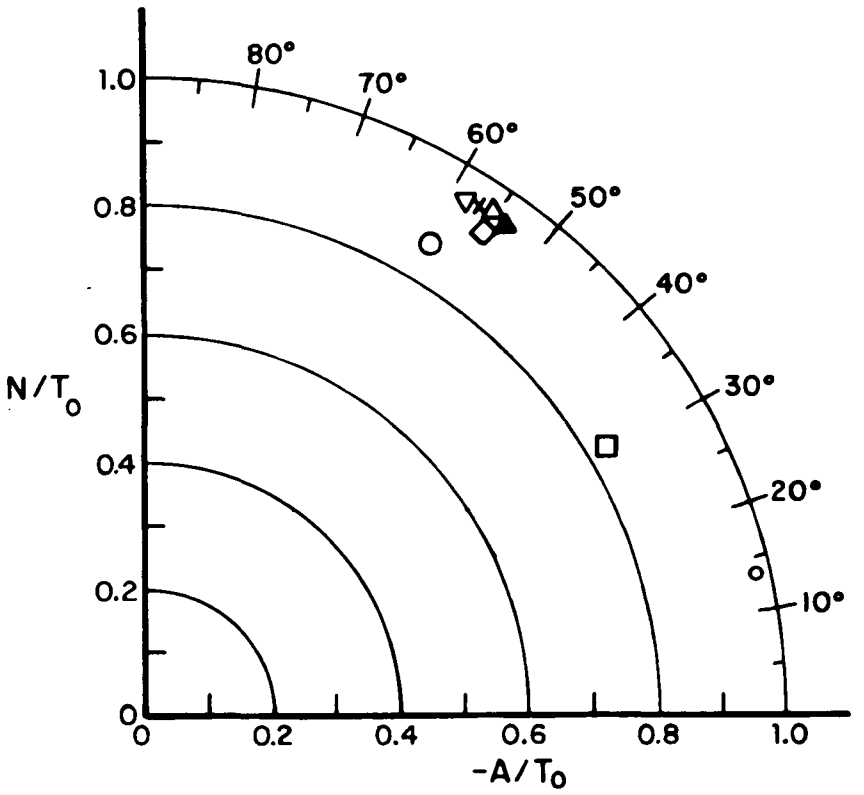

SYMBOL	CONFIGURATION
△	0 AND 1
□	2
○	3
◇	4
▽	5
x	6
▲	7 (BEFORE STALL)

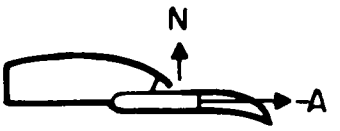

NOTE:
T_0 = CALIBRATION THRUST OF NOZZLE, WITH DEFLECTOR AND WITH FLAP REMOVED.

FIG. 47. STATIC TURNING CHARACTERISTICS OF POROUS FLAP CONFIGURATIONS.

flap setting was imposed) with the result that a number of porous flap configurations were able to turn the flow to the same degree and with approximately the same efficiency as the solid smooth flap.

Some of the configurations stalled prematurely but produced encouraging results at low speeds. The stall originated at the inboard trailing edge location and propagated forward and outboard as speed was increased. This is a result of the very high curvature of the streamlines in that region with a resultant high suction pressure on the local flap surface and the existence of a 90° corner between the flap surface and fence. If the pressure could be redistributed, such as by changing the flap sweep angle, this stall might be delayed or prevented. Forward speed may also be expected to alter or delay the stalling characteristics of the highly porous flaps.

Those porous flaps which did not stall also had encouraging noise reduction characteristics. The results of this aspect of the present study provide the first direct evidence of the aerodynamic viability of the porous surface concept for severe applications, such as propulsive lift systems.

APPENDIX A: MEASUREMENTS OF IMPEDANCE OF THIN POROUS METAL MATERIALS

Although the precise mechanism by which porous surfaces cause flow/surface interaction noise reduction remains to be established, it is essential to characterize the materials in some readily reproducible form to guide future applications of the concept.

A B&K impedance tube was used to measure the dynamic acoustic impedance of the several Brunsmetal* sheets considered as candidate materials. The discussion presented in this section explains how this data can be used to describe analytically the acoustic properties of these Brunsmetal sheets.

Flow Resistance of a Porous Sheet

Consider a thin porous sheet with a pressure drop $\Delta p = p_1 - p_2$ across it which gives rise to an average flow velocity u through it. For sufficiently low pressure drops it is found that the ratio

$$\theta = \frac{\Delta p}{\rho c u} \qquad (A.1)$$

is independent of Δp. This linearity, however, is lost at very high levels where the screen resistance increases monotonically with Δp.

The situation is, in general, slightly different for an oscillating (acoustic) pressure drop across the sheet. In addition to the resistive (frictional) forces, there are also inertial and compliant components associated with the finite mass and compressibility of the air in the screen pores. For a very thin sheet, however, both of these terms are insignificant; the sheet is purely resistive and the quality θ of Eq. A.1 is defined as the acoustic flow resistance.

Porous sheets may be used in conjunction with cavities to obtain a complex impedance

$$\zeta = \theta - i\chi \quad . \qquad (A.2)$$

---

*Trademark of Brunswick Corporation products.

Such a combination, in addition to the resistive component (θ) contributed by the sheet, also possesses a reactive component contributed by the cavity.

Normal Impedance of a Cavity Backed Screen

Consider the screen-cavity combination shown in Fig. A.1. For a normally-incident wave the impedance of a cavity is given by

$$\zeta_c = \frac{p_c}{\rho c u_c} = i \cot kL \qquad (A.3)$$

where L is the cavity depth, $k = \omega/c$, c is the acoustic velocity, ω is the angular frequency and the subscript "c" refers to the "cavity". The impedance ζ of the total combination is given by

$$\frac{p}{\rho c u} = \frac{(p-p_c)}{\rho c u} + \frac{p_c}{\rho c u} = \frac{p-p_c}{\rho c u} + \frac{p_c}{\rho c u_c} \quad . \qquad (A.4)$$

The first term on the right-hand side of Eq. A.4 is none but the screen resistance defined in Eq. A.1 and the second one the cavity impedance given in Eq. A.3. Thus, the normal acoustic impedance of a sheet/cavity combination is

$$\zeta = \theta - i \cot kL \quad . \qquad (A.5)$$

Measurement of Porous Sheet Resistance

To measure the quantity θ associated with a screen, one uses the procedure depicted in Fig. A.2. This involves direct measurement of the steady flow velocity across the sample for a given pressure drop Δp. These conditions for such a measurement, however, are static and the resulting θ_{static} can be expected to be, in general, different than its acoustic counterpart.

The best way for measuring θ is performed in an impedance tube. The porous sheet is combined with a cavity and the total impedance, ζ_t, of the entire combination is extracted. Since the cavity itself has no appreciable resistive component, the acoustic resistance, θ, of the screen is given by

$$\theta = (\text{real } [\zeta_t]) \quad .$$

This procedure was used to evaluate θ for several specimens. The results were obtained with a 2 in. deep cavity. As was shown in Fig. 18, θ increases near resonance, due to non-linear effects

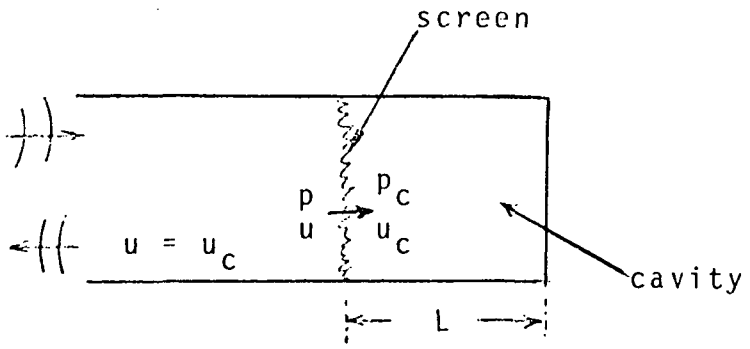

FIG. A.1. ARRANGEMENT FOR DEFINITION OF NORMAL ACOUSTIC IMPEDANCE OF POROUS SHEET/CAVITY COMBINATION.

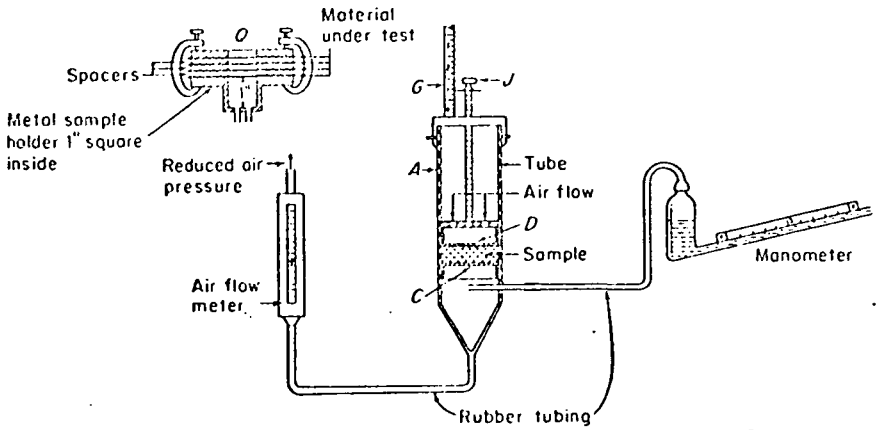

FIG. A.2. ARRANGEMENT FOR MEASUREMENT OF FLOW RESISTANCE OF A POROUS SHEET.

arising from excessively high velocities through the screen. This effect is particularly pronounced for screens with low resistance, i.e., $\theta < 1$ but less pronounced for screens with $\theta > 1$.

A summary of the properties of each material was presented in Table 1 and Fig. 18. The steady flow resistance, θ_s, should be typically equal to the low frequency limit of the acoustic normal resistance θ. There are some discrepancies between θ_s as quoted by the manufacturer and the measured θ in these tests. This is not altogether surprising becausethese specimens may have a partially altered θ due to dirt accumulation in the pores.

REFERENCES

Bohn, A.J., (1976), "Edge Noise Attenuation by Porous Edge Extensions," AIAA Paper 76-80, Presented at AIAA 14*th* Aerospace Sciences Meeting, Washington, D.C., 26-28 January 1976.

Hayden, R.E. and Chanaud, R.C. (1973), "Method of and Structure for Reducing Sound Generation in Fluid Flow Systems Embodying Foil Structures and the Like," U.S. Pat. No. 3,779,338.

Hayden, R.E. and Chanaud, R.C. (1974), "Foil Structures with Reduced Sound Generation," U.S. Pat. No. 3,853,428.

Hayden, R.E., Kadman, Y. and Chanaud, R.C. (1972a), "A Study of the Variable Impedance Surface Concept as a Means for Reducing Noise from Jet Interaction with Deployed Lift-Augmenting Flaps," BBN Report No. 2399 (Nov. 1972), also NASA CR-112166.

Hayden, R.E., Scharton, T.D. *et al.*, (1972b), "A Preliminary Evaluation of Noise Reduction Potential for the Upper Surface Blown Flap," BBN Report No. 2478, NASA CR-112246.

Hayden, R.E. (1973), "Fundamental Aspects of Noise Reduction from Powered Lift Devices," invited paper, 1973 SAE National Air Transportation Meeting, Miami, Florida (published in 1973 *SAE Transactions*), SAE Paper 730376.

Hayden, R.E. (1976), "Reduction of Noise from Airfoils and Propulsive Lift Systems Using Variable Impedance Surfaces," AIAA Paper 76-500, 3*rd* Aeroacoustics Conf., Palo Alto, Calif., July 1976.

NASA Ames Research Center, (1972), "STOL Technology," NASA SP-320, 17-19 October 1972.

NASA Langley Research Center, (1976), "Powered-Lift Aerodynamics and Acoustics," NASA SP-406, 24-26 May 1976. (Subject to limitations of early domestic dissemination restrictions until May 1978.)

Phelps, A.E., III (1975), "Wind Tunnel Investigation of a Twin-Engine Straight-Wing Upper-Surface Blown Jet-Flap Configuration," NASA TND-7778.

Wilby, J.F. and Scharton, T.D. (1974), "Acoustic Transmission Through a Fuselage Sidewall," BBN Report No. 2742, prepared under contract NAS1-11839.